

# **For Reference**

---

**NOT TO BE TAKEN FROM THIS ROOM**



Ex LIBRIS  
UNIVERSITATIS  
ALBERTAENSIS







Digitized by the Internet Archive  
in 2019 with funding from  
University of Alberta Libraries

<https://archive.org/details/Luft1983>



T H E U N I V E R S I T Y O F A L B E R T A

Release Form

NAME OF AUTHOR            Hans Bernd Luft  
TITLE OF THESIS           Film-Cooling Applied To The Insulator Walls  
                              Of An MHD Generator Channel  
DEGREE FOR WHICH THESIS WAS PRESENTED        Doctor of Philosophy  
YEAR THIS DEGREE GRANTED        Spring, 1983

Permission is hereby granted to THE UNIVERSITY OF  
ALBERTA LIBRARY to reproduce single copies of this  
thesis and to lend or sell such copies for private,  
scholarly or scientific research purposes only.

The author reserves other publication rights, and  
neither the thesis nor extensive extracts from it may  
be printed or otherwise reproduced without the author's  
written permission.







THE UNIVERSITY OF ALBERTA

FILM-COOLING APPLIED TO THE  
INSULATOR WALLS OF AN MHD  
GENERATOR CHANNEL

by



HANS-BERND LUFT

A THESIS

SUBMITTED TO THE FACULTY OF GRADUATE STUDIES AND RESEARCH  
IN PARTIAL FULFILLMENT OF THE REQUIREMENT FOR  
THE DEGREE OF DOCTOR OF PHILOSOPHY

DEPARTMENT OF MECHANICAL ENGINEERING

EDMONTON, ALBERTA

SPRING, 1983







05-310

UNIVERSITY OF ALBERTA  
FACULTY OF GRADUATE STUDIES

The undersigned certify that they have read, and recommend to the Faculty of Graduate Studies for acceptance, a thesis entitled "FILM - COOLING APPLIED TO THE INSULATOR WALLS OF AN MHD GENERATOR CHANNEL" submitted by HANS-BERND LUFT in partial fulfillment of the requirements for the degree of Doctor of Philosophy.





## DEDICATION

To my wife Audrey Elaine Rohe-Luft

"It matters not whether one received the prize.  
What really counts is whether one completes the race."

AERL





## ABSTRACT

The possibility of film-cooling the B-wall (insulator wall) of an MHD generator duct has been investigated theoretically. A potassium seeded nitrogen plasma as the primary and secondary fluids is considered and the compressible, turbulent boundary-layer equations are solved numerically using the implicit finite-difference scheme of Patankar and Spalding. This numerical method has been modified in a general way to include the effects of electromagnetic body forces such that it can be applied to other than film-cooling flow problems which involve the action of such body forces. The equations solved are overall continuity, momentum and energy as well as electron conservation and energy to account for electron thermal non-equilibrium and finite-rate ionization in non-equilibrium generators. A mixing-length scheme to model MHD damping of turbulent fluctuations is proposed by exploiting the analogy which can be drawn between MHD and wall suction boundary layer flows.

Results show that the adiabatic film-cooling effectiveness is significantly increased and that MHD turbulent damping noticeably increases the effectiveness even further but to a lesser extent.

An optimum magnetic field intensity exists for which maximum film-cooling effectiveness is obtained for a particular flow condition. The MHD film-cooling process is found to be as sensitive or less to initial flow parameters and geometry as has been observed in





ordinary hydrodynamic flows, but initial magnetic field prescriptions must be as true to physical reality as possible. Non-equilibrium effects are found to produce near-wall current density increases which influence the film-cooling effectiveness in a complicated way, the net outcome of which results in a decreased effectiveness but still significantly larger than its OHD counterpart.



## ACKNOWLEDGEMENTS

The author wishes to express his thanks and acknowledgements to the following:

- (i) Dr. C. M. Rodkiewicz, Professor, for his support and encouragement as supervisor of the thesis.
- (ii) Dr. D. J. Wilson, Professor, Department of Mechanical Engineering, University of Alberta, for his helpful and enlightening discussions on the film-cooling process.
- (iii) The late Dr. R. Gilpin, Professor, Department of Mechanical Engineering, University of Alberta, for his helpful and informative discussions on plasma flows and MHD principles.
- (iv) Dr. R. N. Gupta, Professor, Department of Aeronautical Engineering, Indian Institute of Technology, Kampur, India, (presently with NASA-Langley, Hampton, VA, U.S.A.), for his helpful suggestions and undiminished encouragement and moral support.
- (v) Dr. D. Marsden, Professor, Department of Mechanical Engineering, University of Alberta, for his general consultation on gas dynamics and kinetic theory of gases.
- (iv) My wife, Audrey, for her infinite patience and endurance with never ending support and optimism.
- (vii) Ms. Gail Anderson and Ms. Helen Wozniuk for their diligent efforts and excellent typing of the thesis.





## TABLE OF CONTENTS

	<u>Page</u>
Abstract.....	v
Acknowledgements.....	vii
Table of Contents.....	viii
List of Figures.....	xi
List of Symbols.....	xiii
 CHAPTER I	
STATEMENT OF THE PROBLEM AND ASSOCIATED LITERATURE.....	1
1.1 Introduction.....	1
1.1.1 Adiabatic-Wall Film-Cooling Effectiveness.....	5
1.1.2 Film-Cooling Slot Geometry and Theoretical Flow Model.....	8
1.2 Review of Associated Literature.....	10
1.2.1 Non-Equilibrium MHD Channel-Flow Research and Developments.....	10
1.2.2 MHD Turbulence and Turbulent Flows...	13
1.2.3 OHD Film-Cooling Research and Developments.....	17
1.2.4 MHD Film-Cooling Research and Developments.....	18
 CHAPTER II	
THEORETICAL DEVELOPMENT.....	22
2.1 Boundary Layer Equations.....	22
2.2 Molecular Transport Properties.....	25
2.3 Boundary Conditions.....	27





# TABLE OF CONTENTS (continued)

	<u>Page</u>
CHAPTER II (continued)	
2.4 Calculation of Axial Flow Variables....	32
2.5 Initial Conditions.....	33
CHAPTER III SOLUTIONS TO THE GOVERNING EQUATIONS.....	36
3.1 Numerical Solution Procedure.....	36
3.2 MHD Modifications to Effective Viscosity Hypothesis.....	40
CHAPTER IV UNIVERSAL MHD MODIFICATIONS TO THE PATANKAR AND SPALDING NUMERICAL SOLUTION PROCEDURE.....	49
4.1 MHD Wall Function Modifications.....	49
4.2 Integration of the Couette Flow Equations.....	55
4.3 Curve-Fitting the Integrated Momentum Equation-Shear Stress.....	57
4.4 Curve-Fitting the Integrated Energy Equation-Recovery Factor.....	67
CHAPTER V DISCUSSION OF RESULTS AND CONCLUSIONS.....	71
5.1 General Discussion.....	71
5.2 Evaluation of Computational Procedure for OHD Film-Cooling Flows.....	73
5.3 Thermal and Ionizational Equilibrium, MHD Film-Cooling.....	75
5.3.1 MHD Influence on Film-Cooling Boundary Layer Velocity Profiles and Film-Cooling Effectiveness.....	75
5.3.2 MHD Influence on Film-Cooled Boundary Layer Temperature Profiles and Film-Cooling Effectiveness.....	82
5.3.3 Influence of Variation in Flow Parameters on MHD Film-Cooling Effectiveness at Constant Magnetic Field.....	89



## TABLE OF CONTENTS (continued)

		<u>Page</u>
CHAPTER V	(continued)	
	5.3.4 Influence of Initial Magnetic Field, $B(x)$ , Variation on Boundary Layer Profiles and Film-Cooling Effectiveness.....	93
	5.4 Thermal and Ionizational Non-Equilibrium MHD Film-Cooling.....	101
	5.5 Conclusions.....	108
REFERENCES.....		114
APPENDIX A	"On Flat Plate Boundary Layer Flow Subjected to Suction and Transverse Magnetic Field", H. B. Luft, C. M. Rodkiewicz.....	125





## LIST OF FIGURES

<u>Figure</u>		<u>Page</u>
1.1	Theoretical Model of Film-Cooling Slot.....	4
2.1	Schematic of MHD-Channel Co-ordinate System....	22
2.2	Typical MHD Generator 1-D Core Flow Solution...	31
2.3	Initial Velocity Flow Model Assumed in Present Work.....	35
3.1	Bridging Technique for Effective Viscosity.....	41
3.2	Effective Viscosity, Mixing-Length Model.....	43
4.1	Couette Layer Dimensionless-Velocity Profiles..	58
4.2	Couette Layer Drag Coefficient versus Hartmann Number.....	60
4.3	Couette Layer Drag Coefficient versus Hartmann Number Squared.....	62
4.4	Couette Layer Drag Coefficient, Curve Fitting Parameter 'b' versus Reynolds Number.....	62
4.5	Couette Layer Drag Coefficient, Small Reynolds Number Correction.....	63
4.6	Couette Layer Drag Coefficient, Exact versus Empirical.....	65
4.7	Couette Layer Recovery Factor versus Electric Field Parameter.....	70
5.1	Validation of Computer Program for OHD Film-Cooling Effectiveness.....	74
5.2	MHD Influence on Film-Cooled Boundary Layer Velocity Profiles, Equilibrium Case.....	77
5.3	MHD Influence on Adiabatic Film-Cooling Effectiveness-Equilibrium Case.....	80
5.4	MHD Influence on Film-Cooled Boundary Layer Temperature Profiles, Equilibrium Case.....	83
5.5	Electron Current Density Boundary Layer Profiles, Equilibrium Case.....	85



# LIST OF FIGURES (continued)

<u>Figure</u>		<u>Page</u>
5.6	Equilibrium Electron Mass Fraction Boundary Layer Profiles.....	86
5.7	Equilibrium Plasma Electrical Conductivity Boundary Layer Profiles.....	87
5.8	Influence on MHD Film-Cooling Effectiveness for Constant Magnetic Field and Variable Core Flow Parameters.....	92
5.9	Influence of Initial Condition for $B(x)$ on MHD Film-Cooling Velocity Profiles.....	95
5.10	Influence of Initial Condition for $B(x)$ on MHD Film-Cooling Temperature Profiles.....	96
5.11	Influence of Initial Condition for $B(x)$ on MHD Film-Cooling Effectiveness.....	98
5.12	Developing Boundary Layer Temperature Profiles in MHD Film-Cooling for $B=2$ at $x/y_{C,max}=10$ .....	100
5.13	Effect of Non-Equilibrium on MHD Film-Cooling Velocity Profiles, Near Slot Region.....	102
5.14	Effect of Non-Equilibrium on Boundary Layer Current Density Profiles.....	104
5.15	Effect of Non-Equilibrium on MHD Film-Cooling Velocity Profiles, Far Slot Region.....	105
5.16	Effect of Non-Equilibrium on Boundary Layer Temperature Profiles.....	106
5.17	Influence of Non-Equilibrium on MHD Film-Cooling Effectiveness.....	107





## LIST OF SYMBOLS

$A$	Cross-sectional channel area
$\vec{B}$	Magnetic field induction $\vec{B} = B_x \vec{i} + B_y \vec{j}$ , Fig. 2.1
$B_x$	Induced magnetic field, streamwise component
$c$	Empirical fluid-jet turbulence constant ( $0.13 < c < 0.18$ ), Eq. (1.11)
$C_e$	Electron mass fraction, Eq. (2.7)
$C_p$	Specific heat at constant pressure
$C_{pe}$	Electron specific heat
$C_s$	Mass fraction of species 's' in equation of state, Eq. (2.15)
$^{\circ}\text{C}$	Degrees Celsius
$D$	General turbulence damping function
$\vec{E}$	Electric field strength, $\vec{E} = E_x \vec{i} + E_z \vec{k}$ , Fig. 2.1
$E$	Electric field parameter, Eq. (4.7)
$e$	Electron charge
$F$	Pressure gradient parameter
$F'$	General retarding force per unit duct length due to walls or body forces, Eq. (2.28)
$H$	Total enthalpy
$Ha$	Hartmann number based on Couette layer thickness, Eq. (4.7)
$Ha_L$	Hartmann number based on characteristic length $L$ , $\sqrt{(\sigma/\mu)} BL$
$h$	Static enthalpy
$\bar{h}$	Planck constant, Eq. (2.9)
$h_{aw}$	Adiabatic-wall static enthalpy



$h_C$	Coolant (secondary) flow static enthalpy
$h_e$	Electron enthalpy, $C_{p_e} T_e$
$h_r$	Recovery static enthalpy
$j_{e_z}$	Transverse electron current density
$J_h$	Enthalpy flux
$K$	Turbulence parameter
$K_L$	MHD-channel load factor, Eq. (2.21)
$K_S$	Equilibrium constant, Eq. (2.9)
$\bar{k}$	Boltzmann's constant
$k$	Plasma thermal conductivity
$k_e$	Electron-gas thermal conductivity
$^{\circ}K$	Degrees Kelvin absolute
$L$	General characteristic length
$l$	Mixing length
$M$	Mach number
$\dot{m}$	Channel mass flow, Eq. (2.22)
$m_e$	Electron mass
$m_i$	Ion mass
$n_e^*$	Saha equilibrium electron number density, Eq. (2.7)
$n_G, n_L, n_W$	Exponents in the power law velocity profiles at the film-cooling slot, Eqs. (2.31 - 2.33)
$N_L$	Magnetic interaction number (Stuart number), $\sigma B^2 L / \rho U$
$N_x$	Local magnetic interaction number, $\sigma B^2 x / \rho U$
$p$	Pressure
$p_G$	Channel core flow pressure, Fig. 1.1
$P_r$	Prandtl number



$P_t$	Turbulent Prandtl number
$p_s$	Partial pressure of species 's' in equation of state, Eq. (2.15)
$Q$	Film-cooling blowing parameter $\rho_C U_C / \rho_G U_G$
$Q$	Generalized flow property
$\bar{Q}$	Average value for $Q = \bar{Q} + Q'$
$Q'$	Fluctuating component of $Q = \bar{Q} + Q'$
$Q_{es}$	Electron-particle collision cross section, Eq. (2.14)
$Q_{ei}$	Electron-ion collision cross section
$\dot{q}_w$	Heat transfer at the B-wall
$R$	Gas constant, in equation of state, Eq. (2.15)
$Re$	Reynolds number of the Couette flow
$Re_C$	Reynolds number of the coolant (secondary) flow
$Re_m$	Magnetic Reynolds number
$r$	Recovery factor
$r$	Fluid jet "half-thickness", Eq. (1.11)
$S$	Laminar Schmidt number
$S_t$	Turbulent Schmidt number
$SF$	Seed fraction by mole, Eq. (2.7)
$ST$	Stanton number, Eq. (1.1)
$T$	Main gas temperature
$T_{aw}$	Adiabatic wall temperature
$T_C$	Secondary (coolant) flow temperature, Fig. 1.1
$T_G$	Main gas channel core flow temperature, also referred to free stream temperature
$T_e$	Electron gas temperature





$T_r$	Recovery temperature
$t_L$	Film-cooling slot lip thickness, Fig. 1.1
$U_C$	Coolant (secondary) flow velocity, Fig. 1.1
$U_G$	Channel core-flow velocity or free stream velocity, Fig. 1.1
$u$	Streamwise velocity component
$v$	Transverse velocity component
$W$	Constant $\sqrt{(\tau_w^3/\rho_c)/(-J_{h,w})}$
$x$	Streamwise boundary layer grid coordinate, Fig. 2.1
$y$	Transverse flow Cartesian coordinate, Fig. 1.1
$y_C$	Film-cooling slot height, Fig. 1.1
$y_G$	y-coordinate for edge of boundary layer, Fig. 1.1
$Z$	Compressibility factor, Eq. (2.16)
$Z_{rs}$	Partition function, Eq. (2.10)
$z$	Transverse flow Cartesian coordinate, Fig. 2.1
$\alpha$	Mixing angle, Fig. 1.1
$\beta$	Hall parameter
$\Delta'$	Electron-electron interaction correction, Eq. (2.14)
$\delta_{eff}$	Effective electron-neutron collision energy loss factor, Eq. (2.18)
$\delta_s$	Fraction collision energy loss of species 's' with electrons
$\epsilon$	Eddy viscosity
$\epsilon_i$	Ionization energy, Eq. (1.10)
$\eta$	Film-cooling effectiveness, Eq. (1.5)
$\eta_r$	Film-cooling effectiveness for compressible flow based on recovery temperature reference conditions, Eq. (1.6)
$\theta_u$	MHD turbulence damping factor ( $\theta_u = 1$ for $B = 0$ , $\theta_u = 0$ for $B \rightarrow \infty$ ), Eq. (1.11)



$\theta_v$	Characteristic vibration temperature, Eq. (2.17)
$\mu$	Laminar fluid dynamic viscosity
$\mu_{eff}$	Effective dynamic viscosity, $\mu + \epsilon$
$\mu_H$	Magnetic permeability
$\nu$	Kinematic fluid viscosity
$\nu_{es}$	Momentum collision frequency between electrons and species 's' Eq. (2.18)
$\nu_H$	Magnetic diffusivity, $1/\sigma\mu_H$
$\xi$	Von Mises transformation variable, Eq. (3.1)
$\rho$	Fluid mass density
$\rho_C$	Coolant flow density, Fig. 1.1
$\dot{w}_e$	Electron mass production, Eq. (2.11)
$\rho_G$	Channel core-flow (primary fluid) mass density
$\sigma_0$	Plasma electrical conductivity, first order approximation, Eq. (2.13)
$\sigma_e$	Plasma electrical conductivity
$\sigma_{eff}$	Effective plasma electrical conductivity, Eq. (3.7)
$\tau$	Shear stress
$\tau^+$	$\tau/\tau_w$
$\psi$	Stream function
$\psi_E$	Stream function at outer edge of boundary layer, Fig. 1.1
$\psi_I$	Stream function at inner edge of boundary layer, Fig. 1.1
$\omega$	Normalized stream function, $\psi/\psi_E$ and transverse coordinate of boundary layer grid, Fig. 1.1





## Subscripts

aw	Adiabatic wall
C	Coolant (secondary) flow
c	Couette layer
E	Exterior boundary of general boundary layer
e	Electron species
eff	Effective
emp	Empirical
G	Channel core-flow or free-stream conditions
Go	Initial core-flow or free-stream conditions
I	Interior boundary of general boundary layer
K	Potassium seed
L	Film-cooling slot lip
o	Initial value at $x = 0$ , ie. at location of slot exit
opt	Optimum
r	Recovery conditions
s	General species 's'
w	Wall
x,y,z	Co-ordinate directions

## Superscripts

*	Saha equilibrium conditions, also transformed variable with respect to $K$ , Eq. (4.8)
'	Fluctuating component (except in $F'$ )
$\rightarrow$	Vector quantity
-	Averaged quantity



## Acronyms

JAS	Journal of the Aeronautical Sciences
MHD	Magneto Hydrodynamics
NASA	National Aeronautics and Space Administration
OHD	Ordinary Hydrodynamics



## CHAPTER I

### STATEMENT OF THE PROBLEM AND ASSOCIATED LITERATURE

#### 1.1 Introduction

Magnetohydrodynamic (MHD) gas flows involve, by necessity, the use of high temperature working fluids to ensure an adequate electrical conductivity even with the addition of readily ionizable seed materials such as the alkali metals. In particular, for MHD generators, temperatures of approximately 2500°C are encountered in combustion or open-cycle equilibrium generators whereas somewhat lower fluid temperatures, approximately 1800°C, are required for non-equilibrium, closed cycle generators. Since one of the major obstacles to achieving acceptable generator duty cycles between maintenance shutdown is the problem [1]<sup>†</sup> of materials which can withstand high generator-duct temperatures, it would seem meaningful to investigate the possibility of protecting the MHD duct walls from these high temperatures by cooling techniques which have proven to be extremely effective in ordinary hydrodynamics (OHD) flow applications.

Cooling of MHD channel walls is usually accomplished externally by means of circulating water in contact with the exterior surface of the walls, by water-jacket designs or possibly, when considering the insulator walls, by a specially constructed composite wall designed to have a high overall thermal conductivity to permit a large heat transfer rate while at the same time remaining a good

---

<sup>†</sup>Numbers in square brackets indicate references listed.





electrical insulator. In OHD flows it is known that cooling methods involving mass transfer at the surface in contact with the hot fluid stream are much more effective than cooling the wall on the inside. It was therefore suggested to investigate the possibility of transpiration cooling applied to the insulator or B-walls of an MHD generator and some results representing first order effects obtained from simple integral methods with permeable-wall boundary conditions are presented as a separate study found in Appendix A. Objections to this effort were later raised when considering the practical applications of constructing such a porous MHD duct and a film-cooling technique was instead proposed for this investigation.

The need to protect surfaces which are subjected to high temperature environments has existed for other than MHD flows for a long time. Generally, the high temperature environment is a gaseous one such as those experienced in the ionized air stream surrounding re-entry vehicles, rockets, plasma jets, and high performance gas turbines.

Sophisticated methods of cooling have been employed over the last 30 years which include the introduction of a secondary fluid into the boundary layer of the surface which must be protected. Ablation is another method, which is well known from its application to re-entry vehicles in NASA's space program.<sup>†</sup> In such methods, an added coating to the surface known as a "heat shield" decomposes and, through sublimation and other highly endothermic processes, a large quantity of heat is absorbed by the heat-shield material. Transpiration

---

<sup>†</sup>Brewer, R. A. and Brant, D. N., "Thermal Protection System for the Galileo Mission Atmospheric Entry Probe" AIAA Paper No. 80-0358, 1980.



cooling (ie. cooling by mass transfer or sweat) is a second method which can be applied to a surface made of porous materials. The cooler secondary fluid "diffuses" through such a permeable surface before entry into the boundary layer.

Ablation and transpiration cooling are primarily effective in protecting the region where the materials ablates and the secondary fluid enters the boundary layer. In addition to heat absorption by this material or fluid, the boundary layer is effectively thickened by the mass addition which further reduces the heat transfer rate due to smaller surface gradients. The short-comings of these two methods, however, are that ablation cooling is limited to systems characterized by high heat fluxes of short duration and transpiration cooling requires porous materials which do not possess the necessary structural strength, which in most cases is a necessity in applications where such high temperatures are encountered. The pores, furthermore, have a tendency of becoming clogged resulting in relatively short duty cycles.

A third effective method of cooling involving secondary fluid injection into the downstream boundary layer is termed 'film-cooling'. The primary objective of film-cooling is to keep the surface downstream of the injection slot cool. Figure 1.1 represents schematically a typical film-cooling slot which would be installed at discrete locations along a surface to protect it not only in the immediate region of the fluid injection, but also for a considerable distance downstream. The flow far downstream of the coolant injection slot is, in fact, similar to that downstream of a sweat or ablation-cooled surface. Furthermore, film-cooling could be used to shield



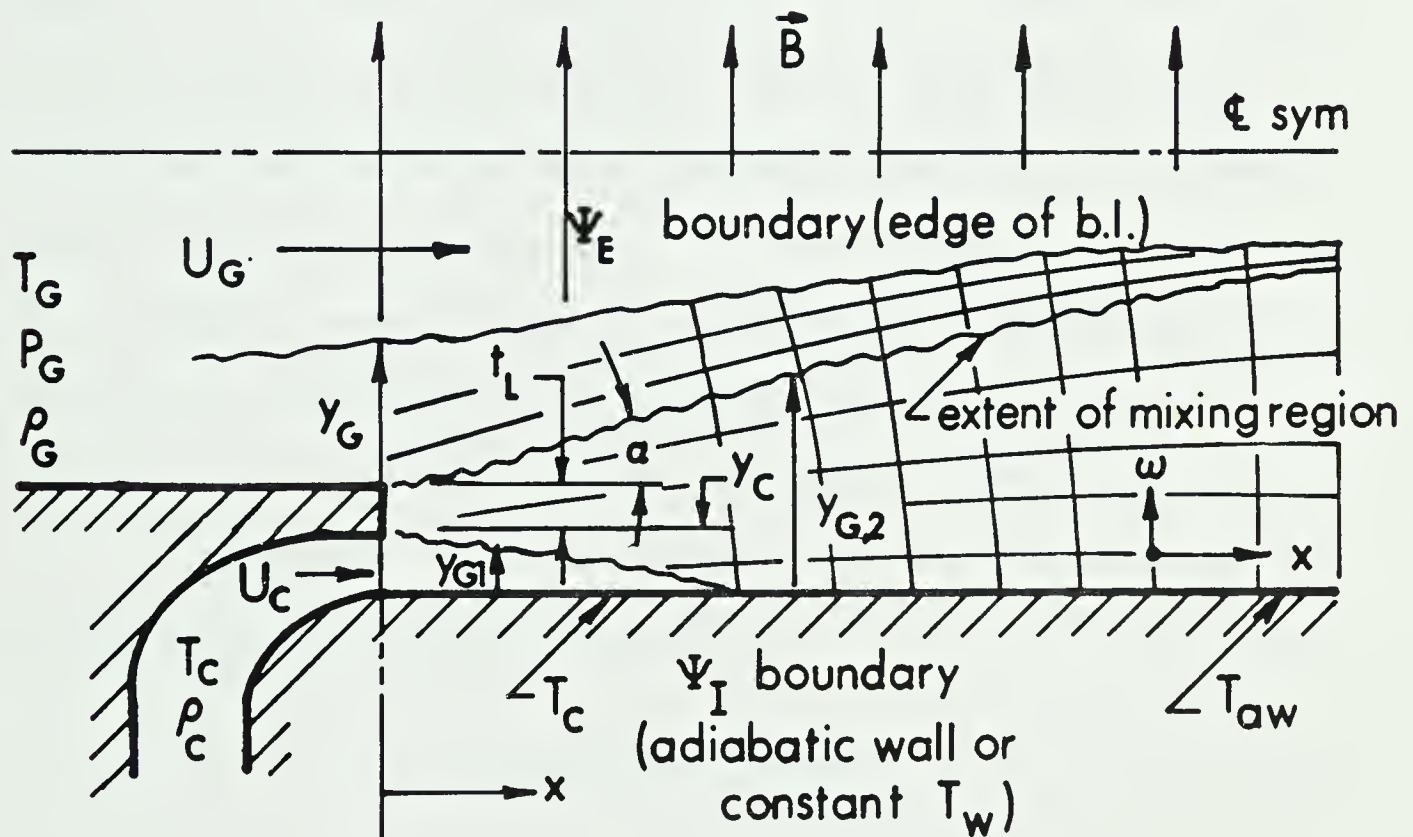


Fig. 1.1 Theoretical Model of Film-Cooling Slot





### 1.1.1 Adiabatic-Wall Film-Cooling Effectiveness

For the thermal design of a surface in contact with a high temperature fluid, the engineer requires information on the heat-transfer rate between the surface and fluid and the variation of the surface temperature along the direction of flow when heat transfer at the fluid/surface interface is prevented. This would represent the maximum temperature to which the surface would be subjected without internal wall cooling and is known as the adiabatic wall temperature,  $T_{aw}$ . The general problem in film-cooling theory is to predict the relationship between the wall temperature distribution and heat transfer, given a certain mainstream flow, secondary injection flow and specific slot geometry. The design problem posed may also be to predict the secondary flow needed to maintain the wall surface temperature below a certain permissible value for a given mainstream flow, slot geometry, and allowable wall heat transfer. The heat transfer is characterized by the Stanton number  $ST$ , and the adiabatic wall temperature by a film-cooling effectiveness,  $\eta$ , and given both these values, the engineer is told all that he needs to know for further design.

The Stanton number  $ST$  in the presence of film-cooling is defined in the conventional way, Eq. (1.1)

$$ST = \dot{q}_w / [(h_r - h_w) \rho_G U_G] \quad (1.1)$$

or since

$$h_r = h_G + \frac{r}{2} U_G^2 \quad (1.2)$$



and

$$h = C_p T \quad (1.3)$$

$$ST = \dot{q}_w / [C_p (T_G - T_w) + \frac{r}{2} U_G^2] \rho_G U_G \quad (1.4)$$

Equation (1.4) is written in terms of quantities which the designer can easily evaluate together with what he desires to know, which is the heat flux,  $\dot{q}_w$ , to the wall.

The adiabatic wall temperature,  $T_{aw}$ , is a function of the primary and secondary flow fields, slot geometry, and temperatures of the two fluid streams. By defining a dimensionless adiabatic wall temperature,  $\eta$ , called the film-cooling effectiveness, this temperature dependence can be eliminated. For constant property flows the film-cooling effectiveness is defined by

$$\eta = \frac{T_{aw} - T_G}{T_C - T_G} \quad (1.5)$$

At the injection slot,  $T_{aw} = T_C$ , and  $\eta = 1$ . Generally  $T_{aw} < T_G$  and  $T_C < T_G$  so that  $\eta$  varies from unity at  $x = 0$  to 0 at  $x = \infty$ , (see Fig. 1.1) where, because of continual mixing of the two gas streams, the adiabatic wall temperature approaches that of the free stream.

For variable property flows, the wall temperature in the slot would be expected to be the recovery temperature of the injected gas whereas far downstream, the adiabatic wall temperature would be the recovery temperature,  $T_r$ , of the mainstream gas. As a consequence, an



appropriate expression often used for compressible film-cooling is

$$\eta_r = \frac{T_{aw} - T_r}{T_c - T_r} \quad (1.6)$$

which is seen to be equivalent to Eq. (1.5) when compressibility effects can be neglected.

For the large temperature differences encountered in high temperature MHD channel flows, an effectiveness similar to Eq. (1.6) will be employed except that the corresponding enthalpies will be substituted for temperatures. Hence in the present work, the film-cooling effectiveness is defined as

$$\eta = \frac{h_{aw} - h_r}{h_c - h_r} \quad (1.7)$$

which can be rewritten in term of temperatures as

$$\eta = \frac{T_{aw} - (T_c + \frac{r}{2} \frac{U_c^2}{C_{pG}})}{(T_G - T_c) + \frac{r}{2C_{pG}} (U_G^2 - U_c^2)} \quad (1.8)$$

from which the designer can determine  $T_{aw}$  in terms of known quantities.

Most investigations into film-cooling have dealt with the determination of heat transfer coefficient and adiabatic wall temperatures as separate studies with a major emphasis on predicting and/or measuring the film-cooling effectiveness,  $\eta$ . A common finding is that the heat transfer coefficient is close to that without injection which implies that it is primarily determined by the mainstream flow. The adiabatic wall temperature, however, varies significantly from that without secondary gas injection which makes it more difficult, and perhaps





more important, to predict. In the present work, only the effects of non-equilibrium flow and MHD body forces (both on average velocities and turbulent fluctuations) on the flow and temperature fields and adiabatic-wall film-cooling effectiveness, will be investigated.

### 1.1.2 Film-Cooling Slot Geometry and Theoretical Flow Model

The film-cooling effectiveness and wall heat flux are dependent on a large number of variables such as slot geometry, properties of both primary and secondary flows, initial velocity and temperature (density) ratios of the two gas streams (often correlated in terms of a blowing parameter  $Q = \rho_C U_C / \rho_G U_G$ ), intensity of freestream turbulence, etc.

Experimental investigations require diligent efforts to obtain many data records and lengthy modifications to change the experimental apparatus. Often the results from experimental measurements proved the effort not to be worth while. If, on the other hand, a reliable theoretical prediction method can be devised which accurately models the film-cooling process, the theoretician needs only change a few statements in the computer program and the results are relatively quickly obtained.

One such prediction method is that devised by Patankar and Spalding [2] and has been successfully applied to OHD film-cooling predictions in Ref. [3]. Unlike many other methods of predicting boundary layer flows, that of Ref. [3] can handle velocity profiles exhibiting maxima. It has therefore also been adopted in the present work and was modified in a general way to allow analysis of MHD flows



as is detailed in Chapter IV. The theoretical model of the MHD film-cooling slot is shown in Fig. 1.1. The boundary layer flow under these conditions will be turbulent and thermal non-equilibrium and finite rate ionization will be considered.

The method of solution is of the finite-difference variety and one main feature is that the computational grid of nodes fits the boundary layer exactly; its width grows or contracts at the same rate as the boundary layer itself. This enables the same number of nodes in the  $y$  (or  $\omega$ ) direction to accurately calculate dependent variable gradients as the marching procedure advances downstream. Furthermore, in the near wall regions of the boundary layer where gradients change rapidly, the Couette flow analysis of the present method precludes the requirement of a very large number of nodal points which is characteristic of other methods which employ constant grid spacings across the entire width of the boundary layer. For such methods the number of nodal points is large by necessity and must increase as downstream solutions develop in order that gradients near the wall may be calculated sufficiently accurate. In the present method the length of computing time is significantly reduced by virtue of a smaller number of grid points which typically may only be of the order of 50 while other methods require of the order of 1000 for similar accuracy.



## 1.2 Review of Associated Literature

### 1.2.1 Non-Equilibrium MHD Channel-Flow Research and Developments

The effects of thermal non-equilibrium and finite rate recombination were studied in the insulator boundary layer of a potassium-seeded nitrogen core-flow MHD Hall-neutralized Faraday accelerator by D. W. Cott [4,5]. The non-similar, compressible boundary layer was assumed to be laminar and two dimensional. The general multi-fluid conservation equations were derived from Boltzmann's equation and a two-fluid model was adopted consisting of the over-all gas and the electron species. A collisionless sheath was assumed and matched with the boundary layer equations which were then solved numerically using the method of Ref. [6]. For the laminar flow considered little accuracy was lost by solving the linearized equations all the way to the wall without a Couette-flow model for the overall gas. For the electron gas boundary layer, however, the Couette-flow concept offered a convenient method of coupling the sheath mixed boundary conditions to the linearized electron diffusion and energy equations. An iteration procedure was devised which matched the sheath transition region, treated as the Couette-flow region, with the finite-difference solution of the outer edge boundary layer flow. It was concluded that thermal non-equilibrium can lead to significant B-wall shorting in long channels, and that Hall effects should not be neglected when large B-fields are encountered and that operation is not noticeably affected by ionizational non-equilibrium or the physics of the electrostatic sheath.





High and Felderman [7], considered the compressible, turbulent, boundary layer flow over the B-wall of an MHD accelerator and solved the equations using the same implicit finite-difference method of Patankar and Spalding [6]. The multi-fluid conservation equations of D. Cott [4,5], were formulated for two-dimensional unsteady turbulent flow over a flat plate. The flow variables were expressed as the sum of a mean part and a fluctuating part of the form  $Q = \bar{Q} + Q'$ . The equations were rewritten into divergence form and then averaged over a time interval that is large compared to the fluctuations. Following classical turbulent boundary-layer theory only perturbations of the form  $(\rho v)'Q'$  were retained.

High and Felderman modified the Couette flow curve fits of Ref. [6], given for the global momentum and energy equations, to include the MHD terms in the solutions. For the electron gas, a free molecular sheath was also assumed to exist near the wall. The electron flux from the continuum analysis is matched to the free-molecular flux across the sheath following the derivations of Sherman, et al. [8]. The resulting expressions used were

$$\frac{\mu}{S} \left( \frac{\partial [C_e (1 + T_e/T)]}{\partial y} \right)_w = \rho_w C_{e_w} \sqrt{(\bar{k} T_e / 2\pi m_i)} \quad (1.9)$$

The continuum expression for the flux on the left hand side contains the gradients of  $C_e$  and  $T_e$  whereas the free molecular expression on the right contains the values of  $C_e$  and  $T_e$ . Equating the continuum electron energy flux at the edge of the sheath to the free-molecular energy flux across the sheath yields a second relation





$$\frac{k_e}{C_{p_e}} \left( \frac{\partial h_e}{\partial y} \right)_w + \frac{\mu}{S} (h_e + \epsilon_i) \left( \frac{\partial [C_e (1 + T_e/T)]}{\partial y} \right)_w$$

$$= C_{e_w} \rho_w \left( \frac{2}{5} \right)^{3/2} \left( \frac{8}{\pi} \right)^{1/2} h_{e_w}^{3/2} \left( \frac{\pi m_e}{8 m_i} \right)^{1/2} \left[ 2 - \ln 4 \left( \frac{\pi m_e}{8 m_i} \right)^{1/2} \right] \quad (1.10)$$

where again a relation resulted between the gradient of  $h_e$  and the value of  $h_{e_w}$  at the wall.

For the Couette-flow curve fits of electron energy and concentration the wall flux could be expressed in terms of the dependent variable at the wall by using the boundary conditions of Eqs. (1.9) and (1.10). The equations were then solved by Runge-Kutta methods and curve fit, with the wall values as parameters. These solutions, however, assumed a constant electron current  $j_z^*$  across the Couette layer and the analysis also did not consider any MHD damping of the turbulent fluctuating quantities.

For the case of finite-rate ionization,  $\sigma = \sigma(n_e, T_e)$ , no significant amount of ionization non-equilibrium was observed in the boundary layer except near the wall in the Couette-flow region. A small amount of electron thermal non-equilibrium was observed which, because of the strong dependence of the electrical conductivity on electron temperature, caused significant differences from calculations using thermal equilibrium. Inclusion of the Hall current was also shown to change the boundary layer characteristics substantially.

Sherman, Yeh, Reshotko, and McAssey Jr. [8,9] studied<sup>†</sup> the compressible boundary layer in a plasma which was in electron

---

<sup>†</sup>The author had an opportunity to discuss various aspects of this study with Dr. E. Reshotko while he was a guest speaker at the University of Alberta, Mechanical Engineering Department.



thermal non-equilibrium and in which ionization and recombination occurred also at finite rates. The surface considered was partly an insulator and partly a thermionically emitting electrode. The flow was laminar and a multi-fluid MHD model was assumed. The governing equations were solved using their own finite-difference scheme and results obtained showed that the electron temperature can differ significantly from the heavy particle temperature. The presence of finite rates influenced the electron density considerably. The heat transfer due to electron impact and electron temperature gradient was considerably less than the heat transfer due to heavy particle temperature gradients and was influenced by the magnetic field and the current.

Other related studies of the effects of thermal non-equilibrium and finite-rate ionization are contained in Refs. [10], [11], and [12].

### 1.2.2 MHD Turbulence and Turbulent Flows

A relatively recent text book entitled "MHD-Flows and Turbulence" [13] contains two excellent sections (Part III and IV) on MHD Turbulence, and General Problems of Turbulence. Both theoretical and experimental studies are presented.

An analytical investigation of both developing and fully developed MHD channel flow was the subject of a PhD thesis by Scaglione [14]. The theoretical derivation of Refs. [15] and [16] for a two-fluid model was utilized to describe the turbulent MHD boundary layer. The eddy diffusion of momentum in the near wall



boundary layer was based on a modified mixing-length theory according to Refs. [17], [18] and [19]. In the outer layer the eddy viscosity was based on a modification of the "intermittent eddy-viscosity" based on studies conducted by Klebanoff [20]. Solutions to the developing turbulent MHD boundary layer equations were arrived at by a linearization technique and solved with an implicit finite-difference method developed by Cebeci and Smith [21,22]. Solutions were presented for channel flow Reynolds numbers ranging from  $10^4$  to  $4 \times 10^5$  and for Hartmann numbers from 0 to 1200. Results showed that for the turbulent flow case, the important physical parameters such as displacement thickness, momentum thickness and skin-friction coefficient showed both a strong Hartmann and Reynolds number dependence. The results also exhibited the effect of detransition from turbulent to laminar flow when the ratio of Hartmann number to Reynolds number exceeded  $1/225$ . Asymptotic solutions for fully developed flow showed quite close agreement with experimental data and with similar theoretical analysis of Lykoudis and Brouillette [17,18]. A correlation of the skin-friction coefficient based on a laminar sub-layer and turbulent core model was derived with Reynolds and Hartmann numbers as parameters. This agreed to within 10% of the experimental data of Ref. [17]. The analysis was limited by the assumptions of incompressible flow, electrically non-conducting channel walls, small magnetic Reynolds number, absence of an externally applied electric field, a magnetic field fixed relative to the channel, negligible Hall effects, electrically neutral fluid, steady state flow, and two-dimensional constant-property flow in which only electromagnetic body forces are present.





Experimental measurements of turbulent friction factors of electrically conducting liquids in pipes and the influence of a longitudinally applied magnetic field were reported by Levin and Chinenkov [23]. This was paralleled with a theoretical study by Levin [24], which adopted a similar approach taken by Lykoudis and Brouillette [18] for deriving a first order effect of the MHD body forces on the turbulent velocity fluctuations. Experimental data was obtained for a wide range of Reynolds and Hartmann numbers and results showed that a substantial increase in the Hartmann number compared to those reported in the literature was required to reduce the friction factor by approximately an order of magnitude.

Other relative theoretical studies of MHD turbulent flows and MHD turbulence modeling including mixing-length theories are found in Ref [25], which consider compressible turbulent MHD boundary layers. The work in Ref. [26] showed that the power output of a Hall generator depends strongly on the wall temperature under laminar, fully developed flow conditions, but that this dependence is greatly reduced when the turbulent boundary layer velocity profile was assumed. This would imply a favourable effect of film-cooling on MHD generator performance, since the injection of a secondary coolant fluid results in a turbulent boundary layer downstream from the slot. Moreau [27], applies spectrum tensor analysis and derives spectrum functions and distribution and transfer of energy in wave-number space for Joule dissipation and induced electric field. The study is restricted to the domain of small magnetic Reynolds numbers,  $Re_m \ll 1$ , so that the



fluctuations of the magnetic field are negligible compared with those of the velocity since  $|b| \approx \text{Re}_m |u'| / u$ . A system of equations is presented in Refs. [28,29] for calculating the average and pulsative velocity and temperature characteristics in a turbulent jet of an incompressible conducting liquid in the presence of a longitudinal or transverse magnetic field ( $\text{Re}_m \ll 1$ ). The semi-empirical Kolmogorov relation for the energy dissipation and the Rotta relation for the exchange term were employed as well as employing the gradient representation of the turbulent diffusion. An MHD analogue of the Prandtl formula for the friction stress and the heat flux were derived. The so-called first Prandtl formula, for example, was written as

$$\frac{\tau}{\rho} = - \overline{uv} = \theta_u \frac{r^{3/2} c}{\kappa^3} \ell^2 \left| \frac{\partial u}{\partial y} \right| \frac{\partial u}{\partial y} \quad (1.11)$$

where  $\theta_u$  is a function of the local interaction parameter,  $\alpha(\sigma\beta^2/\rho)/(\partial u/\partial y)$ , with  $\alpha = 1 - \beta$ , where  $\beta$  is assumed to be constant ( $0 < \beta < 1$ ) and must be determined from experiment.

It is also shown that for some limiting value of the local interaction parameter (Stuart number) there is complete suppression of the turbulent motion which in turn precludes turbulent friction. With an increase in Stuart number, the MHD Prandtl number increases and in the limiting case approaches unity.

Further experimental investigations into the effect of electromagnetic fields on turbulence fluctuations are presented in Refs. [30, [31], and [32].



### 1.2.3 OHD Film-Cooling Research and Developments

An excellent review of film-cooling investigations is presented by Goldstein [33]. The general theory and method of analysis is discussed for two- and three-dimensional film-cooling of both incompressible and compressible flows. Also included is a summary of run conditions and geometry details for 40 experimental investigations including those of Wilson [34,35]. The influence of variable free stream velocity, free stream turbulence, film-cooling slot geometry and foreign gas injection on the film-cooling effectiveness and heat transfer are discussed. An in-depth review of three-dimensional film-cooling is also included.

A general review of the Patankar and Spalding numerical solution procedure [2], is presented by Spalding in Ref. [36]. Both the general behaviour of the film-cooling effectiveness,  $\eta$ , and Stanton number,  $ST$ , are analyzed in reference to variations in parameters such as slot geometry, secondary-to-primary gas velocity ratios, free-stream Mach number, coolant composition, etc. The general method of solution evolved from earlier film-cooling investigations at Imperial College, London, such as those conducted by Cole and Spalding [3]. The method has been compared favourably with experimental measurements involving different  $U_C/U_G$ ,  $T_C/T_G$ ,  $\rho_C/\rho_G$  ratios as well as foreign gas injection. Allowance for free-stream turbulence is incorporated into the numerical finite-difference procedure. Further refinements were necessary, however, for the influence of slot lip thickness for which experimental measurements did not support theoretical predictions.



#### 1.2.4 MHD Film-Cooling Research and Developments

It was mentioned earlier that one potential application of film-cooling techniques is for plasma jets and torches. Shiver [37,38] considered film-cooling a plasma torch as a means of improving the overall energy conversion efficiency of the torch. Regenerative cooling methods had been successfully used to cool plasma torches and have produced higher operating efficiency, defined as the ratio of the energy content of the emerging gas stream to the electrical energy input. Torches with transpiration-cooled anodes have produced efficiencies of 80 to 90 percent compared to 50 to 70 percent efficiencies for the conventional water-cooled torch. The work by Shiver represented the first experimental investigation of film-cooling applied to plasma torches. A gas stabilized constricted-arc type torch was constructed with interchangeable water-cooled copper and film-cooled carbon anodes for the use with argon. A shell and tube calorimeter was constructed to determine the energy content of the torch effluent. Tests were conducted with each torch in which arc current and gas flow rate were selected as the operating variables. Two test runs were also made using the film-cooled torch, during which the arc current and primary gas flow rate were maintained constant, while the secondary (coolant) flow was varied.

The results indicated that, for approximately the same total gas flow rate and arc current, the torch equipped with a film-cooled carbon anode was approximately 20 percent more efficient than a fully water-cooled torch. The film-cooled torch efficiency ranged from 80





to 90 percent, while the water-cooled efficiency ranged from 60 to 70 percent for gas flow rates between 0.20 lbs/min. to 0.57 lbs/min. An error analysis indicated that results obtained were correct to within  $\pm 7\%$ .

Theoretical studies of either transpiration or film-cooling applied to MHD flows include those of D'Sa [39], who considered a hydro-magnetic wall jet. The effect of magnetic forces on the laminar wall jet of an electrically conducting, incompressible fluid of constant properties was studied theoretically. The imposed magnetic field was assumed to be uniform and normal to the wall, which could be porous or slotted to allow suction, blowing or tangential injection. The analysis was limited to laminar, incompressible, constant property flows. The Levy-Lees transformation was used and a series expansion was sought about the non-magnetic solution of the transformed boundary layer equations. The required series was constructed in powers of the so called interaction parameter,  $N_x$ , sometimes referred to as the Stuart number, which physically represents the ratio of magnetic to inertial forces. The resulting linear equations were solved using a modified Runge-Kutta method together with Newton-Raphson iteration for three values of the wall blowing (suction) parameter, representing either an impermeable wall, suction or injection.

Luft and Rodkiewicz [40] applied the Karman-Pohlhausen technique to obtain solutions of the MHD boundary layer flow over an insulated flat plate in the presence of a uniform transverse magnetic field and uniformly applied wall suction. Incompressible, constant



property flow was also assumed and a further transformation of variables following the method of Lew (see Ref.[9] of Appendix A) was performed before deriving the integral equation for MHD flate-plate suction flow. Asymptotic MHD-suction profiles were obtained and fully developed boundary layers illustrated for combined Hartmann numbers and suction coefficients. Developing velocity profiles and average skin friction coefficients were derived.

The similarities observed in this investigation between suction and MHD velocity profiles led to the proposed modification of the constant  $A_0^+$  appearing in the laminar sublayer portion of the two-layer eddy viscosity model of turbulence as discussed in Section 3.2 of this thesis. The complete first order analysis of MHD suction boundary layer flow by Luft and Rodkiewicz is presented in Appendix A and is included as part of the present thesis work.

Sych [41] used a variational method to investigate the steady-state flow of a conducting fluid in a straight channel of rectangular cross section with transverse magnetic field when there is forced flow through the side walls. The liquid viscosity was taken into account as well as the conductivity of the channel walls perpendicular to the external magnetic field. Results obtained were used to assess the losses in an MHD generator.

Jain and Mehta [42] presented an exact solution in a closed form for the hydromagnetic equations for an incompressible, viscous, and electrically conducting fluid flow through an annulus with porous walls in the presence of a radial transverse magnetic field. Solutions were reduced to a simpler form by introducing the normal assumption of



$\nu/\nu_H \ll 1$  ie. low Magnetic Reynolds number, and the pressure distribution was discussed for this case. The analysis was also extended to include parallel MHD Couette flow.

The present work investigates the adiabatic film-cooling effectiveness of film-cooling the insulator (B) wall of both an MHD equilibrium Faraday generator and an MHD non-equilibrium Faraday generator. Turbulent 2-D flow, including the damping of turbulent fluctuations by the electromagnetic fields is considered allowing for plasma electron thermal non-equilibrium and finite-rate ionization. The implicit finite-difference method of Patankar and Spalding [2] is modified in a general way to allow MHD flow calculations. On the basis of the literature review presented here, such a film-cooling investigation has not been undertaken before. Additional research papers consulted in preparation of this thesis are found in Refs. [43] to [58] inclusive.





## CHAPTER II

### THEORETICAL DEVELOPMENT

#### 2.1 Boundary Layer Equations

The development of the equations of motion for a two-dimensional, turbulent, non-equilibrium plasma flow in an MHD duct follows closely the derivation of their laminar counterpart given in detail in Ref.[4]. The classical derivation is performed where the variables are expressed as the sum of a mean part and a fluctuating part after which the equations are averaged over a time interval which is large compared to the period of the fluctuations. The mixing-length concept is used to affect closure of the system of equations and only the boundary layer on the B-wall (insulator wall) is considered. With reference to the coordinate system shown in Fig 2.1, the following equations can be shown to be identical with those given in Ref.[7].

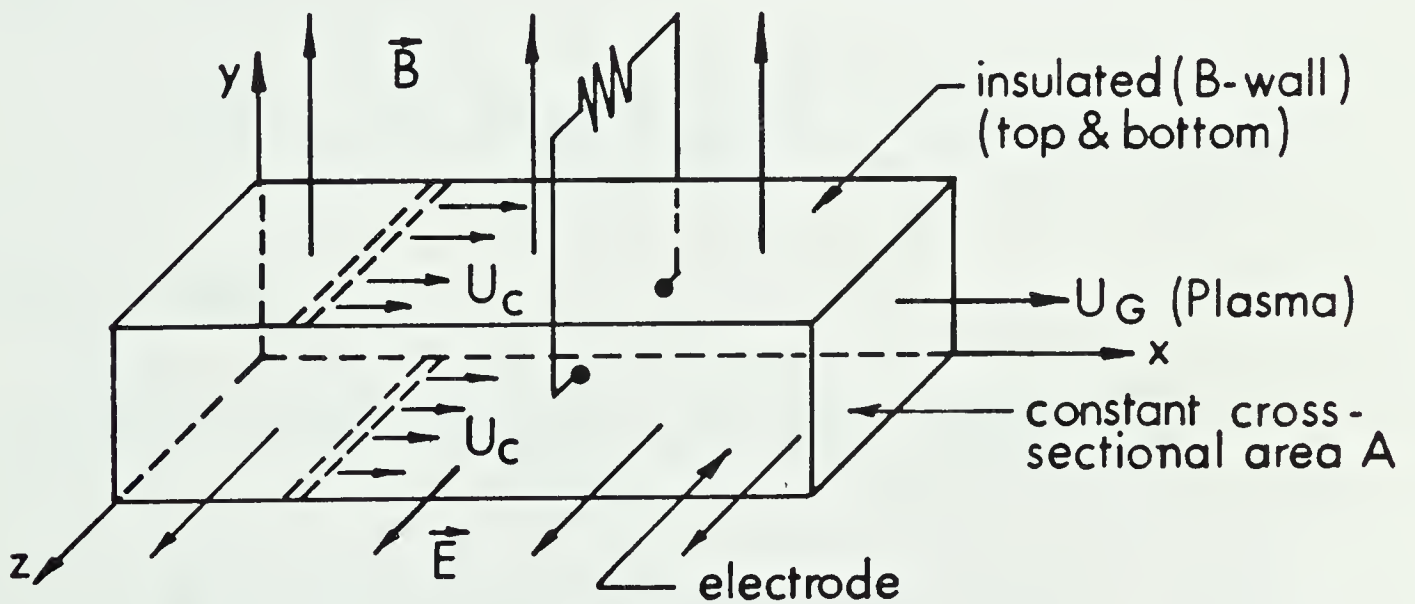


Fig. 2.1 Schematic of MHD-Channel Co-ordinate System



## Overall Continuity

$$\frac{\partial(\rho u)}{\partial x} + \frac{\partial(\rho v)}{\partial y} = 0 \quad (2.1)$$

## Overall Momentum

$$\rho u \frac{\partial u}{\partial x} + \rho v \frac{\partial u}{\partial y} = \frac{\partial}{\partial y} (\mu_{eff} \frac{\partial u}{\partial y}) - (\frac{\partial p}{\partial x} + j e_z B_y) \quad (2.2)$$

## Overall Energy

$$\begin{aligned} \rho u \frac{\partial H}{\partial x} + \rho v \frac{\partial H}{\partial y} &= \frac{\partial}{\partial y} \left( \left( \frac{\mu}{P_r} + \frac{\epsilon}{P_t} \right) \frac{\partial H}{\partial y} \right) \\ &+ \frac{\partial}{\partial y} \left( \left[ \epsilon \left( 1 - \frac{1}{P_t} \right) + \mu \left( 1 - \frac{1}{P_r} \right) \right] \frac{\partial}{\partial y} \left( \frac{u^2}{2} \right) \right) \\ &+ \frac{\partial}{\partial y} \left( \frac{\mu}{S} h_e \frac{\partial}{\partial y} [C_e (1 + T_e/T)] - \left( \frac{\mu}{P_r} + \frac{\epsilon}{P_t} \right) h_e \frac{\partial C_e}{\partial y} + \frac{\epsilon}{S_t} h_e \frac{\partial C_e}{\partial y} \right) \\ &+ j e_z E_z + j e_x E_x \end{aligned} \quad (2.3)$$

## Electron Conservation

$$\rho u \frac{\partial C_e}{\partial x} + \rho v \frac{\partial C_e}{\partial y} = \frac{\partial}{\partial y} \left( \frac{\mu}{S} \frac{\partial C_e (1 + T_e/T)}{\partial y} + \frac{\epsilon}{S_t} \frac{\partial C_e}{\partial y} \right) + \dot{w}_e \quad (2.4)$$

## Electron Energy

$$\begin{aligned} \rho u \frac{\partial C_e h_e}{\partial x} + \rho v \frac{\partial C_e h_e}{\partial y} &= \frac{\partial}{\partial y} \left( \frac{k_e}{C_e C_{p_e}} + \frac{\epsilon_t}{P_t} \right) \frac{\partial C_e h_e}{\partial y} - \frac{\partial}{\partial y} \left( \frac{k_e T_e}{C_e} \frac{\partial C_e}{\partial y} \right) \\ &+ \frac{\partial}{\partial y} \left( \frac{\mu}{S} h_e \frac{\partial}{\partial y} C_e (1 + T_e/T) \right) - \epsilon_i \dot{w}_e + j e_z E_z + j e_x E_x \\ &+ \frac{3}{2} \frac{\bar{k}_e^2 \rho^2}{m_e} \frac{C_e^2}{\sigma_0} \delta_{eff} (T - T_e) \end{aligned} \quad (2.5)$$



## Electron Momentum (Ohm's Law)

$$\begin{aligned}
 j e_z &= \frac{\sigma_e}{1+\beta^2} \left( (E_z + uB) - \beta E_x \right) \\
 j e_x &= \frac{\sigma_e}{1+\beta^2} \left( E_x + \beta(E_z + uB) \right)
 \end{aligned}
 \tag{2.6}$$

Equations (2.1) to (2.3) represent the conservation equations of the heavy species, namely, the nitrogen carrier gas and the potassium seed neutrals and ions. In addition to the conventional boundary layer terms the equations include terms which represent the MHD body force, Joule dissipation, transport of energy by ion and electron diffusion, and heat conduction due to the presence of electron temperature gradients.

Equations (2.4) and (2.5) describe the "electron gas" and included are terms which represent finite-rate ionization-recombination, electron diffusion, energy transport due to electron diffusion, electron temperature gradients, electron production, Joule dissipation and collisional energy losses.

When considering equilibrium ionization, Eq. (2.4) is not used and the electron mass fraction,  $C_e$ , is computed from the Saha relation<sup>†</sup>

$$C_e^* = n_e^* m_e / \rho$$

$$\text{where } n_e^* = (K_s/2) \left[ \sqrt{(1 + \psi_1 SF) - 1} \right] \tag{2.7}$$

$$\psi_1 = 4p/K_s \bar{k}T \tag{2.8}$$

---

<sup>†</sup>Saha, M.N., Philos. Mag., 40, pp. 472 (1920)



$$K_s = \frac{n_i n_e^*}{n_K} = \left( \frac{2\pi m_e \bar{k}T_e}{h^2} \right)^{3/2} Z_{rs} e^{-e\epsilon_i/\bar{k}T_e} \quad (2.9)$$

and the partition function can be approximated by

$$Z_{rs} = 9.115 \times 10^{-1} + 7.33 \times 10^{-5}T - 1.49 \times 10^{-8}T^2 \quad (2.10)$$

(T ≤ 6000°K)

or

$$Z_{rs} = \frac{3.91}{e^{2.895} \times 10^{-4} T - 1} \quad (T > 6000^\circ\text{K})$$

For the case of finite-rate or frozen ionization the mass fraction is obtained from the solution of Eq. (2.5) and the electron production term  $\dot{w}_e$  is approximated by an empirical expression given in Ref. [5].

$$\dot{w}_e = 3.47 \times 10^{-20} T_e^{-4.765} \frac{\rho^3 C_e}{m_e^2} \left[ \left( \frac{C_e^2}{C_K} \right)^* \left( SF - \frac{m_K C_e}{m_e} \right) - C_e^2 \right] \quad (2.11)$$

## 2.2 Molecular Transport Properties

The molecular transport properties required in the governing equations are the viscosity of the gas, the electron thermal conductivity and the electrical conductivity of the gas. Sutherland's viscosity law is used to prescribe the laminar viscosity of the carrier gas

$$\mu = 1.086 \times 10^{-6} T^{3/2} / (T + 100^\circ\text{K}) \text{ N}\cdot\text{sec}/\text{m}^2$$

Other properties have been taken from Ref. [5]. The electron thermal conductivity is obtained from





$$k_e = \left( \frac{e\bar{k}}{m_e} \frac{n_e}{v_0} \right)^2 T_e \left( \frac{1}{\sigma_0} - \frac{1}{\sigma_e} \right) \quad (2.12)$$

where  $v_0$  and  $T_0$  are defined in Refs. [4,59]. The electrical conductivity is given by the expression

$$\sigma_e = \frac{3}{4} \frac{e^2 n_e}{\sqrt{\left(\frac{8m_e \bar{k} T}{\pi}\right)} (1-\Delta') \sum_{s \neq e} n_s Q_{es}} = \frac{\sigma_0}{1-\Delta'} \quad (2.13)$$

with the electron-electron interaction correction given by

$$\Delta' = \frac{2.5 \left( \sum_{s \neq e} A_{es}^{(2)} n_s Q_{es} \right)^2 / \sum_{s \neq e} n_s Q_{es}}{\frac{2\sqrt{2}}{5} \left[ 1 - (2 \ln \Lambda)^{-1} \right] n_e Q_{ei} + \sum_{s \neq e} A_{es}^{(5)} n_s Q_{es}} \quad (2.14)$$

where the expressions for  $A_{es}^{(2)}$ ,  $A_{es}^{(5)}$ ,  $\Lambda$ ,  $Q_{ei}$  are defined in Ref.[60].

The equation of state as used in Ref.[5] is

$$p = \rho Z R T \quad \text{and} \quad p_s = \frac{\bar{k}}{m_s} \rho C_s T_s \quad (2.15)$$

with

$$Z = 1 + 276.6 \left( \frac{3.661 \times 10^{-3} T}{p} \right)^{0.4964} \exp(-55831/T) \quad (2.16)$$

and

$$\begin{aligned} C_p/R = & 3.5 + 1.514 \times 10^{-5} T + \left( \frac{\theta_v/T}{\exp(\theta_v/T) - 1} \right)^2 \exp(\theta_v/T) \\ & + (Z-1) \left[ 1 + (T + 1.125 \times 10^5) \times \left( \frac{0.4964}{T} + \frac{55831}{T^2} \right) \right] \end{aligned} \quad (2.17)$$



where  $T$  is in  $^{\circ}\text{K}$  and  $p$  is in atmospheres.

The collisional energy term in Eq. (2.5) (last term) is derived from the expression  $3\bar{k}C_e \rho \sum_{s \neq e} \frac{\delta_s}{m_s} v_{es}^* (T_s - T_e)$  as is shown in detail in Ref.[4] where  $\delta_s$  is the fractional energy loss during an inelastic collision of an electron with specie "s" ( $\delta_{\text{elastic}}=1$ ) and these inelastic losses are lumped into one term,  $\delta_{\text{eff}}$ , defined by Ref. [61].

$$\delta_{\text{eff}} = \sum_{s \neq e} \frac{2m_e/m_s \delta_s v_{es}^*}{\sum_s v_{es}^*} \quad (2.18)$$

Experiments performed in Ref.[62] indicate that for the nitrogen background gas ( $\delta_{\text{N}_2} = 18$ ) considered here,  $\delta_{\text{eff}}$  remains more or less constant at  $7 \times 10^{-4}$  for  $\text{N}_2$  temperatures in the range of  $2800^{\circ}\text{K}$  to  $5000^{\circ}\text{K}$ . In contrast, for air, Ref.[7] gives  $\delta_{\text{eff}} = 2.93 \times 10^{-3}$  which corresponds to a  $\delta_{\text{air}}$  of about 150. Needless to say, the properties of actual combustion gases in real MHD generator installations must be accurately established before a meaningful comparison between the theory and experiment can be made.

The Prandtl and Schmidt numbers were assumed to be equal with the laminar values of 0.7 and their turbulent counterpart assigned the values of 0.9.

### 2.3 Boundary Conditions

The dependent variables in Eqs. (2.1) to (2.6) must be specified at the channel insulator wall, in the free stream, and at the film-cooling slot exit to begin the integration.



Boundary values at the wall for velocity and enthalpy are:  $u=v=0$  and  $\frac{\partial H}{\partial y} \Big|_w = 0$ . For the electron mass,  $C_{e,w}$ , an electron sheath analysis is performed following the procedure of Sherman, et al. [8,9]. A collisionless free molecular sheath is assumed to exist at the wall and the electron flux across the sheath is matched with the continuum electron flux at the edge of the sheath resulting in [7]:

$$\frac{\mu}{S} \left( \frac{\partial [C_e (1+T_e/T)]}{\partial y} \right) \Big|_w = \rho_w C_{e,w} \sqrt{\frac{\bar{k} T_{e,w}}{m_i}} \quad (2.19)$$

A similar analysis for the electron energy flux results in

$$\begin{aligned} \frac{k_e}{C_{p_e}} \left( \frac{\partial h_e}{\partial y} \right) \Big|_w + \frac{\mu}{S} (h_e + \epsilon_i) \left( \frac{\partial [C_e (1+T_e/T)]}{\partial y} \right) \Big|_w = \\ C_{e,w} \rho_w \left( \frac{2}{5} \right)^{3/2} \sqrt{\left( \frac{8}{\pi} \right)} h_{e,w}^{3/2} \sqrt{\left( \frac{\pi m_e}{8 m_i} \right)} (2 - \ln 4) \sqrt{\frac{\pi m_e}{8 m_i}} \end{aligned} \quad (2.20)$$

Equations (2.19) and (2.20) serve as mixed boundary conditions for the electron mass fraction  $C_e$  and electron enthalpy  $h_e$ , respectively, for the case of frozen and finite-rate ionization-recombination. When equilibrium ionization-recombination is considered, Eq. (2.20) only is used as boundary condition for  $h_e$  from which  $C_e$  can be evaluated using the Saha equilibrium relationship.

The electric and magnetic field parameters  $E_z$  and  $B$  are specified independently and are assumed constant across the generator duct. Actually  $E_z$  is calculated from a given load parameter  $K_L$  (often referred to as either a generator or a pump coefficient) defined by

$$K_L = \pm \frac{E_z}{BU_G} = \frac{\text{applied electric field}}{\text{induced electric field}} \quad (2.21)$$





where the sign of  $K_L$  is positive when  $E_z$  is in the same direction as the induced field (accelerator mode) and negative when  $E_z$  is directed opposite to  $BU_G$  as in the case of a generator. According to a study by Swift-Hook and Wright [63], an optimum generator design is achieved when  $|K_L| \approx .75$  and this is the value prescribed at the film-cooling slot exit. With an appropriate variation in the external load resistance,  $E_z$  can be kept constant by allowing  $K_L$  to vary as  $U_G$  with downstream distance,  $x$ .

The effects of Hall currents can be assessed by setting  $E_x=0$  and by applying an electric field  $E_x$  such that the free stream only is Hall neutralized ( $je_{x,G}=0$ ) with  $E_x$  calculated from Eq. (2.6) evaluated in the free stream. When Hall currents are precluded or neglected then  $je_x=0$  everywhere.

The free stream boundary conditions are specified from the solution of the one-dimensional core-flow equations which may be obtained from Eqs. (2.1) to (2.6) by dropping all transverse gradient terms. Furthermore, previous investigation of non-equilibrium plasma channel flows [5,7], indicate that the core gas is essentially in ionization-recombination equilibrium so that the electron number density or mass fraction can be calculated from the Saha equilibrium relations, Eqs. (2.7) to (2.10), based on the free stream electron temperature,  $T_{eG}$ .

The resulting equations are then

$$\rho_G U_G A = \dot{m} = \text{constant mass flow} \quad (2.22)$$



$$\rho_G U_G \frac{dU_G}{dx} = - \left( \frac{\partial p}{\partial x} + j_{e_{x,G}} B \right) \quad (2.23)$$

$$\rho_G U_G \frac{dH_G}{dx} = j_{e_{z,G}} E_z + j_{e_{x,G}} E_x \quad (2.24)$$

$$\rho_G U_G \frac{d}{dx} (C_e^* h_e)_G = j_{e_{z,G}} E_z + j_{e_{x,G}} E_x + \frac{3}{2} \frac{\bar{k}_e^2 \rho_G^2 C_e^{*2}}{m_e^3 \sigma_0} \delta_{eff} (T - T_e) \quad (2.25)$$

$$j_{e_{z,G}} = \sigma_{e,G} U_G B (1 + K_L) \quad (2.26)$$

$$p_G = Z \rho_G R T_G \quad (2.27)$$

Since there are only six equations with nine unknowns, namely  $\rho_G$ ,  $p_G$ ,  $U_G$ ,  $H_G$ ,  $j_{e_{z,G}}$ ,  $h_{e,G}$ ,  $A$ ,  $B$ , and  $E_z$  (or  $K_L$ ) three of these must be specified independently. Cott [4,5] specifies  $T_G$ ,  $j_{e_{z,G}}$ , and  $B$  whereas High and Felderman [7] specify  $h_G$ ,  $E_z$ , and  $B$ . A constant area duct is considered here so that  $A$ ,  $B$ , and  $E_z$  (or  $K_L$ ) have been assigned independently.

Numerous solutions for one-dimensional constant area non-equilibrium generators have been presented by Heighway and Nichols, [10] for both supersonic and subsonic velocities and a typical solution providing the outer boundary conditions is depicted in Fig 2.2.



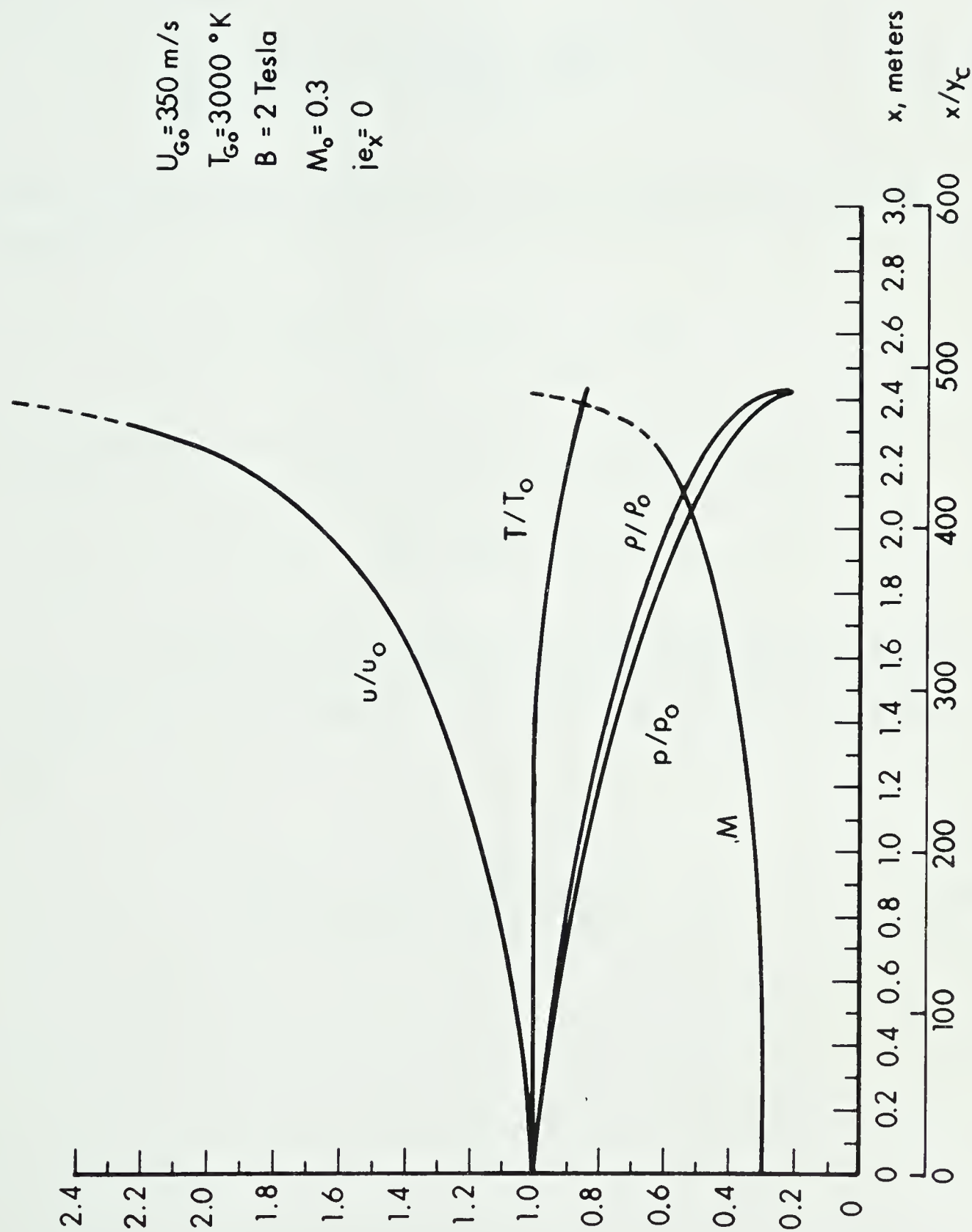


Fig. 2.2 Typical MHD 1-D Core Flow Solutions, Equilibrium Case



## 2.4 Calculation of Axial Flow Variables

Downstream pressure is calculated in accordance with Patankar and Spalding's procedure for handling confined flows [2] using the plug-flow formula<sup>†</sup>

$$\frac{dp}{dx} = - \frac{\frac{F'}{A} - \frac{2\bar{u}}{A} \frac{d\dot{m}}{dx} - \frac{\dot{m}\bar{u}}{A\bar{T}} \frac{d\bar{T}}{dx}}{1 - \dot{m}\bar{u}/Ap} \quad (2.28)$$

where  $\bar{T}$  is an average temperature,  $\bar{u}$  is the mass-average velocity defined by

$$\bar{u} = \int_{\text{duct}} \rho u^2 dy / \int_{\text{duct}} \rho u dy$$

and the retarding force per unit duct length  $F'/A$  is given by

$$\frac{2\tau_w}{h} + j e_z B$$

Once the pressure gradient has been obtained from Eq.(2.28) the downstream local enthalpy in the core flow may then be evaluated from

$$\frac{dh_G}{dx} = \frac{1}{\rho_G} \frac{dp}{dx} + \frac{j e_{z,G}}{\rho_G} (K_L + 1) B \quad (2.29)$$

---

<sup>†</sup> A misprint in Ref. [2] is noted here in the denominator which is incorrectly written as  $1 - \dot{m}\bar{u}/A\bar{p}$





Previous investigations by Cott [4,5] and High and Felderman [7], showed that ionizational equilibrium exists in the core flow so that the downstream electron enthalpy can be determined from

$$\frac{dh_{eG}}{dx} = \frac{K_L B j_{e,z,G}}{\rho_G C_{eG}} + \frac{eB(K_L+1)}{m_e} \beta_G + \frac{3}{2} \frac{\bar{k}_e^2}{m_e^3 \sigma_0} \frac{\delta_{eff} \rho_G C_{eG}}{U_G} (T_G - T_{eG}) \quad (2.30)$$

and the downstream electron mass fraction can then be computed from the Saha relation using the electron enthalpy computed from Eq. (2.30).

## 2.5 Initial Conditions

The velocity profile shown in Fig. 2.3, at the slot exit is based on a power-law variation of  $u$  with  $y$  and is one of several profiles considered by Cole and Spalding [3] in their work to assess, along with other parameters, the influence of different initial profiles on the theoretical prediction of the film-cooling effectiveness. It is essentially a power-law profile prescribed as follows:

$$\text{For } \delta_w \quad u/U_c = (y/\delta_w)^{n_w} \quad (2.31)$$

$$\text{For } \delta_L \quad (u-U_L)/(U_C-U_L) = \left[ (y_C-y)/\delta_L \right]^{n_L} \quad (2.32)$$

$$\text{For } \delta_G \quad (u-U_L)/(U_G-U_L) = \left[ (y-y_C-t_L)/\delta_G \right]^{n_G} \quad (2.33)$$



To define the initial velocity profile, therefore, the quantities  $U_C$ ,  $U_L$ ,  $U_G$ ,  $\delta_L$ ,  $\delta_G$ ,  $\delta_w$ ,  $n_w$ ,  $n_L$ , and  $n_G$  must be specified. The initial thickness of the boundary layer,  $y_G$ , identifies the grid line  $\omega = 1$ , which defines the outer edge of the layer as it develops downstream. The inner edge of the layer at  $y = 0$ , coincides with the film-cooled wall where the grid line has the value  $\omega = 0$ .

Initial gas and electron temperature profiles were assumed equal and uniform across the slot and in the free stream and varying linearly across the slot lip. Hence for

$$0 \leq y < y_C : T_C = \text{constant} \quad (2.34)$$

$$y_C \leq y < (y_C + t_L) : (T - T_C) / (T_G - T_C) = (y - y_C) / t_L \quad (2.35)$$

$$y \geq (y_C + t_L) : T_G = \text{constant} \quad (2.36)$$

Finally, the electron mass fraction,  $C_e$ , was calculated assuming ionizational equilibrium from Eq. (2.7). Thermal and ionizational equilibrium are assumed in defining initial boundary layer profiles for both equilibrium and non-equilibrium MHD flows considered in this work.

Because of numerical computation problems experienced by assuming a step function for the magnetic field parameter  $B$  (from 0 to  $B = \text{constant}$  at  $x/y_C = 0$ ), the initial value for  $B$  was applied as a



linear function of  $x$  until a finite value of  $x/y_c$  was reached, after which  $B$  remained constant with  $x$ . The effect of choosing different values of  $x/y_c$  at which  $B$  becomes a constant is assessed and discussed in Section 5.3.4. Typical values of  $x/y_c$  assigned were 20, 10, and 1, where the smaller value of  $x/y_c$  approaches closer to a step function for  $B(x)$ .

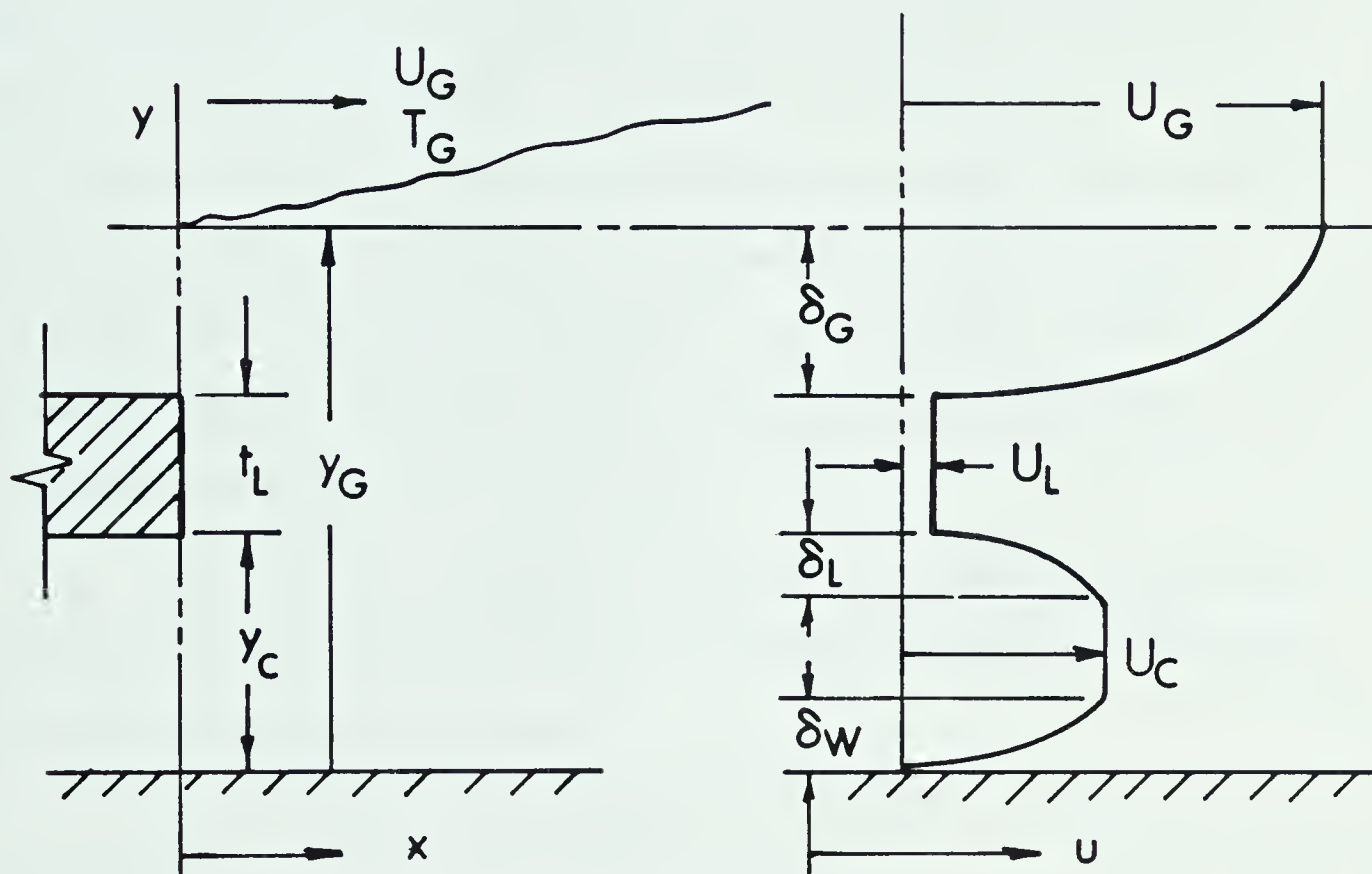


Fig. 2.3 Initial Velocity Flow Model Assumed in Present Work



# CHAPTER III

## SOLUTIONS TO THE GOVERNING EQUATIONS

### 3.1 Numerical Solution Procedure

The numerical method adopted here to solve the MHD boundary layer equations is that of Patankar and Spalding first described in detail in Refs. [2] and [6]. Its particular application to the OHD film-cooling process is described in generality in Ref. [64] and a specific application to evaluate the effects of such parameters as slot lip thickness, free-stream turbulence, initial velocity profiles, free-stream to slot velocity ratios etc. on theoretical film-cooling predictions is demonstrated in Ref. [3].

The Patankar-Spalding formulation transforms the governing equations from the Cartesian to the Von Mises coordinate system with the change of variables defined by:

$$\xi = x, \psi = \int \rho u dy$$

such that

$$\frac{\partial}{\partial x} = \frac{\partial}{\partial \xi} - \frac{v}{u} \frac{\partial}{\partial y}, \quad \frac{\partial}{\partial y} = \rho u \frac{\partial}{\partial \psi} \quad (3.1)$$

The transformed momentum equation (2.2), for example, is then readily developed by substitution of (3.1) to obtain

$$\rho u \left( \frac{\partial u}{\partial \xi} - \frac{v}{u} \frac{\partial u}{\partial y} \right) + \rho v \frac{\partial u}{\partial y} = - \left( \frac{\partial p}{\partial \xi} - \frac{v}{u} \frac{\partial p}{\partial y} + j e_z B_y \right) + \rho u \frac{\partial}{\partial \psi} \left( \mu_{\text{eff}} \rho u \frac{\partial u}{\partial \psi} \right) \quad (3.2)$$





Replacing  $\xi$  by  $x$  after having performed the differentiation and rearranging, Eq. (3.2) becomes

$$\frac{\partial u}{\partial x} = \frac{\partial}{\partial \psi} \left( \mu_{\text{eff}} \rho u \frac{\partial u}{\partial \psi} \right) - \frac{1}{\rho u} \left( \frac{\partial p}{\partial x} + j e_z B_y \right) \quad (3.3)$$

The  $x - \psi$  grid is next confined to the boundary layer region only, by a non-dimensionalizing of Eq.(3.3) with respect to  $\psi$  by defining a dimensionless stream function

$$\omega = \frac{\psi - \psi_I}{\psi_E - \psi_I} \quad (3.4)$$

where  $\psi_I$  and  $\psi_E$  are the values of the stream functions at the inner and outer boundaries respectively. The effect is a grid which grows along with the boundary layer in a continuous manner and a cross-stream variable which varies always between zero and unity.

The momentum equation (3.3) in terms of  $x$  and  $\omega$  then becomes

$$\frac{\partial u}{\partial x} + \left( \frac{\dot{m}_I'' + \omega(\dot{m}_E'' - \dot{m}_I'')}{\psi_E - \psi_I} \right) \frac{\partial u}{\partial \omega} = \frac{\partial}{\partial \omega} \left( \frac{\mu_{\text{eff}} \rho u}{(\psi_E - \psi_I)^2} \frac{\partial u}{\partial \omega} \right) - \frac{1}{\rho u} \left( \frac{\partial p}{\partial x} + j e_z B_y \right) \quad (3.5)$$

For the sake of completeness, the remaining boundary layer equations (i.e. Eqs. (2.3) through (2.5)) in terms of  $x$  and  $\omega$  are written as follows:

Overall Energy

$$\frac{\partial H}{\partial x} + \left( \frac{\dot{m}_I'' + \omega(\dot{m}_E'' - \dot{m}_I'')}{\psi_E - \psi_I} \right) \frac{\partial H}{\partial \omega} = \frac{\partial}{\partial \omega} \left( \frac{\rho u \mu_{\text{eff},H}}{(\psi_E - \psi_I)^2 \sigma_{\text{eff},H}} \frac{\partial H}{\partial \omega} \right)$$



$$\begin{aligned}
& + \frac{\partial}{\partial \omega} \left[ \frac{\rho u \mu_{\text{eff,H}}}{(\psi_E - \psi_I)^2} \left( 1 - \frac{1}{\sigma_{\text{eff,H}}} \right) \frac{\partial}{\partial \omega} \left( \frac{u^2}{2} \right) + \frac{\rho u h_e}{(\psi_E - \psi_I)^2} \left( \frac{\mu_{\text{eff,C}_e}}{\sigma_{\text{eff,C}_e}} - \frac{\mu_{\text{eff,H}}}{\sigma_{\text{eff,H}}} \right) \frac{\partial C_e}{\partial \omega} \right. \\
& \quad \left. + \frac{\mu}{S} \frac{\rho u h_e}{(\psi_E - \psi_I)^2} \frac{\partial}{\partial \omega} \left( \frac{T_e}{T} \right) \right] + \frac{j e_x E_x + j e_z E_z}{\rho u} \quad (3.6)
\end{aligned}$$

where

$$\frac{\mu_{\text{eff,C}_e}}{\sigma_{\text{eff,C}_e}} = \frac{\mu}{S} \left( 1 + \frac{T_e}{T} \right) + \frac{\epsilon}{S_t} \quad (3.7)$$

$$\frac{\mu_{\text{eff,H}}}{\sigma_{\text{eff,H}}} = \frac{\mu}{P_r} + \frac{\epsilon}{P_t} \quad (3.8)$$

Electron Conservation

$$\begin{aligned}
\frac{\partial C_e}{\partial x} + \left( \frac{\dot{m}_I'' + \omega(\dot{m}_E'' - \dot{m}_I'')}{\psi_E - \psi_I} \right) \frac{\partial C_e}{\partial \omega} &= \frac{\partial}{\partial \omega} \left( \frac{\rho u}{(\psi_E - \psi_I)^2} \frac{\mu_{\text{eff,C}_e}}{\sigma_{\text{eff,C}_e}} \frac{\partial C_e}{\partial \omega} \right) \\
&+ \frac{\dot{w}_e}{\rho u} + \frac{\partial}{\partial \omega} \left( \frac{\rho u}{(\psi_E - \psi_I)^2} C_e \frac{\mu}{S} \frac{\partial}{\partial \omega} \left( \frac{T_e}{T} \right) \right) \quad (3.9)
\end{aligned}$$

Electron Energy

$$\begin{aligned}
\frac{\partial C_e h_e}{\partial x} + \left( \frac{\dot{m}_I'' + \omega(\dot{m}_E'' - \dot{m}_I'')}{\psi_E - \psi_I} \right) \frac{\partial C_e h_e}{\partial \omega} &= \frac{\partial}{\partial \omega} \left( \frac{\rho u}{(\psi_E - \psi_I)^2} \frac{\mu_{\text{eff,e}}}{\sigma_{\text{eff,e}}} \frac{\partial C_e h_e}{\partial \omega} \right) \\
&+ \frac{\partial}{\partial \omega} \left( h_e \frac{\mu}{S} \frac{\rho u}{(\psi_E - \psi_I)^2} \frac{\partial}{\partial \omega} \left( C_e \left( 1 + \frac{T_e}{T} \right) \right) - \frac{k_e T_e}{C_e} \frac{\rho u}{(\psi_E - \psi_I)^2} \frac{\partial C_e}{\partial \omega} \right) \\
&- \frac{\dot{w}_e \epsilon_i}{\rho u} + \frac{E_z j e_z + E_x j e_x}{\rho u} + \frac{e C_e}{m_e} \left( \frac{j e_x}{\sigma_o} - E_x \right) + \frac{3}{2} \frac{\bar{k} e^2 \rho C_e^2 \delta_{\text{eff}}}{m_e^3 \sigma_o u} (T - T_e) \quad (3.10)
\end{aligned}$$



where

$$\frac{\mu_{eff,e}}{\sigma_{eff,e}} = \frac{k_e}{c_{p_e} c_e} + \frac{\varepsilon}{P_t} \quad (3.11)$$

These equations share the common form

$$\frac{\partial \phi}{\partial x} + (a+b\omega) \frac{\partial \phi}{\partial \omega} = \frac{\partial}{\partial \omega} \left( c \frac{\partial \phi}{\partial \omega} \right) + d \quad (3.12)$$

with convection terms on the left, conduction terms first on the right and all other terms not involving  $\frac{\partial \phi}{\partial \omega}$  lumped into one source term "d".

The terms  $\dot{m}_I''$  and  $\dot{m}_E''$  defined by  $\frac{d\psi_I}{dx} = -\dot{m}_I''$  and  $\frac{d\psi_E}{dx} = -\dot{m}_E''$  represent the rates of mass transfer across the I and E boundaries. At a line of symmetry the mass-transfer rate is zero while at a wall the mass flux is derived from given boundary conditions. When the E boundary corresponds to the "edge" of a boundary layer, as in the problem considered here, an expression for  $\dot{m}_E''$  ( $\equiv \dot{m}_G''$ ) must be derived to determine the amount of mass entrained by the boundary layer at its junction with the free stream. The momentum equation (2.2) in the free stream reduces to

$$\rho u \frac{\partial u}{\partial x} = - \left( \frac{\partial p}{\partial x} + j e_z B_y \right) \quad (3.13)$$

Since in the limit as  $y$  approaches  $y_G$ , expression (3.13) must also hold true just inside the G boundary, substitution back into the momentum equation yields the desired expression for the entrainment rate

$$\dot{m}_G'' = \lim_{y \rightarrow y_G} \left( \frac{\frac{\partial}{\partial y} \left( \mu_{eff} \frac{\partial u}{\partial y} \right)}{\partial u / \partial y} \right) \quad (3.14)$$



This limit will exist and be finite if the mixing-length concept is employed since  $\mu_{\text{eff}}$  will vanish simultaneously as  $\partial u / \partial y$  approaches zero. For example, substitution of Prandtl's mixing-length hypothesis  $\mu_{\text{eff}} = \rho \ell^2 \left| \frac{\partial u}{\partial y} \right|$  into expression (3.14) yields for the entrainment rate

$$m_G'' = \lim_{y \rightarrow y_G} \left( 2\rho \ell^2 \frac{\partial^2 u}{\partial y^2} \right) \quad (3.15)$$

It is perhaps worth noting at this point that film-cooling mathematical computational-techniques employing a simple mixing-length, eddy-viscosity hypothesis have been shown to be capable of correctly describing the trends and magnitudes of important properties of wall-jet and wall-wake flows. Additional references include the work of Kacker and Whitelaw [65] who employed the Prandtl-Kolmogorov model of turbulence with a simple empirical expression for the length scale to obtain satisfactory predictions over a wide range of film-cooling flow situations.

### 3.2 MHD Modifications to Effective Viscosity Hypothesis

The effective viscosity hypothesis assumes that in the expression for the effective shear stress  $\tau_{\text{eff}} = \mu_{\text{eff}} \frac{\partial \bar{u}}{\partial y}$ ,  $\mu_{\text{eff}}$  is composed of a laminar viscosity  $\mu$  plus an eddy viscosity which, upon the adoption of Prandtl's mixing-length theory, may be written as<sup>†</sup>

$$\epsilon = \rho \ell^2 \left| \partial u / \partial y \right| \quad (3.16)$$

Various empirical relations have been derived for the mixing-length " $\ell$ " and many of these can be expressed by the general form

---

<sup>†</sup>Often Klebanoff's intermittency factor  $\Gamma$  is included in the expression for  $\epsilon$  for the region away from the wall, but it will be assumed unity here.





$$\ell = Dy_\ell f(x, y/y_\ell) \quad (3.17)$$

where "D" is a general damping function which is zero at the wall and equal to unity at large distances from the wall, " $y_\ell$ " is some characteristic thickness of the boundary layer and "f" is some function which permits the mixing-length to vary with downstream and cross-stream directions.

Several models for " $\ell$ " have been proposed for the region near a film-cooling slot and attempts to account for the effects of relaxation or slot-lip thickness for example have resulted in fairly accurate predictions by a judicious choice of the function "f" and appropriate modifications of the effective diffusivity profiles near the slot exit. In Ref.[66] a bridging technique is employed as shown in Fig.3.1 to preclude the unrealistic occurrence of a vanishing diffusivity at points of velocity extremum. In Ref.[67] further modifications are imposed on the bridged profile to represent the effect of slot lip thickness in the form of an "additive" diffusivity also shown in Fig.3.1.

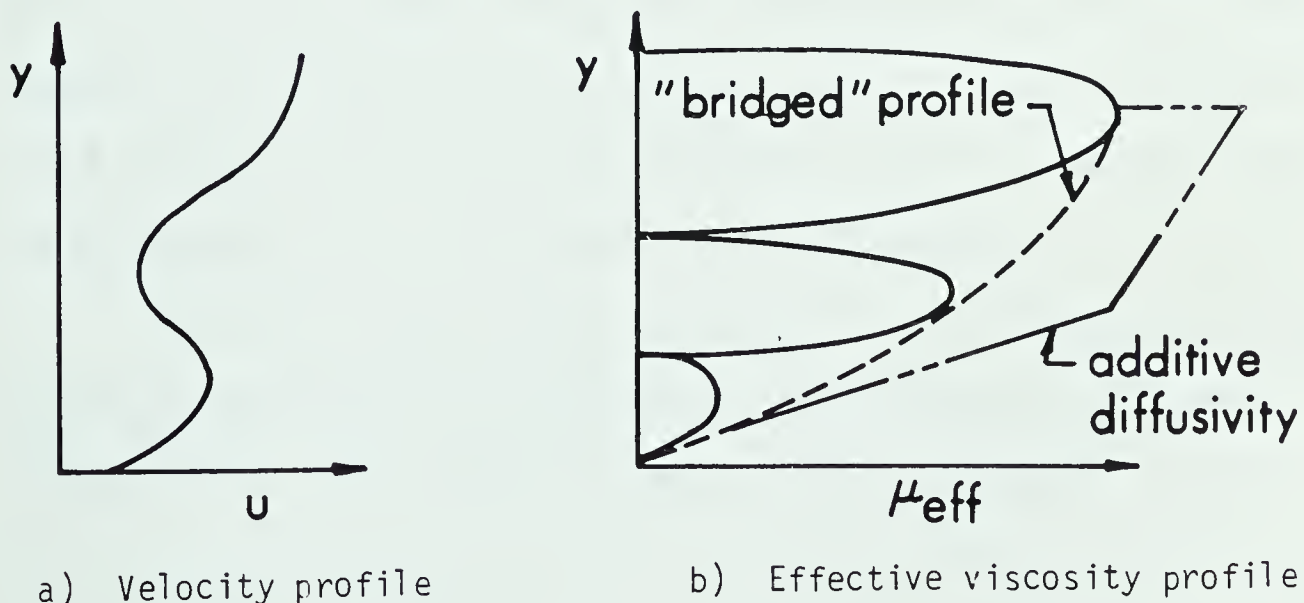


Fig. 3.1 Bridging technique for effective viscosity



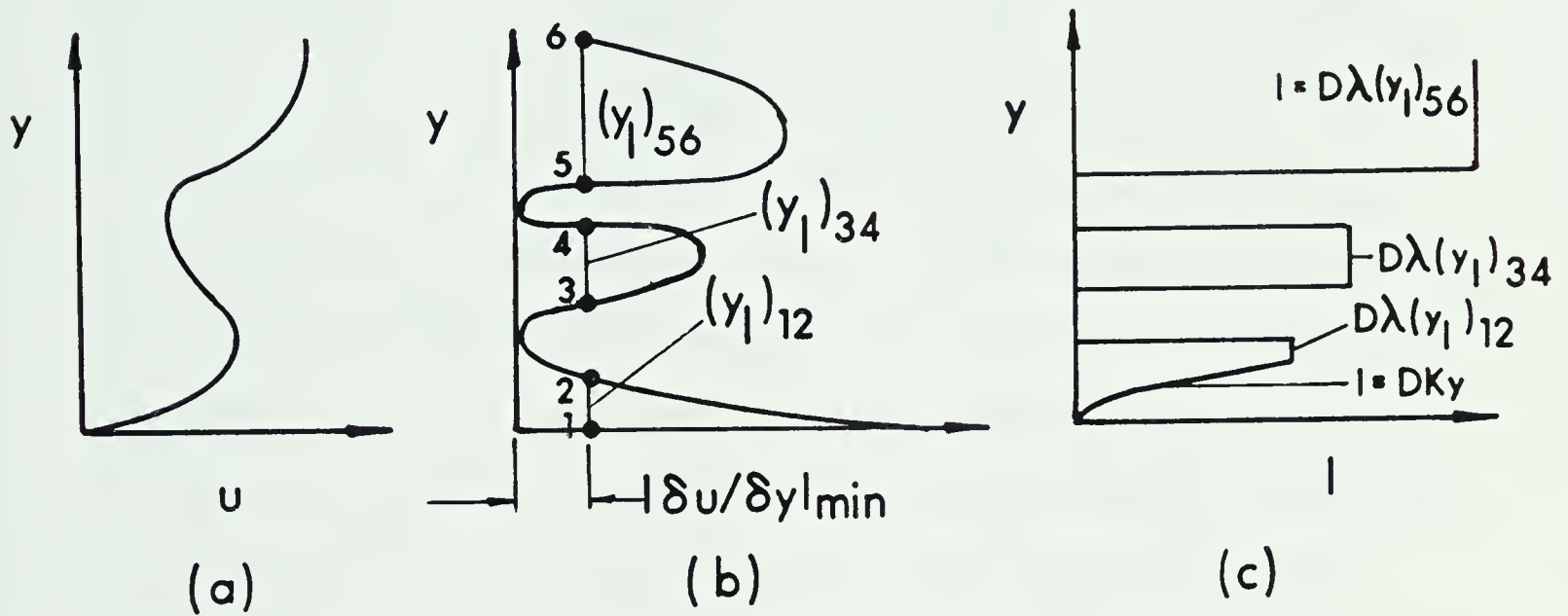
For Mach 3 and higher Mach number flows, Bushnell [68] reports good agreement with experimental velocity profiles and heat transfer rates by assuming a certain value for the mixing angle  $\alpha$ , (Fig.1.1) and prescribing a mixing-length proportional to the local boundary-layer thickness  $\delta_i$ . Flow relaxation down-stream of the cooling slot is divided into three regions and a maximum mixing-length  $\ell_{\max} = .08 \delta_i$  is prescribed where  $\delta_i = y_C/2$ ,  $y_{G,2} - y_{G,1}$  and  $y_G - y_{G,1}$  respectively. The simplified procedure is claimed to be applicable to the near slot ( $x/y_C < 30$ ) as well as the far slot ( $x/y_C > 30$ ) regions even though the boundary-layer equations are not valid in the near slot region.

Relaxation effects could be approximately accounted for in Ref.[69] by assuming that the mixing-length is a function of a velocity profile shape factor. According to the work of Maise and McDonald [70] mixing-length values for equilibrium incompressible flows can be used for compressible equilibrium flows with adiabatic walls up to Mach number 5. The function  $f(x, y/y_C)$  was therefore chosen as a function of the incompressible form factor which is defined as the ratio of the displacement thickness to the momentum thickness. Three functional variations derived from experimental results were tried with a quadratic variation giving the best agreement near the end of the relaxation region for recovery from wall blowing.

In the present work the effective viscosity,  $\mu_{\text{eff}}$  is assigned in much the same manner as was done by Cole and Spalding [3] with further modifications introduced in an attempt to account for the



influence of the magnetic body force. The contribution to  $\mu_{\text{eff}}$  of shear-generated turbulence is accomplished by adopting a mixing-length profile illustrated in Fig. 3.2 which is appropriate to a velocity profile as expected from a tangential injection slot.



(a) Velocity profile

(b) Absolute tangential-velocity gradient

(c) Mixing-length

Fig. 3.2 Effective viscosity, mixing-length model

In Fig. 3.2(b) a selected minimum value  $\left| \frac{\partial u}{\partial y} \right|_{\min}$  determines characteristic lengths  $(y_\ell)_{12}$ ,  $(y_\ell)_{34}$  and  $(y_\ell)_{56}$ . For these far wall regions  $f(x, y/y_\ell)$  is assigned an empirical mixing-length constant  $\lambda$  and the corresponding mixing-lengths are then  $\ell_{12} = D\lambda(y_\ell)_{12}$ ,  $\ell_{34} = D\lambda(y_\ell)_{34}$  and  $\ell_{56} = D\lambda(y_\ell)_{56}$ . The value of  $\lambda$  is taken as 0.075 and the MHD damping function  $D$  will be derived below. The value of  $\left| \frac{\partial u}{\partial y} \right|_{\min}$  is also established from the gross shape of the velocity profile and equated to  $F_R U_G / y_G$  with  $F_R$  as another empirical constant taken as 0.15 for best agreement with experiment, Ref.[3].



Equation (3.16) used in conjunction with an  $\ell \sim y$  profile such as Fig. 3.2(c) would result in vanishing  $\epsilon$  in some regions of the boundary-layer. An unrealistic zero value for  $\epsilon$  is precluded by making an allowance for local "free stream" turbulence and postulating that  $\left| \frac{\partial u}{\partial y} \right|$  never falls below a value typical of the fluctuating component of the local "free stream" velocity. This minimum fluctuating component,  $u'_{\min}$ , is assumed to be proportional to the local velocity, namely  $u'_{\min} = F_u u$  where  $F_u$  is yet another empirical constant taken as 0.02.

Near the wall the mixing-length is prescribed by the usual linear variation  $\ell = DKy$  with  $K = 0.435$ . Here the damping function,  $D$ , will be a modified Van Driest function which is derived in the following manner. To account for the increasingly predominant influence of the laminar viscosity,  $\nu$ , upon approaching a solid boundary, Van Driest [19] considered the velocity distribution normal to an oscillating semi-infinite plane (Stoke's 2nd problem) given by

$$u(y) = u_0 \exp \left[ -\sqrt{\left( \frac{n}{2\nu} \right) y} \right] \cos \left[ nt - \sqrt{\left( \frac{n}{2\nu} \right) y} \right] \quad (3.18)$$

Identifying  $u$  as the fluctuating velocity  $u'$  and taking the inverse situation with the plane fixed

$$u' = u_0' (1 - e^{-y/A_1}), \quad (3.19)$$

where

$$A_1 = \sqrt{(2) \nu} / \sqrt{(n \nu)}$$





The quantity  $\sqrt{(\nu)}$  with units of velocity is then replaced by the "friction velocity"  $\sqrt{(\tau_w/\rho_w)}$  and the constant  $A_1$  is now replaced by  $A$  given as  $A = A_0^+ \nu / \sqrt{(\tau_w/\rho_w)}$  with  $A_0^+$  chosen to agree with experiments.

Generalizing this damping effect to include blown plates or adverse pressure gradients for which the local shear stress can vary markedly with  $y$  in the region near the wall, Kays [71] among others, argue that the local shear stress is more likely to effect the local damping and ought to be used in the constant  $A$  rather than the shear stress at either extremity of the boundary layer. Hence the first contribution to the function  $D$  due to viscous damping can be written as

$$D_1 = 1 - \exp(-y^+ \sqrt{(\tau^+)}/A_0^+) \quad (3.20)$$

where  $y^+ = (y/\nu)\sqrt{(\tau/\rho)}$ ,  $A_0^+ = (A/\nu)\sqrt{(\tau/\rho)}$ , and  $\tau^+ = \tau/\tau_w$

The obvious extension to include MHD effects is to resolve Stoke's 2nd problem with the magnetic body force term included. In its simplest form the equation to solve is <sup>†</sup>

$$\frac{\partial u}{\partial t} = \nu \frac{\partial^2 u}{\partial y^2} - \frac{\sigma B_y^2}{\rho} u \quad (3.21)$$

with boundary conditions

$$u(t,0) = u_0 \cos(nt) \text{ and } u = \text{finite at } y = \infty, t > 0$$

---

<sup>†</sup> Stoke's first problem using Eq.(3.21) was first solved by Rossow [72]



The solution by Laplace transforms gives

$$u = u_0 \exp \left[ -y \sqrt{\left( \frac{1}{2\nu} \sqrt{(m^2 + n^2) + m} \right)} \right] \cos \left[ nt - y \sqrt{\left( \frac{1}{2\nu} \sqrt{(m^2 + n^2) - m} \right)} \right] \quad (3.22)$$

where

$$m = \sigma B_y^2 / \rho$$

By reasoning similar to the one used for viscous damping we deduce that the second contribution to the function D is given by

$$D_2 = 1 - \exp \left( -y^+ \sqrt{\frac{\tau^+}{A_0^+}} \sqrt{\left( \left( \frac{A_0^{+2} m^+}{2} \right)^2 + 1\right) + \frac{A_0^{+2} m^+}{2}} \right) \quad (3.23)$$

or

$$D_2 = 1 - \exp(-y^+ \sqrt{\tau^+} / A^+)$$

where now

$$A^+ = A_0^+ / \sqrt{\left( \left( \frac{A_0^{+2} m^+}{2} \right)^2 + 1\right) + \frac{A_0^{+2} m^+}{2}} \quad (3.24)$$

and

$$m^+ = m\mu / \tau_w$$

Finally, outside the viscous sublayer, damping due to electromagnetic forces still persists although viscous damping is negligible. Resolving Eq. (3.21) without including  $\nu$  results in  $u = u_0 e^{-A_2 m^+}$  from which the third contribution to the damping function D is taken to be

$$D_3 = e^{-A_2 m^+} \quad (3.25)$$

Experiments performed by Lykoudis and Brouillette [17,18] indicate that best agreement was obtained with  $A_2 = 700$ .

Since the  $v'$  fluctuations are not damped by the B field (ie. they are parallel to the magnetic lines of force) and since  $|v'| = 0|u'|$ ,  $D_1$  is used to represent wall damping of the  $v'$  fluctua-



tions,  $D_2$  is used to represent both wall and MHD damping of  $u'$  and  $D_3$  is used to account for MHD damping away from the wall. The final expression for  $D$  in Eq. (3.17), therefore, is written as

$$D = \sqrt{(D_1 D_2 D_3)} \quad (3.26)$$

One final refinement introduced in this dissertation, in an attempt to account for the shape alteration of the gross velocity profile by the magnetic body force, involves a modification of the constant  $A_0^+$ . In OHD flows,  $A_0^+ = 26$  is often assumed even though it has been shown to be influenced appreciably by other factors such as transpiration and/or pressure gradients represented by parameters  $v^+$  and  $p^+$ . An empirical correlation of experimental results is given by Kays [71] as

$$A_0^+ = A_{0,0}^+ / \left( 5.15 \left[ v^+ + \frac{5.86 p^+}{1 + 5v^+} \right] + 1.0 \right) \quad (3.27)$$

where  $A_0^+ = A_{0,0}^+ = 26$  when  $m^+ = p^+ = v^+ = 0$

An analogy between wall suction and magnetic body force influence on the gross shape of the velocity profiles was first pointed out by Lykoudis [73]. The simultaneous presence of wall suction and magnetic field was investigated further, by Luft and Rodkiewicz [40]. Equation (3) of this paper (which appears as Appendix A in this work) may be re-written in terms of the variables defined here, namely  $m^+$  and  $y^+$ , so that

$$\bar{u} = 1 - e^{-\sqrt{(m^+)} y^+} \quad (3.28)$$

Comparing this with the well known asymptotic suction profile (Ref. [74],



for example) and defining  $v^+ = v_w / (\sqrt{(\tau_w)/\rho_c})$  this suction profile may be written as

$$\bar{u} = 1 - e^{-|v^+|y^+} \quad (3.29)$$

It is immediately apparent that  $\sqrt{m}^+$  in (3.28) plays an identical role as suction plays in the velocity profile given by Eq. (3.29). Equation (10) of Ref. [40] is also seen to return the asymptotic suction profile when the magnetic parameter  $I$  defined there is set to zero and noting that  $|v^+|y^+ \equiv \eta$  (not to be confused with the definition of  $\eta$  for film-cooling effectiveness here). Thus the turbulence parameter  $A_0^+$  in the functions  $D_1$  and  $D_2$  is evaluated in accordance with Eq.(3.27) but with  $v^+$  replaced by  $\sqrt{m}^+$  so that

$$A_0^+ = \frac{26}{5.15 \left[ \sqrt{m}^+ + \frac{5.86p^+}{1+5\sqrt{m}^+} \right] + 1} \quad (3.30)$$





CHAPTER IV  
UNIVERSAL MHD MODIFICATIONS TO THE PATANKAR  
AND SPALDING NUMERICAL SOLUTION PROCEDURE

#### 4.1 MHD Wall Function Modifications

The method of Patankar and Spalding involves a 'Couette flow' analysis near a wall wherein the x-wise convection is neglected, by virtue of the velocity component  $u$  being small. The fluxes of mass, momentum, and energy are determined from the solution of ordinary differential equations which can be solved once for all. The momentum equation including the MHD term may then be written for an impermeable wall as

$$\frac{d\tau}{dy} = \rho v \frac{du}{dy} + \frac{dp}{dx} + j e_z B_y$$

or

$$\tau = \tau_w + \int_0^y \left( \frac{dp}{dx} + j e_z B_y \right) dy$$

where

$$j e_z = \frac{\sigma}{1+\beta^2} \left[ (E_z + u B_y) - \beta E_x \right]$$

and

$$\tau = \mu_{\text{eff}} \frac{du}{dy}$$

In terms of dimensionless variables (defined in the nomenclature) this equation can be written as



$$\tau^+ = 1 + \frac{1}{\tau_w} \int_0^{y^+} \left( \frac{p + \tau_w}{\mu_c} \sqrt{(\tau_w \rho_c)} + j e_z B_y \right) \frac{\mu_c}{\sqrt{(\tau_w \rho_c)}} dy^+$$

This suggests the definition

$$j e_z^+ = \frac{\mu_c}{\sqrt{(\tau_w^3 \rho_c)}} (j e_z B_y)$$

such that

$$\tau^+ = 1 + \int_0^{y^+} (p^+ + j e_z^+) dy^+$$

Since  $\tau^+ = \mu^+ \frac{du^+}{dy^+}$  the equation to be integrated is then

$$\frac{du^+}{dy^+} = \frac{1 + \int_0^{y^+} (p^+ + j e_z^+) dy^+}{\mu^+} \quad (4.1)$$

Defining further (similar to the Lykoudis parameter  $\lambda^2$  introduced in Ref. [73])

$$\sigma^+ = \frac{\sigma}{\sigma_c}, \quad m^+ = \frac{\sigma_c B_y^2 \mu_c}{\rho_c \tau_w}$$

and  $E_z^+ = \frac{E_z}{B_y \sqrt{(\tau_w / \rho_c)}}$ ,  $E_x^+ = \frac{E_x}{B_y \sqrt{(\tau_w / \rho_c)}}$ ,  $j e_z^+$  may

be expressed as

$$j e_z^+ = \frac{m^+ \sigma^+}{1 + \beta^2} \left[ E_z^+ + u^+ - \beta E_x^+ \right] \quad (4.2)$$



For the electromagnetic field influence on the recovery factor it turns out to be more convenient to define an electric field parameter without reference to the magnetic field. Hence let  $e^+ = E_z \sqrt{(\sigma_c \mu_c)/\tau_w}$  and if we further restrict the solutions to be valid for negligible Hall effect in the Couette region the current density can be expressed as

$$je_z^+ = m^+ \sigma^+ [E_z^+ + u^+] \quad (4.3)$$

The evolution of the parameter  $e^+$ , which is related to  $E_z^+$  by  $e^+ = \sqrt{(m^+)} E_z^+$  will be demonstrated in the following section dealing with the integration of the Couette flow equations.

The global energy equation in the Couette region may be written as

$$\rho v \frac{dH}{dy} = - \frac{d}{dy} \{J_h - u\tau\} + je_z E_z$$

where

$$J_h = - \frac{\mu_{eff}}{Pr_{eff}} \frac{\partial h}{\partial y} = - k \frac{\partial T}{\partial y} - k_e \frac{\partial T_e}{\partial y} + \sum_s \rho_s v_s h_s \quad (4.4)$$

or, in terms of the dimensionless variables (defined in the nomenclature),

$$\frac{d\phi^+}{dy^+} = \frac{Pr_{eff}}{\mu^+} + \frac{W}{2} \left[ (1 + Pr_{eff}) \frac{du^{+2}}{dy^+} - 2 \frac{Pr_{eff}}{\mu^+} \int_0^{y^+} je_z^+ E_z^+ dy^+ \right] \quad (4.5)$$

Treating  $u^+$ ,  $Pr_{eff}$  and  $\sigma^+$  as known functions of  $y^+$ , the solutions to Eqs. (4.1) and (4.5) may be written formally as functions of the



various parameters, namely  $u^+ = f_u(m^+, p^+, E_z^+, y^+)$

and  $\phi^+ = f_{\phi,1}(m^+, p^+, E_z^+, y^+, Pr) + \frac{W}{2} f_{\phi,2}(m^+, p^+, E_z^+, y^+, Pr)$

Specifying these solutions appropriate to the outer edge of the Couette region, the rates of transfer of momentum, heat, and mass (in the general case) across the Couette flow may be expressed in terms of a drag coefficient  $s$ , a Stanton number  $ST$ , and a recovery factor  $r$ . It may be shown that

$$s = f_{u,c}^{-2} = \tau_w / (\rho_c u_c^2)$$

$$ST = (f_{u,c} f_{\phi,1,c})^{-1} = - J_h / \{ (H_{ad} - H_{w,ad}) \rho_c u_c \} \quad (4.6)$$

$$r = 1 - f_{\phi,2} f_{u,c}^{-2} = (h_{w,ad} - h_c) / (u_c^2 / 2)$$

Finally, the parameters pertinent to the solution of the equations above, may be combined in such a way that expressions for  $s$ ,  $St$  and  $Re$  can be derived as functions of the more common dimensionless numbers. These are: the Reynolds number of the Couette flow  $Re$ ; a pressure gradient parameter  $F$ ; the Hartmann number  $Ha$  based on the thickness of the Couette layer; and a newly introduced electric field parameter,  $E$ . Their definitions are





$$\begin{aligned}
Re &= u_c^+ y_c^+ \equiv (\rho u y / \mu)_c \\
F &= p^+ y_c^+ / (u_c^+)^2 \equiv (y_c / \rho_c u_c^2) dp / dx \\
F &= e^+ y_c^+ / u_c^+ \equiv \frac{E_z y_c}{u_c} \sqrt{(\sigma_c / \mu_c)} \\
Ha &= \sqrt{(m^+) y_c^+} \equiv B y_c \sqrt{(\sigma_c / \mu_c)}
\end{aligned} \tag{4.7}$$

Before the integration of Eqs. (4.1) and (4.5) is carried out, it is possible to eliminate the turbulence parameter  $K$  by a further change of variables defined as follows:

$$\begin{aligned}
y^* &= K y^+ \\
u^* &= K u^+ \\
\phi^* &= K \phi^+ \\
A^* &= K A^+ \\
p^* &= \frac{p^+}{K} \\
m^* &= \frac{m^+}{K^2} \\
E_z^* &= K E_z^+ \\
j e_z^* &= j e_z^+ / K \\
e^* &= e^+
\end{aligned} \tag{4.8a}$$



$$R^* = K^2 Re$$

$$F^* = F/K^2$$

$$Ha^* = Ha$$

$$E^* = E$$

$$s^* = \frac{s}{K^2}$$

then the following relations also hold

$$R^* = u_c^* y_c^*$$

$$F^* = (p^* y^* / u_*^2)_c$$

$$E_z^* = e^* / \sqrt{m^*} \quad (4.8b)$$

$$Ha^* = \sqrt{(m^*)} y_c^*$$

$$E^* = (e^* y^* / u^*)_c$$

The equations to be integrated then become

$$\frac{du^*}{dy^*} = \frac{\tau^+}{\mu^+}$$

with

$$\tau^+ = 1 + \int_0^{y^*} (p^* + j e_z^*) dy^* \quad (4.10)$$

$$j e_z^* = m^* [E_z^* + u^*] \quad (4.11)$$

and



$$\frac{d\phi^*}{dy^*} = \frac{Pr_{eff}}{\mu^+} + \frac{W}{2K} \left[ (1-Pr_{eff})2u^* \frac{du^*}{dy^*} - 2 \frac{Pr_{eff}}{\mu^+} \int_0^{y^*} je_z^* E_z^* dy^* \right] \quad (4.12)$$

#### 4.2 Integration of the Couette Flow Equations

Assuming both the pressure gradient and current density to be independent of  $y$  across the Couette layer, Eq. (4.10) can be integrated to yield

$$\tau^+ = 1 + (p^* + je_z^*) y^* \quad (4.13)$$

and the curve-fitted solutions of Patankar and Spalding could be used by merely defining an effective pressure gradient parameter such that

$$F_{eff} = (p^+ + je_z^+) \frac{y_c^+}{(u_c^+)^2} \quad (4.14)$$

This was the approach adopted in Ref. [7] although the authors concede<sup>†</sup> that perhaps  $je_z^*$  should be allowed to vary with  $y$  as is evident from expression (4.11). In this thesis relations will be presented which do allow  $je_z^*$  to vary as prescribed by Eq. (4.11) although, as was done in the general OHD method of Patankar and Spalding, a constant property Couette flow will be assumed such that  $\sigma^+ = 1$  will also be imposed.

Substitution of Eq. (4.11) into Eq. (4.10) yields

$$\tau^+ = 1 + (p^* + m^* E_z^*) y^* + m^* \int_0^{y^*} u^* dy^* \quad (4.15)$$

$$\tau^+ = 1 + p_{eff}^* y^* + m^* \int_0^{y^*} u^* dy^* \quad (4.16)$$

$$\text{with} \quad p_{eff}^* = p^* + m^* E_z^* \quad (4.17)$$

---

<sup>†</sup>Private communication.



which can be interpreted as an effective pressure gradient parameter. It is evident from this that, in the presence of a magnetic field ( $m^* \neq 0$ ), the effective pressure gradient is altered only if an electric field is also present; that is,  $E_z^*$  must not be zero.

Now, strictly speaking, in addition to  $Re$ , there are three independent parameters,  $p^*$ ,  $m^*$ , and  $E_z^*$ , which can influence the solution to Eq. (4.9). Fortunately as Eq. (4.16) shows, however, there are effectively only two free parameters, namely,  $P_{eff}^*$  and  $m^*$ , since  $p^*$ ,  $m^*$  and  $E_z^*$  appear as a group to form a single coefficient of  $y^*$  in Eq. (4.16). The equation for the shear stress, Eq. (4.9), may then be integrated and curve fit for two special cases: one with  $P_{eff}^* = 0$  and the other with  $m^* = 0$ . For  $m^* = 0$  no electromagnetic effects are present and the solution given by Patankar and Spalding for the effect of pressure gradient on drag, must be recovered. This provided a convenient check on the computer routine written for the drag coefficient  $s$ . The curve-fitted solution for this case is given as [2].

$$\frac{s^*}{s_0^*} = 1 - \left( \frac{4F^*R^*}{[12.8^{2.5} + R^{*2.5}]^{0.4}} \right)^{1.6} \quad (4.18)$$

where  $s_0^*$  is the value of  $s^*$  as a function of  $R^*$  with  $P_{eff}^* = m^* = 0$ . Then, if a curve-fitted solution for  $P_{eff}^* = 0$  could also be found, the resultant expression for  $s^*/s_0^*$  as a function of  $R^*$ ,  $p^*$ ,  $m^*$  and  $E_z^*$  could be assumed<sup>†</sup> to be formed of the product of this solution with Eq. (4.18) in which  $F^*$  would be replaced by an effective pressure

---

<sup>†</sup>This assumption must be tested by comparing the results it yields with an exact integration which is done in Table 1.





gradient parameter  $F_{\text{eff}}^*$  computed by replacing  $p^*$  with  $P_{\text{eff}}^*$ , that is

$$F_{\text{eff}}^* = (p^* + m^* E_z^*) y_c^* / u_c^{*2} \quad (4.19)$$

Before proceeding with the details of curve fitting the solutions for  $P_{\text{eff}}^* = 0$ , the equation for total enthalpy with  $m^*$  and  $P_{\text{eff}}^*$  as parameters will now also be written for completeness:

$$\begin{aligned} \frac{d\phi^*}{dy^*} = & \frac{Pr_{\text{eff}}}{\mu^+} + \frac{W}{2K} \left[ (1 - Pr_{\text{eff}}) 2u^* \frac{du^*}{dy^*} - \right. \\ & \left. \frac{2Pr_{\text{eff}}}{\mu^+} P_{\text{eff}}^* \left( \frac{P_{\text{eff}}^*}{m^*} y^* + \int_0^{y^*} u^* dy^* \right) \right] \end{aligned} \quad (4.20)$$

Furthermore, substituting the results of Section 3.2 for  $\mu^+$  prior to integration, the velocity equation (4.9) becomes

$$\frac{du^*}{dy^*} = \frac{2\tau^+}{1 + \sqrt{(1 + 4y^{*2}\tau^+ D_1 D_2 D_3)}} \quad (4.21)$$

with Eq. (4.16) providing the link for  $\tau^+$ . Figure 4.1 shows typical results obtained from the numerical integration of Eq. (4.21). The curve of  $u^*$  vs  $y^*$  for  $m^* = 0$  corresponds exactly to the curve labelled  $p^* = 0$  in Ref. [2] as it should.<sup>†</sup>

### 4.3 Curve-Fitting the Integrated Momentum Equation - Shear Stress

A convenient feature of the method of Patankar and Spalding [2] for OHD flows is the ability to condense the integrated Couette flow

---

<sup>†</sup> Note that in Ref. [2],  $m^*$  represents a mass transfer parameter and is not to be confused with the magnetic field parameter  $m^*$  as defined in this thesis.



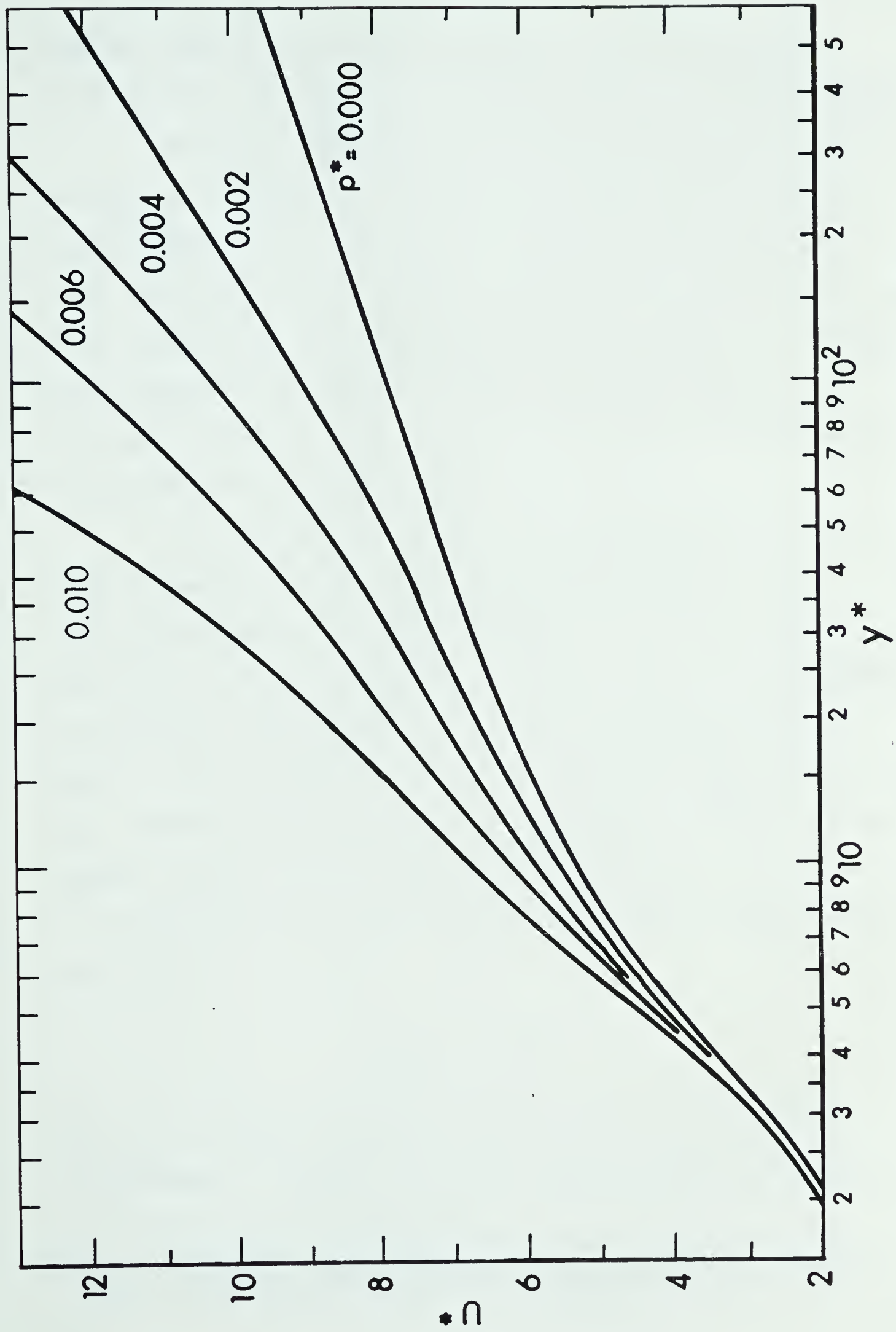


Fig. 4.1 Couette Layer Dimensionless-Velocity Profiles  $P_{\text{eff}}^* = 0$



equations into a set of algebraic equations. Such equations will now be derived in this section for MHD flows with the following results:

We require a single equation for the curves shown in Fig. 4.1 for  $P_{\text{eff}}^* = 0$ . Figure 4.2 is a plot of  $s^*/s_0^*$  against  $Ha^*$  for various Reynolds numbers,  $R^*$ . Analogous to the effect of mass transfer on drag<sup>†</sup> illustrated by similar curves in Ref. [2] it is observed that the horizontal distance between any two curves of constant  $R^*$  is approximately uniform for all values of  $s^*/s_0^*$ . This suggests that all the curves could be made to collapse on to a single curve if the abscissa were multiplied by a function of  $R^*$ .

In the technique of curve fitting and parameter correlation (see, for example, Ref. [75], [76]) one usually strives to obtain linear relationships among these parameters. In plotting  $s^*/s_0^*$  against  $Ha^*$  on rectangular graph paper, linear curves are, unfortunately, not obtained. Referring back to Eq. (4.15) it is observed that the magnetic field parameter  $m^*$  appears only to the first power and previous formulation shows  $m^*$  related to  $Ha^*$  through  $m^* = Ha^{*2}/y_c^{*2}$ . This suggests trying a plot of  $s^*/s_0^*$  against  $Ha^{*2}$  as is done in Fig. 4.3. It is evident that the general form of the equation for these curves for all  $R^*$  is

$$\frac{s^*}{s_0^*} = a - b Ha^{*2}$$

where  $a$  and  $b$  must be regarded as functions of  $R^*$ . Now, for all curves shown,  $s^* = s_0^*$  when  $Ha^* = 0$  as it should by definition; hence

---

<sup>†</sup>This result further substantiates the analogy between wall suction (mass transfer) and MHD effects first proposed by Lykoudis, [73].



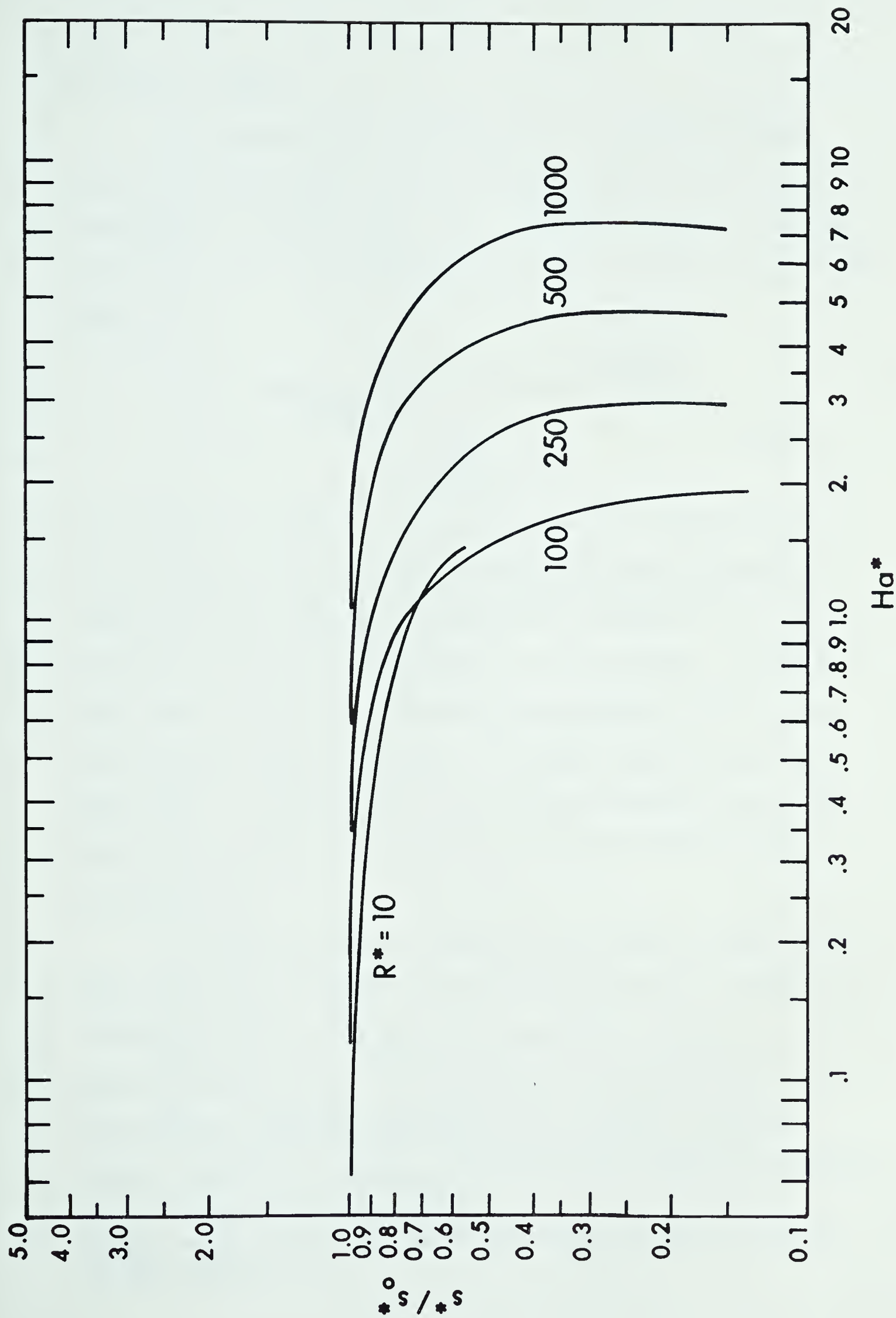


Fig. 4.2 Couette Layer Drag Coefficient vs. Hartmann Number,  $Pe_{eff} = 0$





$a = 1$  and  $b = b(R^*)$ .

To evaluate  $b$  as a function of  $R^*$ , a straight line was eventually obtained when plotting the slope  $b$  against  $R^*$  on log-log coordinates as is shown in Fig. 4.4. Evidently,  $b$  has the functional relation;  $b = nR^{*-m}$ , and graphically we find  $n = 117.55$ , and  $m = 1.345$ . Hence

$$\begin{aligned} (s^*/s_0^*)_{\text{emp},1} &= 1 - 117.55 R^{*-1.345} Ha^{*2} \\ &= 1 - \frac{Ha^{*2}}{0.0085 R^{*1.345}} \end{aligned} \quad (4.22)$$

If the empirical values of  $s^*/s_0^*$  computed from Eq. (4.22) are now plotted against the exact values of  $s^*/s_0^*$  taken from the numerical integration of the Couette-flow equations, a 45 degree line is expected if a one-to-one correspondence is to be obtained. Figure 4.5 shows such a plot and it is observed that agreement is fairly good over a certain range of  $s^*/s_0^*$  and for Reynolds numbers greater than about 100. For smaller values of  $R^*$  the curves deviate excessively from the exact values and a correction for small Reynolds numbers must be derived.<sup>†</sup>

In order to derive a suitable small-Reynolds number correction, the obvious solution is to plot the difference  $\delta = (s^*/s_0^*)_{\text{exact}} - (s^*/s_0^*)_{\text{emp}}$  against  $(s^*/s_0^*)_{\text{emp}}$  for various  $R^*$  and hope for a family of straight lines. This procedure failed and a plot of  $\delta$  versus  $Ha^{*2}$  was attempted with equal lack of success. Finally, a plot of  $\delta$  against  $1 - (s^*/s_0^*)_{\text{emp}}$  yielded a set of reasonably straight

---

<sup>†</sup>Typical values of  $R^* = u^*y^*$  are in the range of about 10 to 1000 as seen from Fig. 4.1.



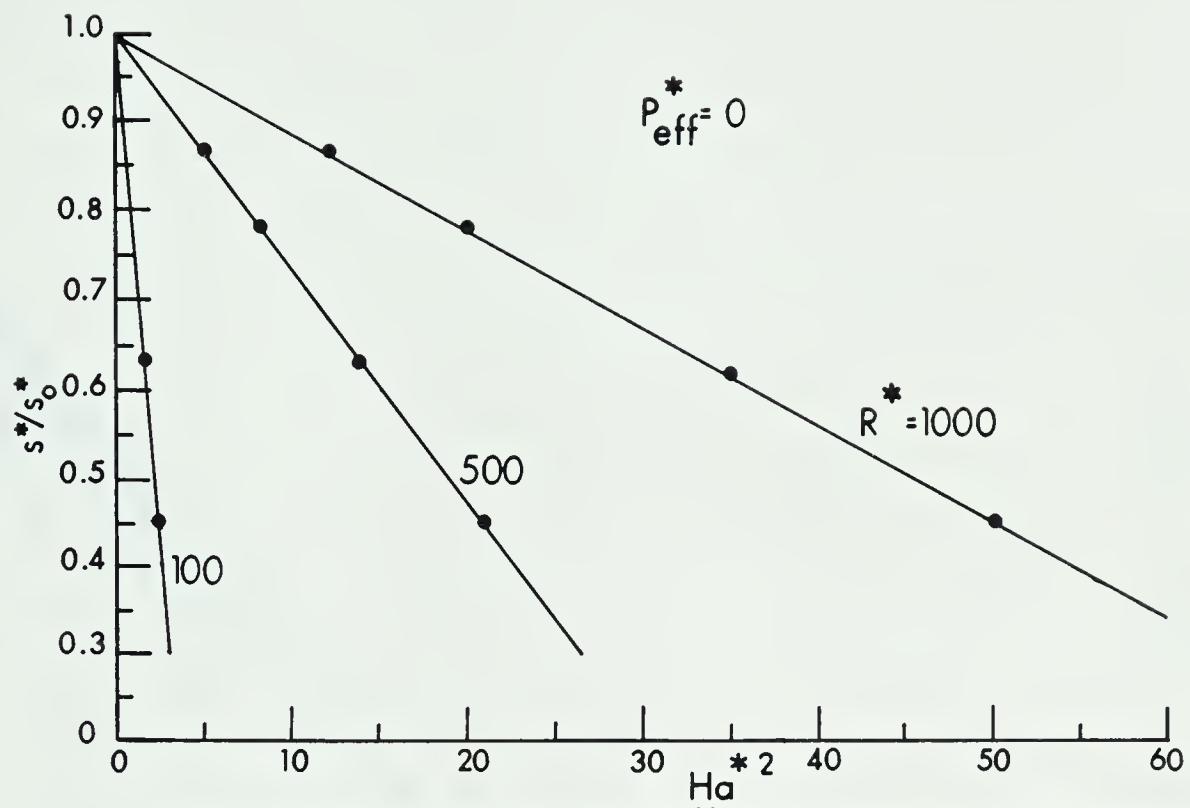


Fig. 4.3 Couette Layer Drag Coefficient vs. Hartmann No. Squared

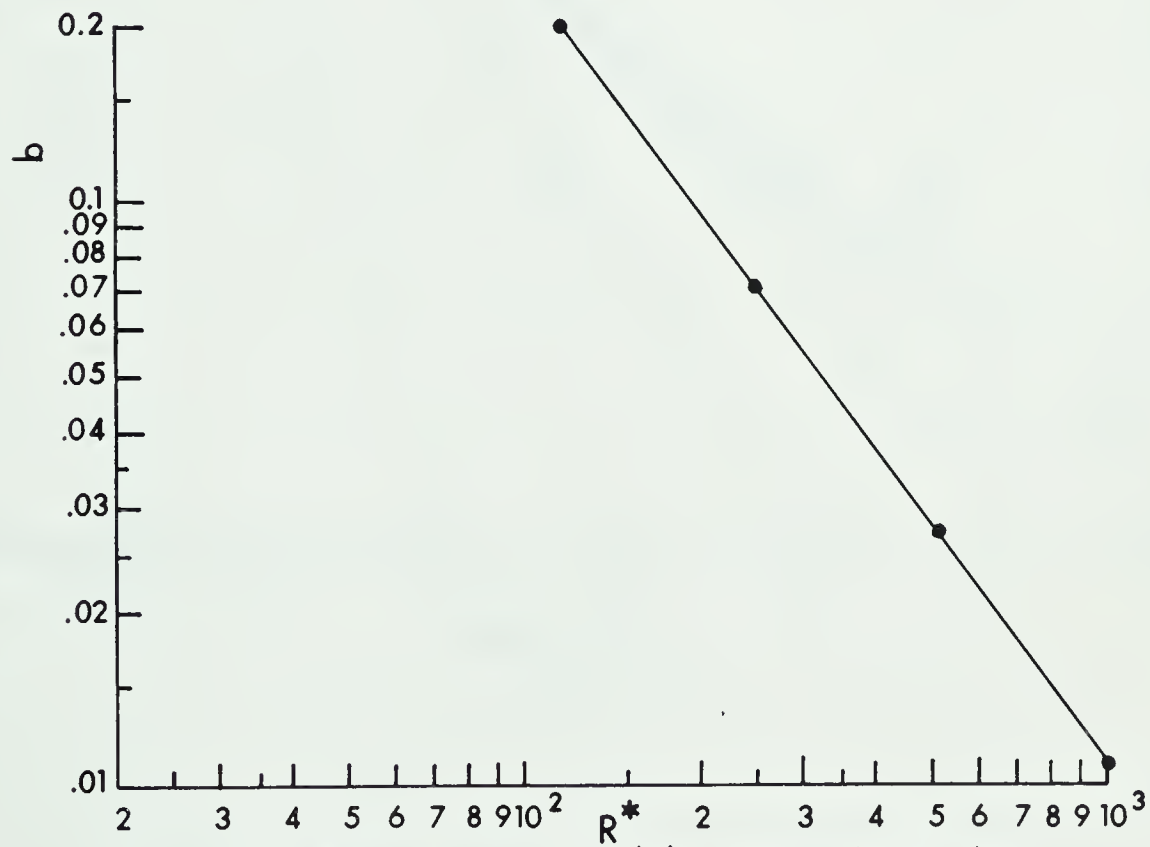


Fig. 4.4 Curve Fitting Parameter 'b' vs. Reynolds Number



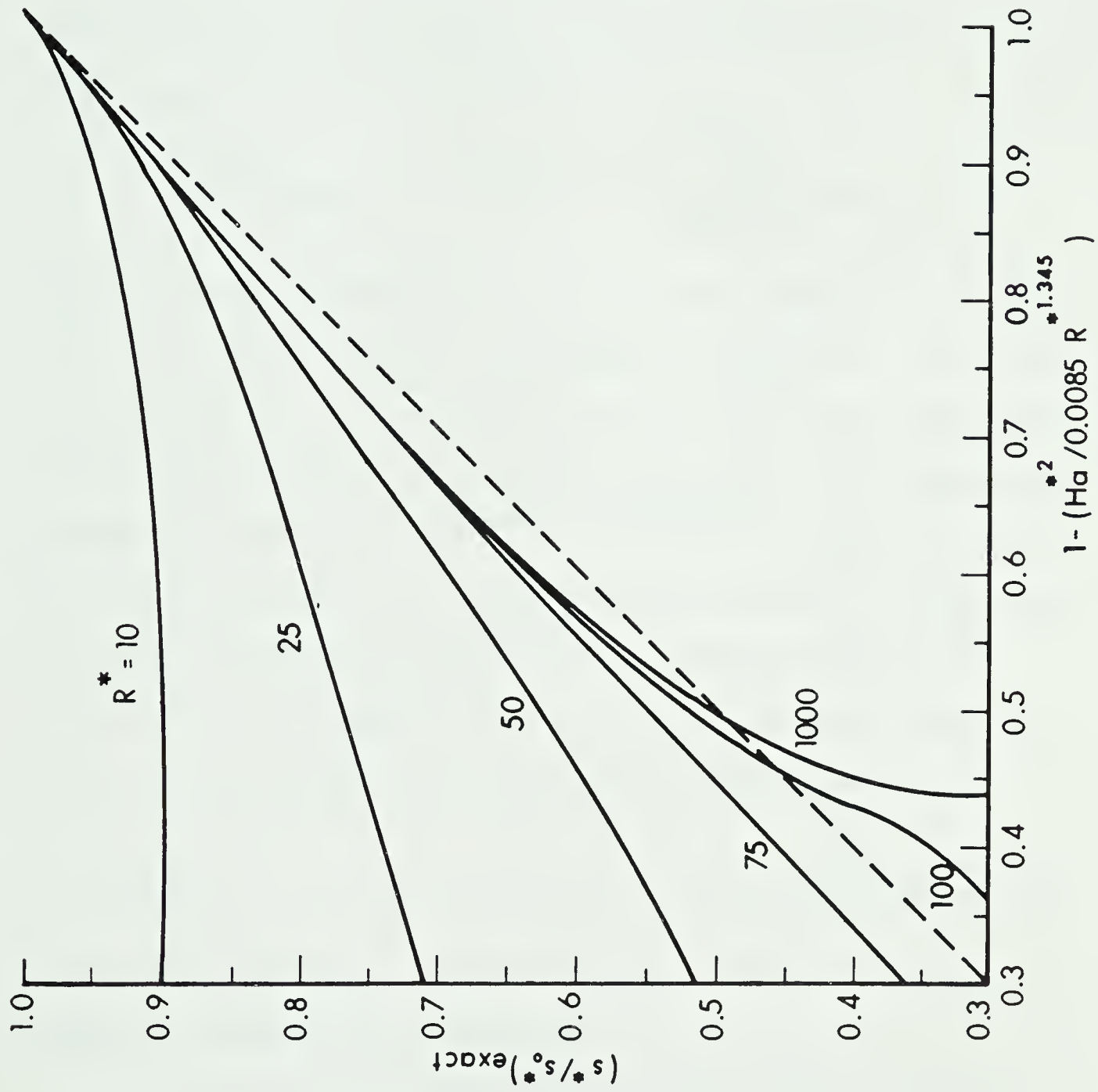


Fig.4.5 Couette Layer Drag Coefficient  
Small Reynolds No. Correction



lines such that the general form of the equation for  $\delta$  could be written as

$$\delta = b(R^*) \frac{Ha^{*2}}{0.0085 R^{*1.345}}$$

The new expression for  $(s^*/s_0^*)_{\text{emp},2}$  (which ideally equals  $(s^*/s_0^*)_{\text{exact}}$ ) may now be written as  $(s^*/s_0^*)_{\text{emp},1} + \delta$  or

$$(s^*/s_0^*)_{\text{emp},2} = 1 + [b(R^*) - 1] \frac{Ha^{*2}}{0.0085 R^{*1.345}} \quad (4.23)$$

Evidently the function  $b(R^*)$  in Eq. (4.23) must possess the property:  $b(0) = 1$ , so that the second term remains finite (which, incidentally, is an obvious flaw in expression (4.22)) and also it must somehow approach zero asymptotically for large values of  $R^*$ . This immediately suggests the form  $b(R^*) = 10^{-nR^{*m}} = e^{-2.303nR^{*m}}$ . A trial and error solution of plotting  $b(R^*)$  on semi-log paper revealed a linear curve for  $m = 1.5$  from which the constant  $n$  was finally evaluated as  $1.31 \times 10^{-3}$ . Hence the resulting empirical expression for the magnetic field influence on the drag coefficient takes the form

$$(s^*/s_0^*)_{\text{emp},2} = 1 - [1 - \exp(-3.02 \times 10^{-3} R^{*1.5})] \frac{Ha^{*2}}{0.0085 R^{*1.345}} \quad (4.24)$$

Figure 4.6 illustrates a plot of  $(s^*/s_0^*)_{\text{exact}}$  versus  $(s^*/s_0^*)_{\text{emp}}$  and agreement is deemed to be reasonable.

It now remains to deal with the most general situation, namely that for which all the parameters  $R^*$ ,  $p^*$ ,  $m^*$ , and  $E_z^*$  are prescribed independently and where, specifically, the pressure gradient is non-zero or the electric field parameter  $E_z^*$  takes on values other





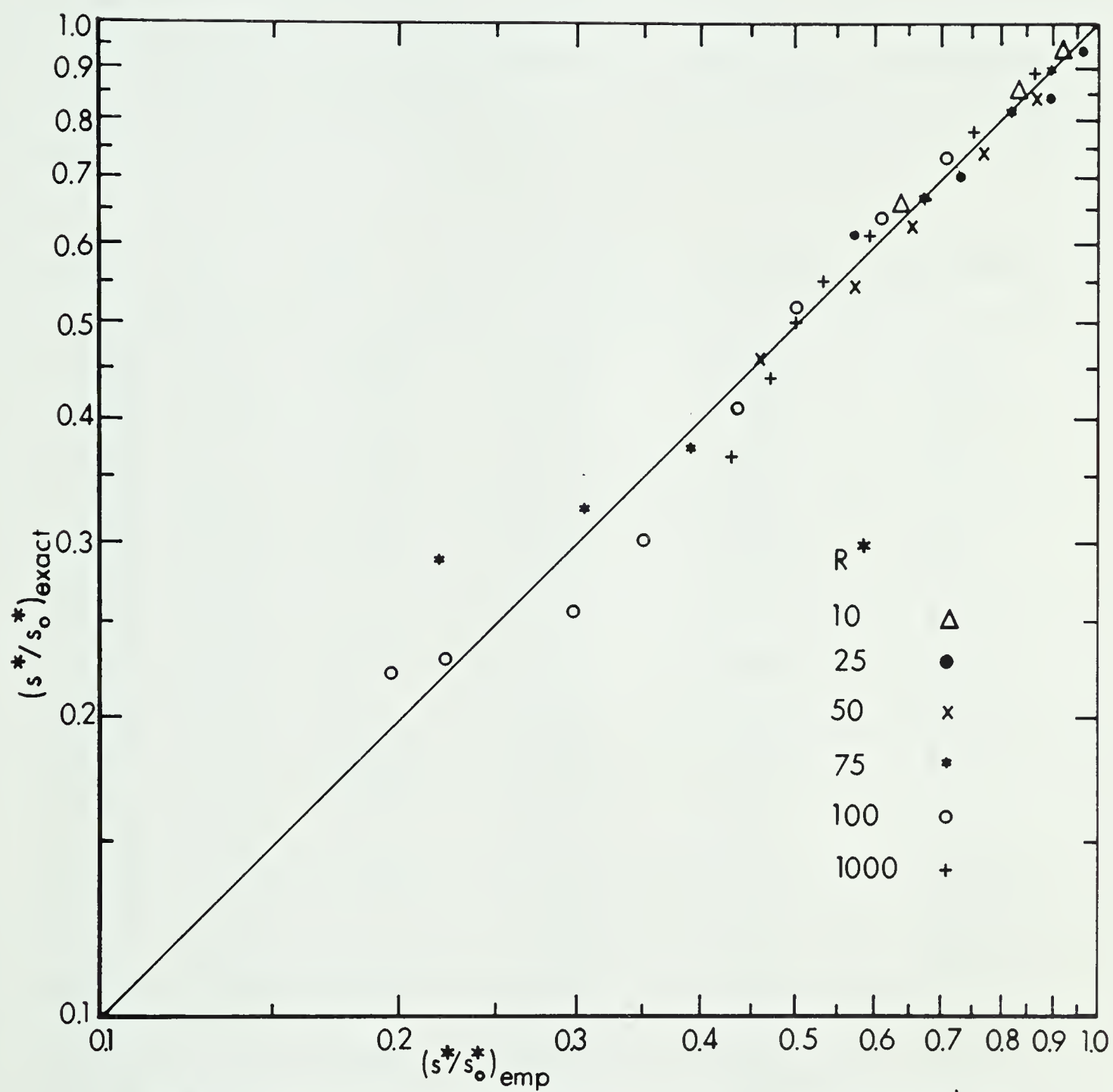


Fig. 4.6 Couette Layer Drag Coefficient, Exact vs. Empirical ( $P_{\text{eff}}^* = 0$ )



than those dictated by  $E_z^* = -p^*/m^*$ .<sup>†</sup> The approach adopted in Ref. [2] to a similar situation implies that a general formula be assumed by forming the product of Eqs. (4.24) and (4.18) with  $F^*$  replaced by  $F_{\text{eff}}^*$  defined in Eq. (4.19). In Table 1 is given a comparison of such a product solution with the exact values for  $s^*/s_0^*$ . The agreement is seen to be satisfactory for a range of representative flow parameters.

Table 1

$R^*$	$Ha^*$	$F_{\text{eff}}^*$	$(s^*/s_0^*)_{\text{exact}}$	$(s^*/s_0^*)_{\text{emp}}$	% Deviation
14.69	0	0.0148	0.890	0.920	4.00
15.94	0.179	0.0252	0.800	0.850	6.40
18.33	0	-0.0148	1.050	1.080	3.20
18.76	0.223	-0.0178	1.020	1.070	5.40
19.52	0.050	-0.0033	0.970	1.020	5.10
20.47	0.224	0	0.910	0.970	7.60
51.44	0.900	-0.0138	0.806	0.741	8.17
86.54	0.150	-0.0045	0.998	1.020	2.46
101.16	0.716	0	0.883	0.885	0.22
102.97	0.810	-0.0275	1.080	1.010	6.75
103.28	0.510	-0.0046	0.960	0.970	0.75
105.11	1.160	0	0.730	0.710	2.70
328.38	0	-0.1002	1.673	1.715	2.51
491.71	2.680	0	0.818	0.797	2.62
503.33	0.700	-0.0135	1.068	1.073	0.43
903.86	4.470	0	0.763	0.751	1.58
973.34	0	0.0528	0.668	0.684	2.42
1035.05	6.320	0	0.598	0.586	2.07
1047.57	3.900	-0.0200	0.988	0.956	3.35
1107.97	0	0.0815	0.529	0.532	0.59

<sup>†</sup> Expression (4.24) is valid for non-zero pressure gradients also as long as the electric field  $E_z^*$  satisfies this relation.



It is evident from Table 1 that within a deviation of plus or minus 10% the wall shear stress can be calculated from

$$s^*/s_{0,emp}^* = \left( 1 - \frac{4F_{eff}^* R^*}{[12.8^{2.5} + R^{*2.5}]^{0.4}} \right)^{1.6} \times \left( 1 - [1 - \exp(-3.02 \times 10^{-3} R^{*1.5})] \frac{Ha^{*2}}{0.0085 R^{*1.345}} \right) \quad (4.25)$$

It should be pointed out that in using Eq. (4.25) the magnitude of the parameters such as  $Ha^*$  must be limited so as to avoid zero or negative values of  $(s^*/s_{0,emp}^*)$  since this would indicate boundary layer separation. Calculations reveal, for example, that for  $F_{eff}^* = 0$ , and  $R^* = 25$ ,  $Ha^*$  must be  $\leq 1$  in order that Eq. (4.25) be accurate to within 10%. If  $Ha^* = By_c \sqrt{(\sigma_c/\mu_c)}$  is calculated for typical values of  $B = 5$  Tesla (webers/m<sup>2</sup>),  $y_c = 5 \times 10^{-4}$  m,  $\sigma_c = 10$  mho/m and  $\mu_c = 10^{-4}$  kgm/m-sec, then  $Ha^* = 0.78$ . Hence Eq. (4.25) does not pose any physical limitations since, to the author's knowledge, maximum magnetic fields which can be generated by present day super-conducting magnets are of the order of 7.5 Teslas.

#### 4.4 Curve Fitting the Integrated Energy Equation - Recovery Factor

In order to formulate the effect on the recovery factor,  $r/r_0$ , due to the magnetic and electric fields in a similar manner as was done for  $s^*/s_0^*$ , it is evident that Eq.(4.20), with  $m^*$  and  $P_{eff}^*$  as parameters, must be re-written since, as expression (4.27) shows,  $E_z^*$  cannot be assigned different values via  $P_{eff}^*$  with  $m^* = 0$ . Furthermore, with  $m^*$  appearing in the denominator, integration of Eq. (4.20)



cannot be performed with  $m^* = 0$ .

Recalling Eq. (4.12), the integral  $\int_0^{y^*} j e_z^* E_z^* dy^*$  can be rewritten in the following way. First, the integrand may be written as

$$j e_z^* E_z^* = \frac{\sigma_c \mu_c E_z^2}{\tau_w^2} + \frac{\sigma_c \mu_c E_z B u}{\tau_w^2}$$

Next, by introducing a previously defined electric field parameter

$$E^* = \frac{E_z y_c}{u_c} \sqrt{\left(\frac{\sigma_c}{\mu_c}\right)} = \frac{e^* y^*}{u^*}$$

we obtain

$$j e_z^* E_z^* = e^{*2} + \sqrt{(m^*)} e^* u^* \quad (4.26)$$

The simultaneous equations to be integrated then become Eq. (4.21) with  $\tau^+$  given by

$$\tau^+ = 1 + (p^* + e^* \sqrt{m^*}) y^* + m^* \int u^* dy^* \quad (4.27)$$

and the energy equation by

$$\begin{aligned} \frac{d\phi^*}{dy^*} = & \frac{Pr_{eff}}{\mu^+} + \frac{W}{2K} \left[ (1 - Pr_{eff}) 2u^* \frac{du^*}{dy^*} \right. \\ & \left. - \frac{2Pr_{eff}}{\mu^+} [e^{*2} y^* + e^* \sqrt{m^*} \int u^* dy^*] \right] \end{aligned} \quad (4.28)$$

Figure 4.7 shows integration results with  $p^* = m^* = 0$  when  $r/r_0$  is plotted against  $E^{*2}$ . Curve fitting these results gives the following





empirical expressions:

$$r/r_0 = 1 + \exp(-0.01875R^*)(E^*)^2 \quad R^* \leq 55 \quad (4.29)$$

$$r/r_0 = 1 + 24(R^*)^{-1.04}(e^*)^2 \quad R^* > 55$$

In Table 2 are given the results obtained from expressions (4.29) and compared with the exact values.

Table 2

$R^*$	$\pm E^*$	$(r/r_0)_{\text{exact}}$	$(r/r_0)_{\text{emp}}$	% Deviation
11	3.33	10.00	10.03	0.3
53	5.69	12.57	12.99	3.3
102	2.83	2.58	2.56	0.8
200	13.49	18.91	18.67	1.3
527	0.93	1.04	1.03	1.0
1060	47.75	41.16	40.07	2.7

Integration results with non-zero pressure gradient ( $p^* \neq 0$ ) and magnetic field ( $m^* \neq 0$ ) revealed  $r/r_0$  to be a weak function of  $p^*$  and not a direct function<sup>†</sup> of  $H_a^*$  when  $E^* = 0$ . For small non-zero values of  $E^*$  the influence of  $H_a^*$  on  $r/r_0$  appears to be negligible so that Eq. (4.19) can be considered to account for the primary electromagnetic effects on the recovery factor. For large electric fields, however, such as those encountered in MHD accelerators, a further modification to these expressions would be necessary.

---

<sup>†</sup>Note however that even in this case,  $r/r_0$  will be an indirect function of  $H_a^*$  since this parameter influences the wall shear stress which in turn affects the viscous dissipation.



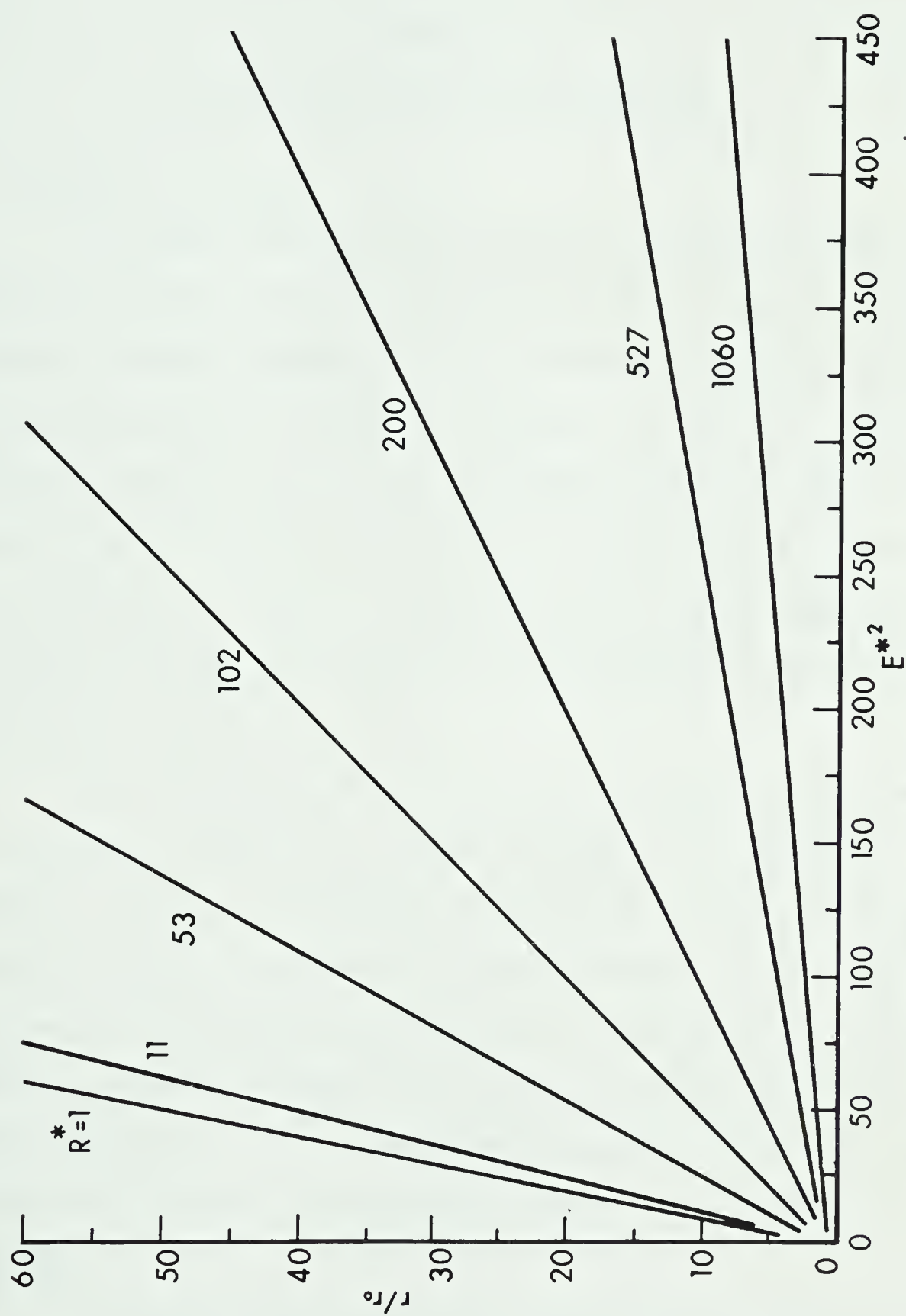


Fig. 4.7 Couette Layer Recovery Factor vs. Electrical Field Parameter ( $m^*=0$ )



## CHAPTER V

### DISCUSSION OF RESULTS AND CONCLUSIONS

#### 5.1 General Discussion

In order to assess the fundamental influences of MHD body forces and Joulean dissipation on the adiabatic film-cooling effectiveness, several computations were performed by assuming thermal and ionizational equilibrium as discussed in Section 5.3. This assumes that the electron gas is at the same temperature as the plasma and that the mass electron number density can be calculated from the Saha relation, Eq. (2.7). These results will also be required for assessing the effects of thermal non-equilibrium and finite rates as discussed in Section 5.4.

The MHD effects on the adiabatic film-cooling effectiveness,  $\eta$ , are clearly shown in the figures discussed in the following Sections. However, to research and understand the causes for the observed effects, it becomes necessary to examine a more intimate picture of the phenomena; examination of the velocity and temperature profiles across the boundary layer helps to provide this insight. These profiles as well as corresponding electric current and plasma conductivity profiles are examined in detail in the following Sections.

Previous research into OHD film-cooling has shown that the process depends on many factors. Examples of these would be the



geometry of the film-cooling injection slot, the properties of the primary and secondary (coolant) flows, the rate of coolant blowing represented by a blowing parameter  $Q = \rho_C U_C / \rho_G U_G$ , ratios such as those of temperatures,  $T_C/T_G$  (or densities) and velocities,  $U_C/U_G$ , magnitude of free stream turbulence intensity, magnitudes of favourable or adverse pressure gradients, chemical composition of coolant fluid etc. Clearly, a reliable theoretical prediction procedure can be an expedient computation tool to assess the effects of many of these parameters, without resorting to costly and time consuming experimental measurements, by simply changing a few program statements or data cards. Any theoretical computational method must, however, agree to within acceptable limits with experimental measurements whenever these are available.

Section 5.2 assesses the reliability of the present numerical procedure by comparing its predictions with experimental results as well as with predictions obtained with a similar procedure when applied to OHD film-cooling problems.

For the numerical solution techniques, it also becomes important to investigate the sensitivity of predictions to the initial conditions. These are assumed to exist at the beginning of the numerical marching procedure and, in this case, represent assumed conditions at the film-cooling slot exit. If results prove to be strongly dependent on the prescribed initial conditions, then it becomes necessary to solve the fully developed MHD channel flow upstream of the slot and then adopt these solutions to obtain the initial conditions at the slot exit. Section 5.3.4. includes an analysis of the influence of initial magnetic field variation on the





boundary layer velocity and temperature profiles and hence on the film-cooling effectiveness.

Section 5.4 considers the influence of thermal non-equilibrium and finite-rate ionization on the MHD film-cooling effectiveness. Core flow or free-stream conditions are chosen such that little or no electron thermal non-equilibrium would exist. This insures that any differences from the equilibrium solutions will be boundary layer effects and not due to free stream effects.

Furthermore, in order to preclude complications for the non-equilibrium analysis resulting from Hall currents,  $je_x$ , the assumption of infinitely segmented electrodes will be made such that  $je_x=0$  everywhere. To assess Hall current effects in the boundary layer, this restriction is later replaced with the assumption of free-stream Hall-neutralized flow,  $je_{x,G}=0$  and finally the condition  $E_x=0$  is imposed which represents an MHD channel for which the Hall potential is short-circuited.

## 5.2 Evaluation of Computational Procedure for OHD Film-Cooling Flows

For the purposes of testing the lengthy computer program written for this thesis, the film-cooling effectiveness predictions derived from it for ordinary hydrodynamic flows (OHD) were compared both with similar calculation techniques [3], and with experimental data, [64].

The present computer method was compared with that of Cole and Spalding [3] for which their "standard case" results are shown for comparison in Fig.5.1. The initial flow parameters are



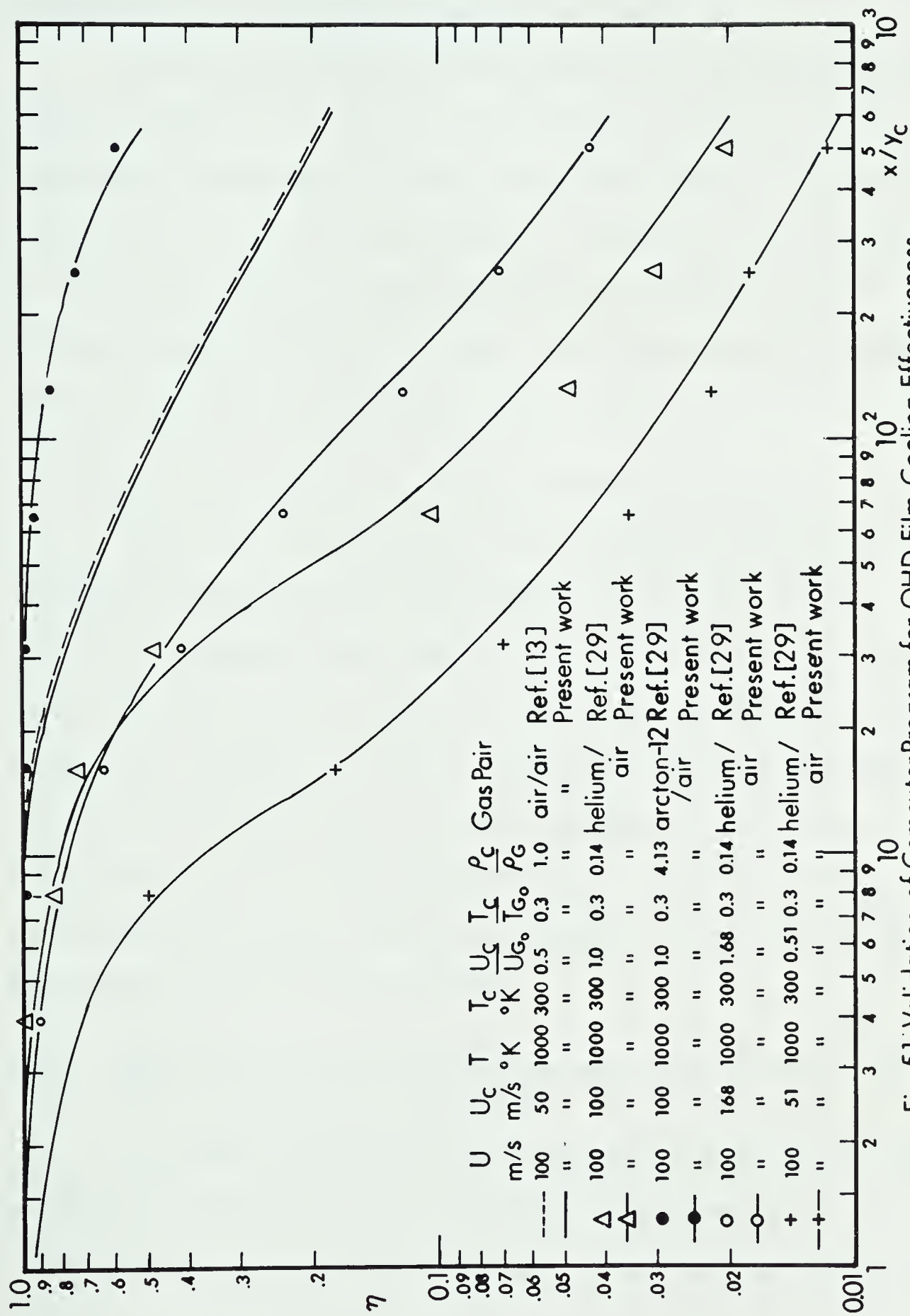


Fig.5.1 Validation of Computer Program for OHD Film-Cooling Effectiveness



detailed in a tabular form in Fig. 5.1. It can be seen that both computer predictions are virtually identical from which it may be concluded that the program is functioning properly.

Additional validation and credence to the numerical technique, in general, is provided by favourable comparison with the experimental measurements of Burns and Stollery [64] for different combinations of main and coolant gases. Figure 5.1 displays results for helium and argon-12 coolant injection at different coolant-main-gas velocity and density ratios. It is concluded that agreement between prediction and experiment is satisfactory.

### 5.3 Thermal and Ionizational Equilibrium MHD Film-Cooling

Many non film-cooled MHD flows have been studied under the assumption of thermal equilibrium between the electron gas and carrier gas temperature with the electron number density,  $n_e$  (or mass fraction  $C_e$ ), calculated from the Saha equilibrium relation. This assumption is generally valid for open-cycle combustion MHD generators. Equilibrium conditions have also been assumed in this Section so that the influence of electromagnetic body forces and Joule dissipation on the film-cooling effectiveness can be assessed in the light of general MHD effects on plasma channel flows.

#### 5.3.1 MHD Influence on Film-cooled Boundary Layer Velocity Profiles and Film-Cooling Effectiveness

The close agreement achieved both with the prediction method of Cole and Spalding [3] and with experiment as shown in Fig. 5.1 is, in part, due to having chosen identical initial velocity profiles at the



film-cooling slot exit in the prediction method. This initial profile was also chosen for the developing MHD flow field and is shown plotted in Fig. 5.2a as represented by  $x/y_C=0$ .

Many computer runs were performed with different combinations of the parameters available, such as  $B$ ,  $U_C/U_{Go}$ ,  $Q$ , etc. A typical case is represented in Fig. 5.2 where two identical runs were performed except that one is for OHD flow ( $B=0$ ) and the other is for MHD flow (ie.  $B=2$ ). The run conditions are detailed on Fig. 5.2a, which compares developing velocity profiles in MHD and OHD flows in the near-slot region. Similar velocity profiles for larger down-stream distances are plotted in Fig. 5.2b.

The developing velocity profiles for OHD film-cooling are typical of what is obtained by other procedures and experimental measurements. Spalding [51] makes note of developing velocity profiles becoming gradually fuller "... but, that even at 100 slot-heights downstream, the profiles have not lost all trace of their original depression." A similar trend is observed with the OHD profiles shown in Fig. 5.2 where the velocity profiles appear not to be fully developed even at larger downstream distances for these run conditions.

It can be seen that the OHD velocity profiles lose their maxima relatively quickly compared to those for MHD flow which are seen to develop the characteristics of a sustained wall jet flow. The MHD velocity profiles are showing a relative acceleration of the boundary layer fluid with that of the free stream (core flow), since the  $\vec{j} \times \vec{B}$  retarding force is less intense in the boundary layer where





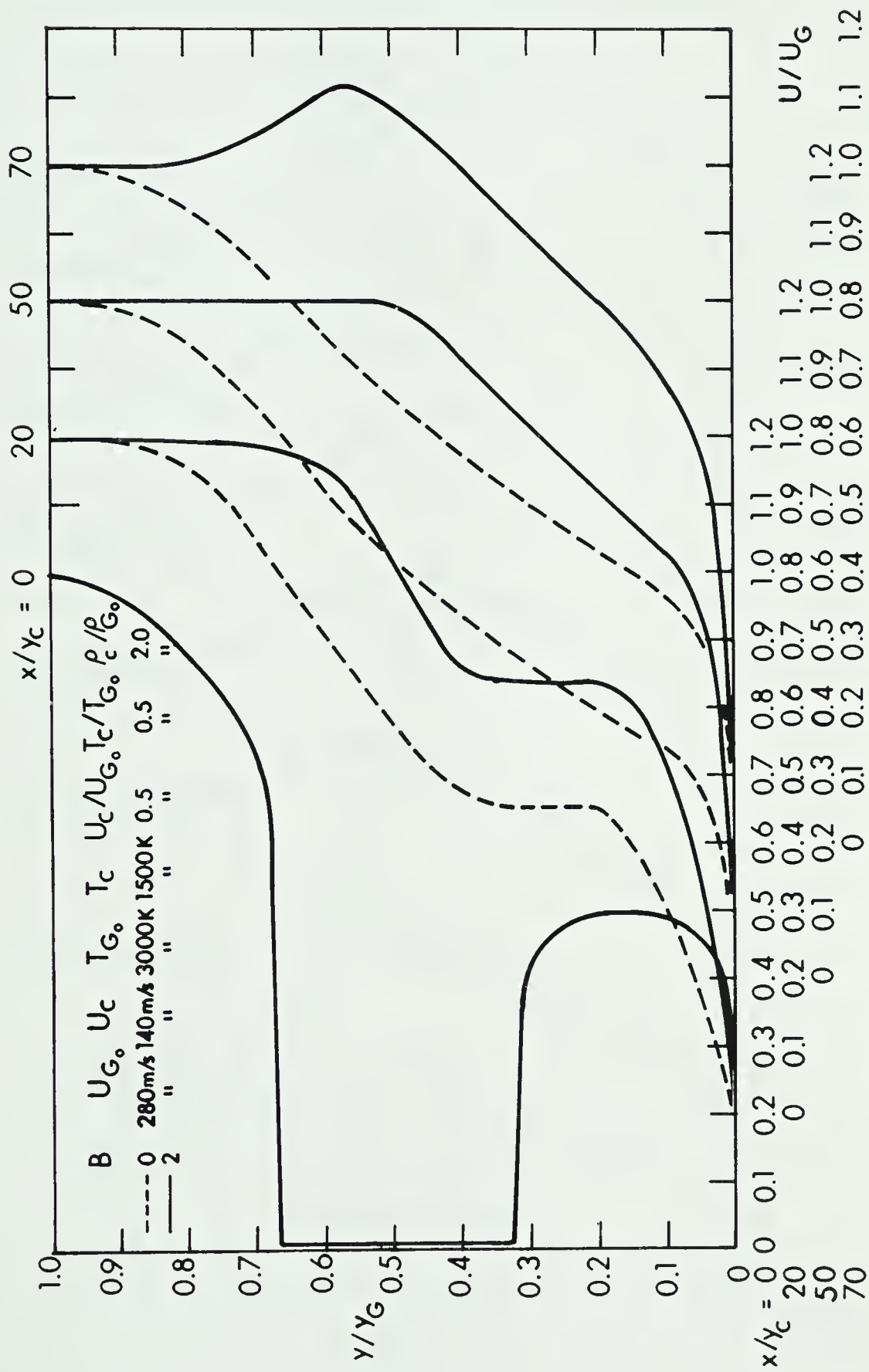


Fig. 5.2a MHD Influence on Film-Cooled Boundary Layer Velocity Profiles -Near Slot Region  
Equilibrium Case



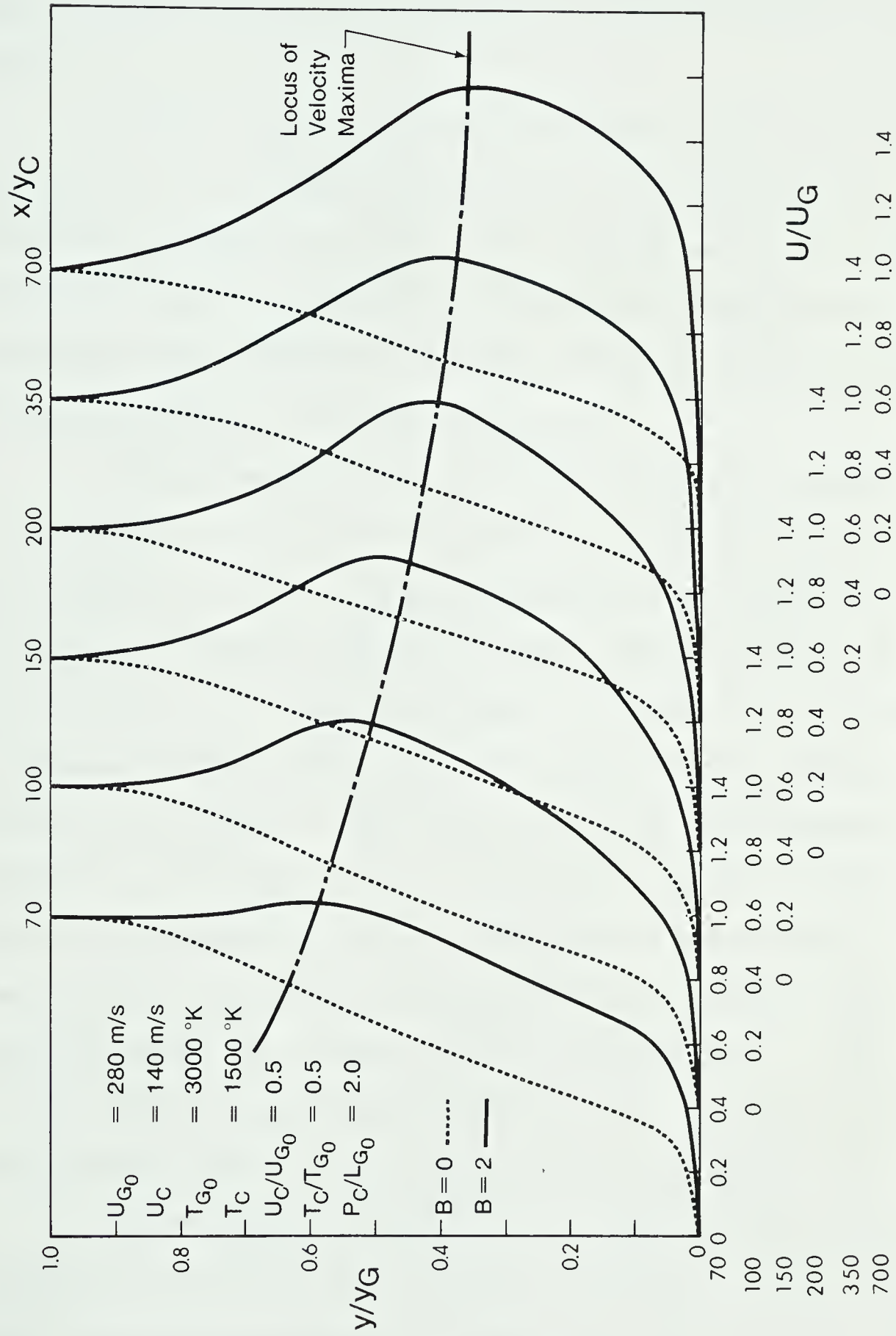


Fig.5.2b MHD Influence on Film-Cooled Boundary Layer Velocity Profiles - Far Slot Region Equilibrium Case.



lower temperatures result in lower plasma electrical conductivity. The corresponding electrical current and conductivity profiles at the same downstream distances are shown in Fig. 5.5 and Fig. 5.7, respectively.

The MHD velocity profiles imply that as the magnetic field strength,  $B$ , is increased, more mass flow in the channel gets confined in the boundary layers of the insulator walls. The sustaining of a wall jet type flow by the magnetic body forces would be expected to have a beneficial influence on the film-cooling effectiveness, at least for smaller values of  $B$ .

With reference to Fig. 5.2, the wall jet can be imagined as originating near the mid point of the upper slot lip and emerging into a quiescent fluid. The jet flow would act as a barrier to mixing of the primary (core) and secondary (coolant) gases. At larger values of  $B$ , however, the higher  $\vec{j} \times \vec{B}$  forces in the free stream would direct most of the channel mass flow into the boundary layers of the  $B$  walls. The hotter core flow gas would therefore be forced into the boundary layer in sufficient quantity to rapidly heat up the coolant, resulting in a decrease in effectiveness. It would also be expected, by the observed large difference in velocity profiles between OHD and MHD flow, that the difference in  $\eta$  would also be relatively large although the difference in  $\eta$  from one non-zero value of  $B$  to another would be expected less pronounced.

The film-cooling effectiveness is shown on Fig. 5.3 and plotted for different values of magnetic field,  $B$ . It can be seen that the expected behaviour of  $\eta$  from studying the velocity profiles of



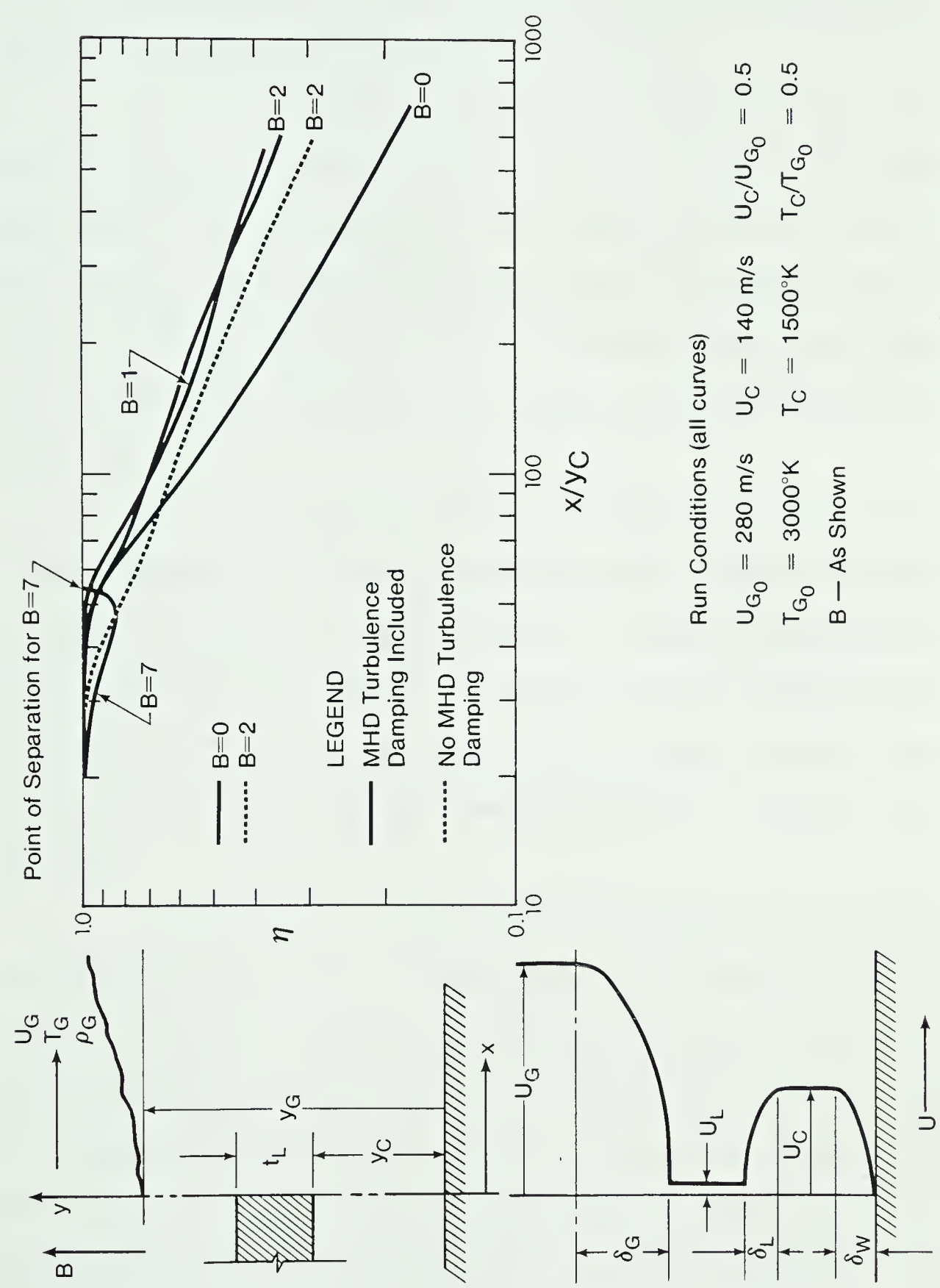


Fig.5.3 MHD Influence on Adiabatic Film - Cooling Effectiveness — Equilibrium Case.





Fig. 5.2, is borne out by the observed behaviour of  $\eta$  which indeed supports the predicted observations. All runs were performed with the flow parameters as shown, and only the magnetic field,  $B$ , was varied. Curves plotted are for  $B=0, 1, 2$ , and  $7$ .

It is seen that the increase in  $\eta$  from  $B=0$  to  $B=1$  is relatively much greater than that for  $B=1$  to  $B=2$ . In fact, the predicted decrease in  $\eta$  for larger values of  $B$  is borne out by the curves for  $B=2$  and  $B=7$ . The latter actually shows that the magnetic field retarding force for  $B=7$  is sufficiently strong enough to cause flow separation at approximately 55 slot heights downstream from the slot exit.

The optimum magnetic field intensity resulting in the largest increase in film-cooling effectiveness is seen from Fig. 5.3 to occur for values of  $B$  between 1 and 2. By way of comparison, the OHD film-cooling effectiveness is reduced to 50% at 120 slot heights downstream whereas a similar reduction by 50% does not occur until approximately 250 slot heights downstream have been reached in the MHD case.

The influence of the magnetic field damping of the turbulent velocity fluctuations on the film-cooling effectiveness is also illustrated in Fig. 5.3. Because any damping of turbulent fluctuations would reduce the rate of mixing of the primary and secondary streams, the film-cooling effectiveness would be expected to increase and this is verified in Fig. 5.3. The average increase in  $\eta$  for a magnetic field parameter  $B=2$  is seen to be 15% for the run conditions shown.



The plot of the velocity profiles in Fig. 5.2b also shows the locus of velocity maxima in the MHD boundary layer flow. The gradual decreasing trend of this curve can be attributed to the increase of electron current density,  $je_z$ , at closer distances from the walls. These currents, in turn, result from higher plasma conductivities which are strong functions of temperature and electron number density which, as seen from Fig. 5.4, are increasing at points closer to the wall as the downstream flow develops. (The natural variation of  $T_e$  with temperature (or degree of ionization) behaves according to the following pattern: For degrees of ionization less than 0.1%,  $T_e$  is an exponential function of  $T$ , rising rapidly; as the ionization exceeds this value,  $T_e \sim T^{3/2}$ ). The equilibrium electron mass-fraction profiles,  $C_e^* / C_{eG}$ , are plotted in Fig. 5.6 for similar run conditions and with  $B=0$  and  $B=2$ . All computational runs presented in this work include electromagnetic field damping of turbulent fluctuations.

### 5.3.2 MHD Influence on Film-Cooled Boundary Layer Temperature Profiles and Film-Cooling Effectiveness

The characteristics of a wall jet flow for the MHD velocity profiles shown in Fig. 5.2 would result in the upper half of the jet drawing into it the hotter fluid of the core flow while the lower half of the jet would do the same for the coolant fluid.

As discussed in the previous Section 5.3.1, the effect of this jet in keeping two fluid streams "separated" for a considerable distance downstream, results in a reduced heat transfer between them since the rate of mixing is reduced and velocity fluctuations are damped. This would result in lower boundary layer temperatures near



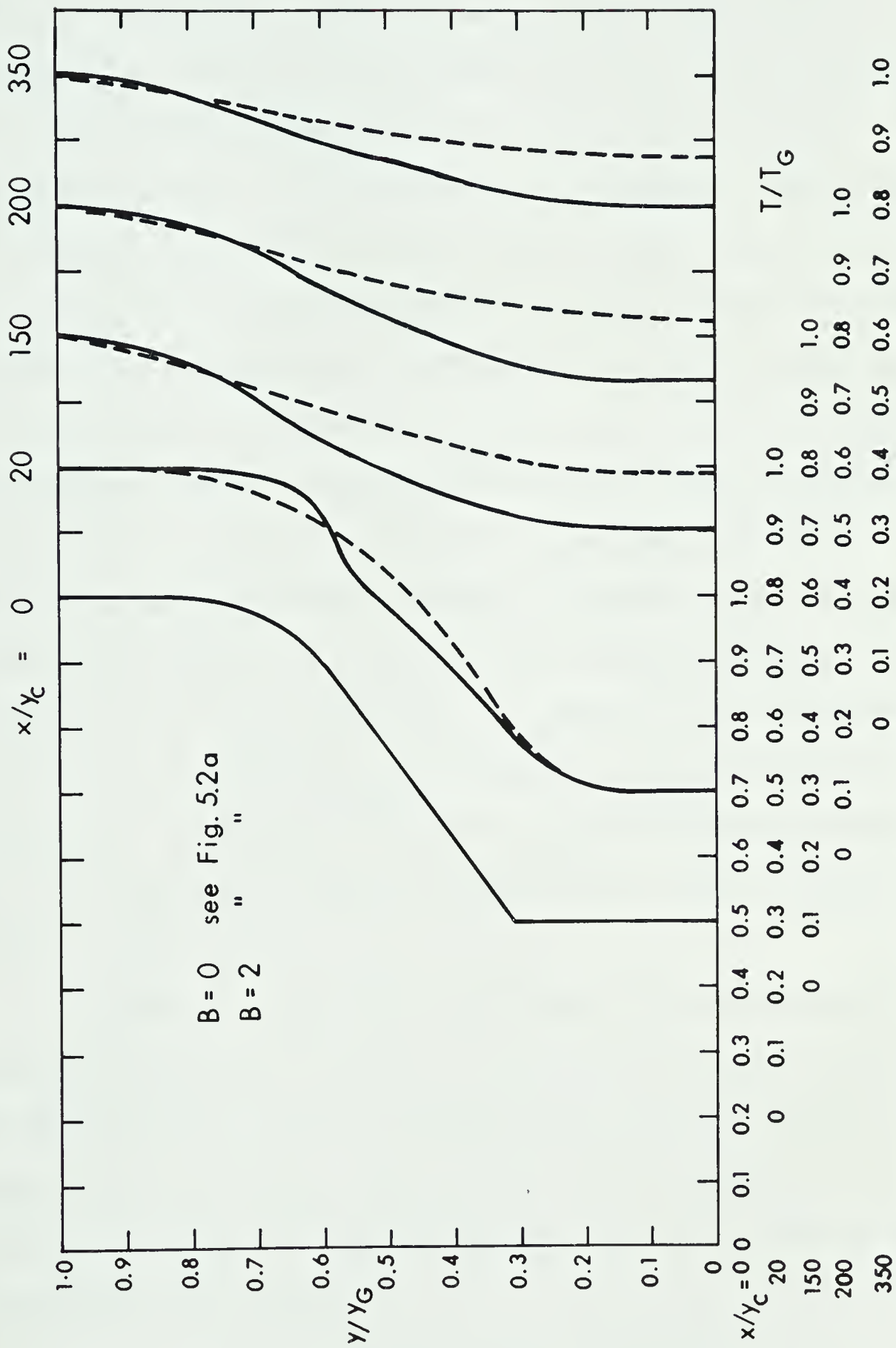


Fig. 5.4 MHD Influence on Film-Cooled Boundary Layer Temperature Profiles-Equilibrium Case



the wall and hence an increased effectiveness. Both these observations are substantiated from Figs. 5.3, 5.4 where the expected trends are easily seen. With the run conditions used for Fig. 5.4, the reduction in boundary-layer temperatures near the wall, when going from OHD flow to MHD film-cooling ( $B=2$  in this case), is approximately 10% at downstream distances of interest. The corresponding increase in film-cooling effectiveness is seen from Fig. 5.3, and, for a particular downstream position of  $x/y_C=200$ , amounts to approximately 55%. The temperature profile given for twenty slot-heights in Fig. 5.4 shows the effect of convective heat transfer resulting from the core flow mass entrained into the mixing region as depicted by the velocity profile depression for  $x/y_C=20$  and, at the same normal distance from the wall, as seen by comparing Figs. 5.2 and 5.4. The core flow temperature difference for a zero and non-zero ( $B=2$ ) magnetic field are not significant, so that the normalized temperature curves in Fig. 5.4 can be compared directly as actual temperature differences. For example, at  $x/y_C=150$ , the free stream temperature,  $T_G$ , for the OHD flow, is  $2995^\circ\text{K}$  and for  $B=2$  this value is  $2946^\circ\text{K}$  - a nominal 2% lower value.

Because of some primary and secondary flow mixing and resulting convection heat transfer as well as heat transfer through conduction, the temperature at increasing distances from the slot increases at closer points to the wall. This trend is clearly evident on Fig. 5.4 which results in part from the decreasing locus of the velocity maxima as discussed in Fig. 5.2b.





$$U_{G_0} = 280 \text{ m/s}$$

$$U_C/U_{G_0} = 0.5$$

$$U_C = 140 \text{ m/s}$$

$$T_C/T_{G_0} = 0.5$$

$$T_{G_0} = 3000^\circ\text{K}$$

$$\rho_C/\rho_{G_0} = 2.0$$

$$T_C = 1500^\circ\text{K}$$

$$B = 2.0$$

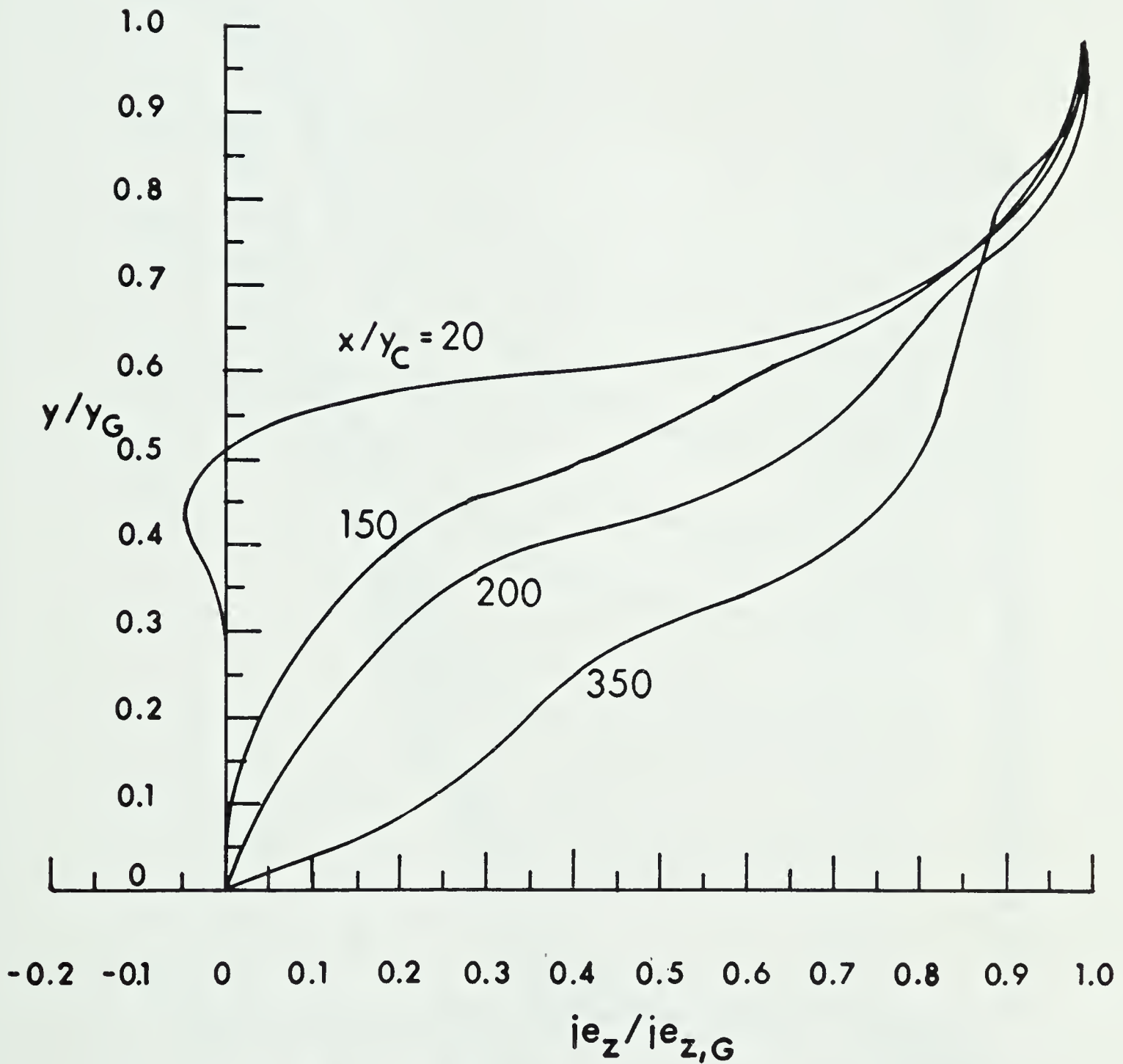


Fig. 5.5 Electron - Current Density Boundary - Layer Profiles, Equilibrium Case



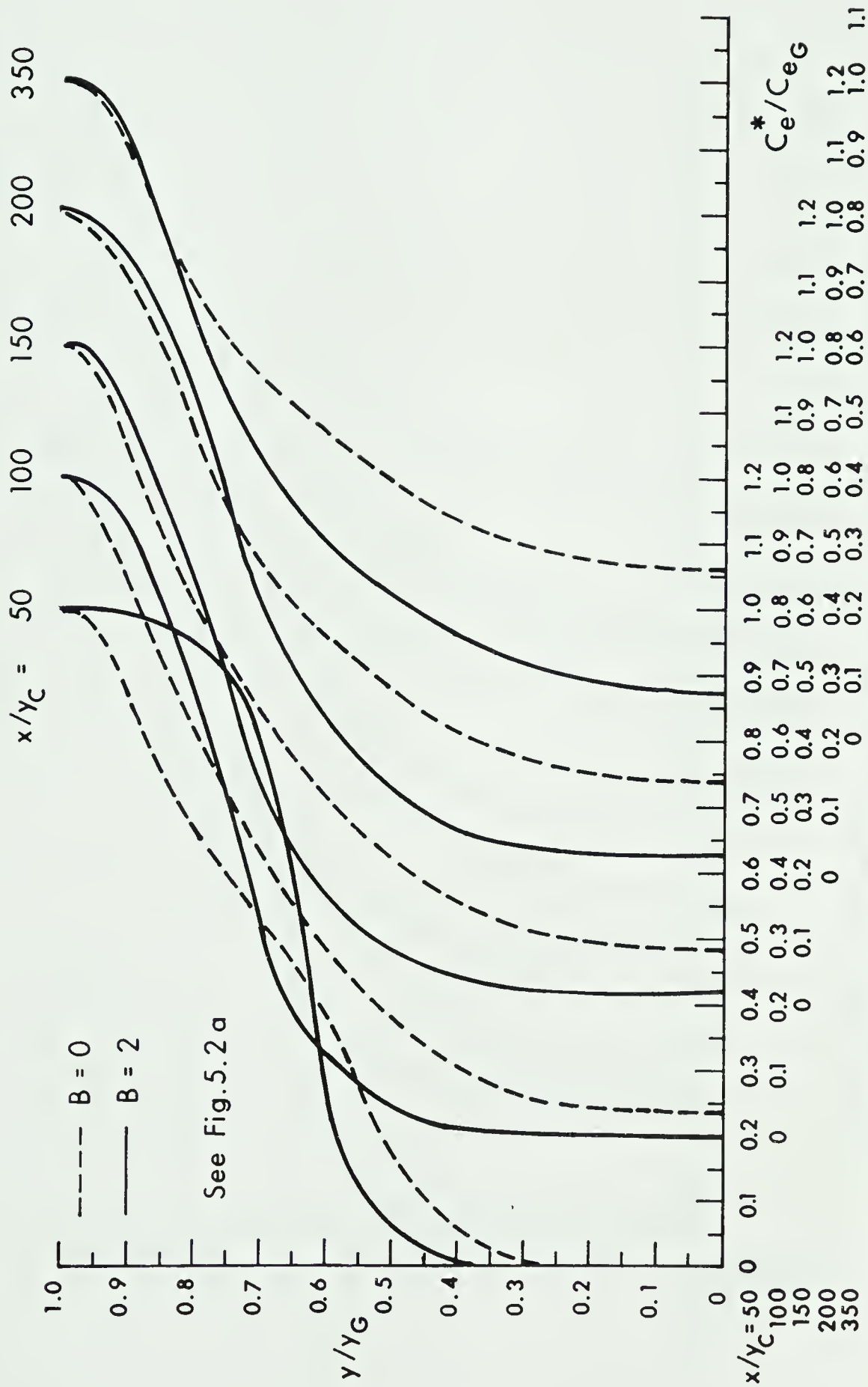


Fig. 5.6 Equilibrium Electron Mass Fraction Boundary-Layer Profiles



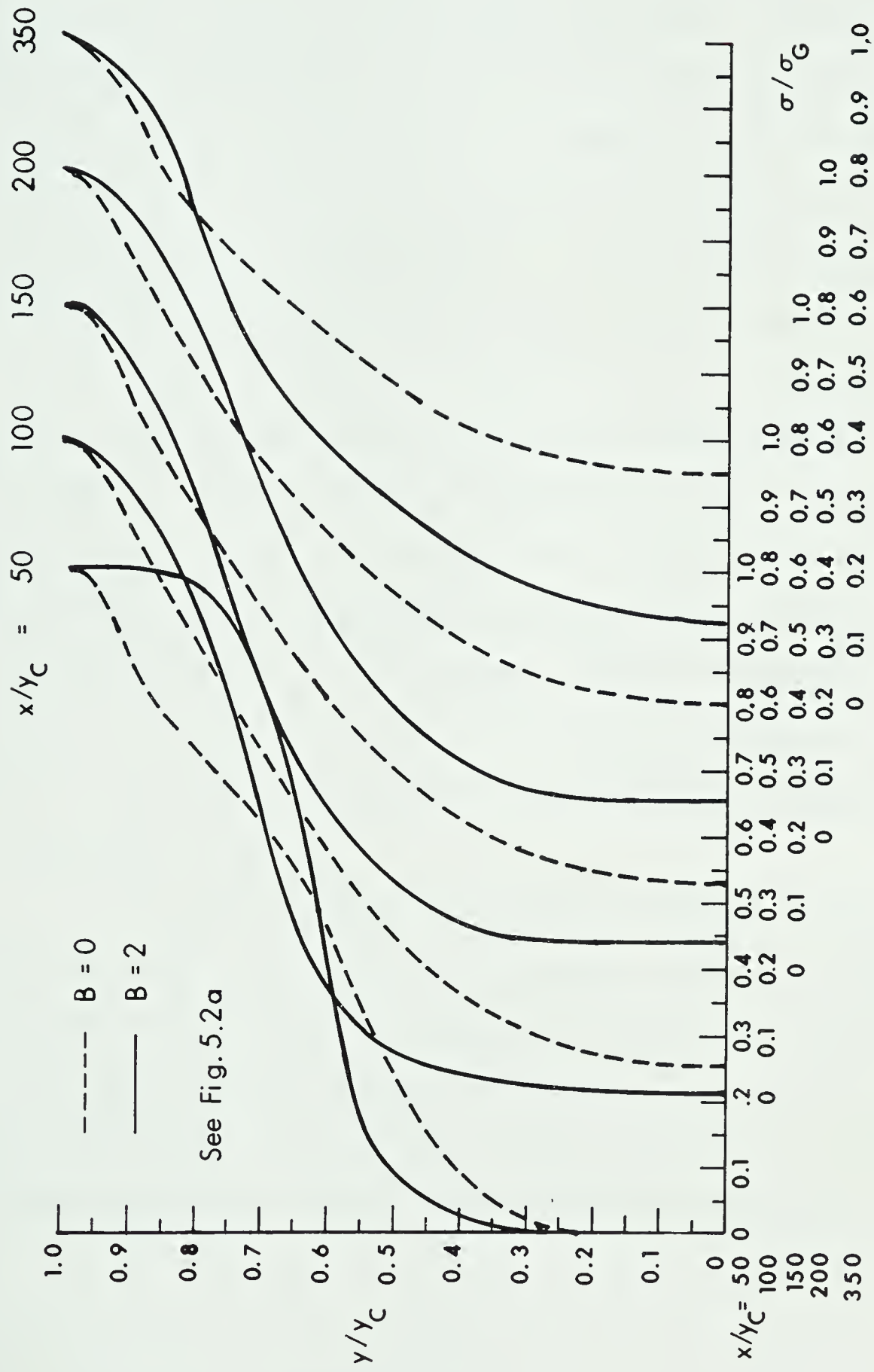


Fig. 5.7 Equilibrium Plasma Electrical Conductivity Boundary-Layer Profiles



The temperature boundary layer profiles observed for the run conditions of Fig 5.4 do not display any sign of Joule dissipative heating, even at 350 slot heights downstream. The profiles show that the temperature in the film-cooled boundary layer is everywhere less than that of the free stream. Joule dissipation effects are, of course, more pronounced in electrode boundary layers where high electric currents prevail. Viscous dissipative heating is seen to be insignificant as well for these run conditions.

Actual MHD generator channel B-walls will, of course, not be completely adiabatic especially when high temperature gas flows are encountered. The heat transfer experienced in actual channel walls would reduce boundary layer temperatures so that Fig 5.4 represents the maximum possible temperatures attainable in the boundary layer. As mentioned earlier, this is the most important information required by the design engineer for the generator design although the heat transfer rate would have to be known to predict MHD generator performance and efficiency.

In comparing Fig 5.2, 5.3, and 5.4 together it is apparent that, for equilibrium plasma flow, the major cause for the observed increase in the film-cooling effectiveness over that in OHD flows, is the significant alteration of the boundary-layer velocity profiles with appreciable contributions to higher  $\eta$  resulting from MHD turbulence damping and reduced boundary layer temperatures at the wall.





### 5.3.3 Influence of Variation in Flow-Parameters on MHD Film-Cooling Effectiveness at Constant Magnetic Field

As mentioned in Section 1.2.3, extensive research both experimental and theoretical, has been undertaken for OHD film-cooling to investigate the influences of different flow parameters on the film-cooling effectiveness. Some of the studies relevant to the tangential-injection slot geometry (chosen for the present investigation) are briefly discussed here. Whitelaw [77] presented measurements of the impervious wall effectiveness of a two dimensional wall jet. The measurements were obtained using slot heights of 0.5, 0.25, 0.132 and 0.074 inches, several slot-to-free-stream velocity ratios  $U_C/U_{Go}$  ranging from 0.288 to 2.66, and coolant Reynolds numbers,  $745 \leq Re_C \leq 44,000$ . The measurements confirmed results from other investigators that the optimum effectiveness is obtained when  $U_C/U_{Go}$  is close to unity but that the magnitude of  $\eta_{opt}$  is dependent upon the slot height to a considerable extent.

Eckert and Birkebak [78] studied the effect of slot geometry on film-cooling in a system which used air in the primary and secondary flows. Experiments were made with a tangential-injection slot and velocity and temperature boundary-layer profiles were measured from which the film-cooling effectiveness was calculated. Wider slots gave better performance in the sense that less mixing occurred at the slot exit resulting in somewhat higher values of  $\eta$ . Results when compared to measurements of Seban and Back [79,80] indicated that the optimum slot geometry depends on the ratio of the mass velocities in the main (primary) stream and in the coolant (secondary) stream and also on its range of variation.



Cole and Spalding [3] applied their finite-difference numerical procedure to investigate the influence of the initial velocity profile shape and slot lip thickness,  $t_L$ , on  $\eta$  and made comparisons with the experimental measurements of others. The shape of the initial velocity profile was found to have a weak influence on the adiabatic wall effectiveness although a more realistic initial velocity profile, also prescribed in the present work, gave better agreement with experiment for the near slot region over the range of velocity ratios computed,  $0.5 \leq U_C/U_{Go} \leq 1.7$ . The effect of  $t_L$  was not completely resolved and further refinement was planned for improved comparison with experimental measurements.

Measurements made by Kacker and Whitelaw [81] related to the influence of initial velocity profiles at the tangential-injection slot, supported conclusions that such film-cooled boundary layers have short lived memories. The effect on the impervious wall effectiveness of the thickness of the initial boundary layer on the upper lip of the slot was shown to be not greater than 5 per cent. The range of velocity ratios considered was  $0.3 \leq U_C/U_{Go} \leq 2.05$ . The same authors [65] also used a numerical procedure for solving the steady, two-dimensional, constant property form of the Navier-Stokes equations to obtain predictions of mean and fluctuating properties downstream of a tangential-injection film-cooling slot. Among the parameters studied, which influence film-cooling effectiveness, were the velocity ratio, Reynolds number, upper lip boundary-layer thickness, shape of the slot velocity profiles, slot and free-stream turbulence intensities, and the slot lip thickness.



In order to assess the corresponding influence of some of these parameters on the MHD film-cooling effectiveness, several runs were performed where the magnetic field was kept constant ( $B=2$  in this case) and other parameters were varied. Figure 5.8 shows the film-cooling effectiveness at different magnitudes of primary and secondary flow velocities and temperatures. Two computations are also shown at similar temperatures and velocities but with  $B=0$  to illustrate the relative influence of  $B$  compared with the effects of other flow parameters.

It can be seen that the influence of velocity and temperature on the OHD film-cooling effectiveness (curves 6 and 7) is much more pronounced than the corresponding influence of the same parameters on the MHD film-cooling effectiveness (curves 1 and 4). In other words, the existence of electromagnetic body forces suppresses the magnitude of the influence that these same parameters exert on  $\eta$  in OHD film-cooling flows.

It is observed furthermore, that the magnitude of change in  $\eta$  from OHD to MHD film-cooling effectiveness depends significantly on the magnitudes of the initial velocities and temperatures of the primary and secondary flows (curves 1 and 7 and 4 and 6).

The difference in magnitude as well as in direction depends also on the downstream position of the region in question. For example, at 200 slot heights the increase in  $\eta$  from OHD to MHD flow was only about 18% for  $U_{Go}=250$ ,  $U_C=125$ ,  $T_{Go}=2500$ ,  $T_C=1250$  (curves 1 and 7) while the corresponding increase in  $\eta$  was approximately 250%





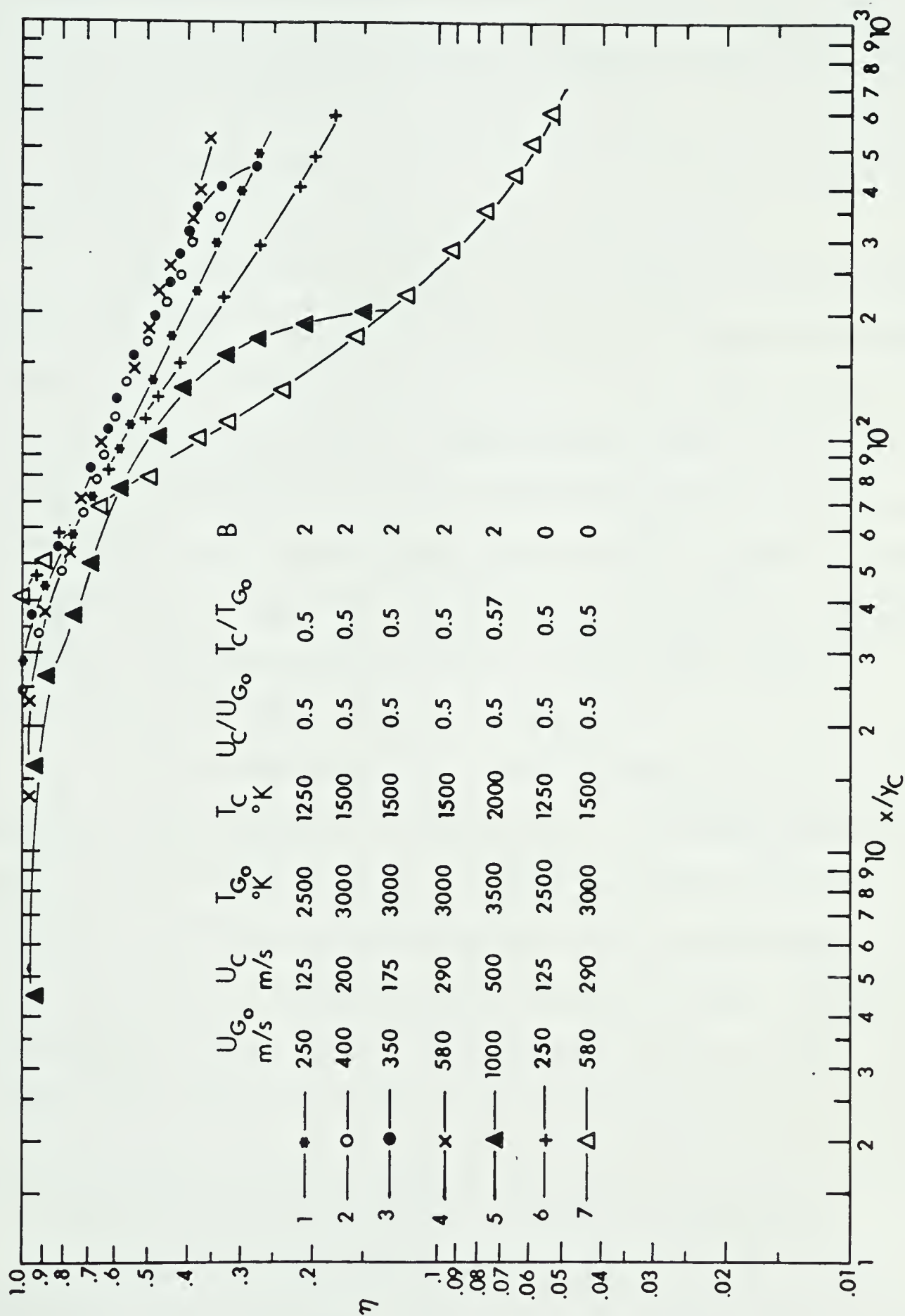


Fig.5.8 Influence on MHD Film-Cooling Effectiveness for Constant  $B$  and Variable Core Flow Parameters - Equilibrium Case





for  $U_{Go}=580$ ,  $U_C=290$ ,  $T_{Go}=3000$ ,  $T_C=1500$  (curves 4 and 6)! For both run comparisons it is observed that in the near-slot region (small  $x/y_C$ ) the film-cooling effectiveness is reduced for MHD flows. The cross over point occurs at  $x/y_C \approx 80$  for the lower initial velocities and temperatures (curves 1 and 7) while a similar change occurs at  $x/y_C \approx 60$  for the higher initial values (curves 4 and 6).

The results shown on Fig. 5.8 also indicate that for a specific value of magnetic field ( $B=2$  in this case), the film-cooling effectiveness remains a fairly constant function of  $x/y_C$  after certain values of initial velocity and temperature have been reached. For example, at  $x/y_C=200$  the increase in MHD film-cooling effectiveness was approximately 19% in changing from  $U_{Go}=250$ ,  $U_C=125$ ,  $T_{Go}=2500$ ,  $T_C=1250$  to  $U_{Go}=350$ ,  $U_C=175$ ,  $T_{Go}=3000$ ,  $T_C=1500$  (curves 1 and 3). Any further increase in these parameters resulted in a negligible change of film-cooling effectiveness (curves 2, 3, and 4).

A final observation made in Fig. 5.8 concerns curve 3 with  $U_{Go}=1000$ ,  $U_C=500$ ,  $T_{Go}=3500$ ,  $T_C=2000$ , and  $B=2$ . The effectiveness is seen to drop off rapidly to zero at approximately 200 slot heights downstream. This would indicate that the flow has become choked at  $x/y_C \approx 200$  which is a consequence of the physical channel size and slot geometry chosen in the present work and the fact that the initial Mach number was already close to unity ( $M_{Go}=0.86$ ).

#### 5.3.4 Influence of Initial Magnetic Field, $B_o(x)$ , Variation on Boundary Layer Profiles and Film-Cooling Effectiveness

Because of computational problems arising in the finite-difference technique, Sherman, et al. [8] were forced to allow a



gradual but rapid increase in axial variation of the assumed initial magnetic-field  $B_0(x)$ . Similar difficulties arose also in the present investigation where computational problems were encountered in using a step function for  $B_0(x)$  at  $x=0$ .

It has been shown in OHD film-cooling research, for example Refs. [3] and [65], that the shape of the initial boundary layer profiles have relatively small effects on  $\eta$  at downstream distances of main interest. Computations performed in the present work indicate that similar conclusions can be stated for the MHD film-cooling effectiveness. The functional relationships for  $B_0(x)$ , assumed as initial condition for the MHD finite-difference procedure, however, have shown to be of more significance. Several runs were therefore performed with a linearly increasing function,  $B_0(x)$ , whose slope was varied in a gradual approach to a step function. Figure 5.9 compares the developing velocity profiles for the identical run conditions shown except that  $(x/y_C)_{\max}=1$  and 10, respectively, in the relation  $B_0=B_{\max}$  at  $x/y_C=(x/y_C)_{\max}$ , where  $B_{\max}=2$ . The shape of the profiles are similar in each case but, as expected, the magnetic field which reaches its maximum at closer distances to the slot, induced a greater acceleration of the boundary layer fluid relative to that in the freestream. The difference in velocity profiles is still evident at approximately 150 slot heights although its magnitude has negligible influence on the film-cooling effectiveness (shown on Fig. 5.11) for the same run conditions (curves 1 and 2).

Figure 5.9 also shows how the MHD velocity boundary-layer profiles become fuller with an increase in the velocity ratio maxima



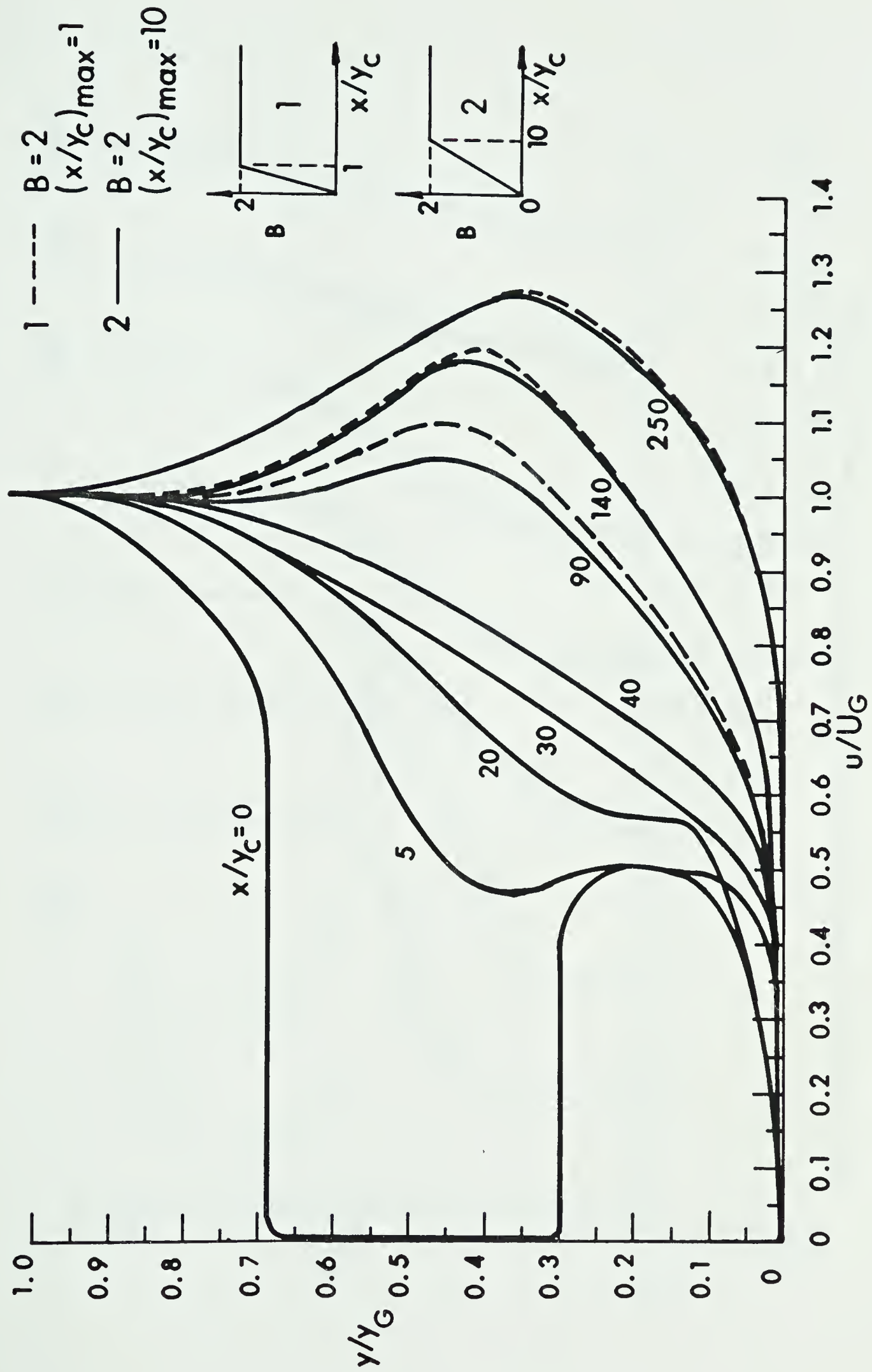


Fig. 5.9 Influence of Initial Condition for  $B(x)$  on MHD Film-Cooling Velocity Profiles





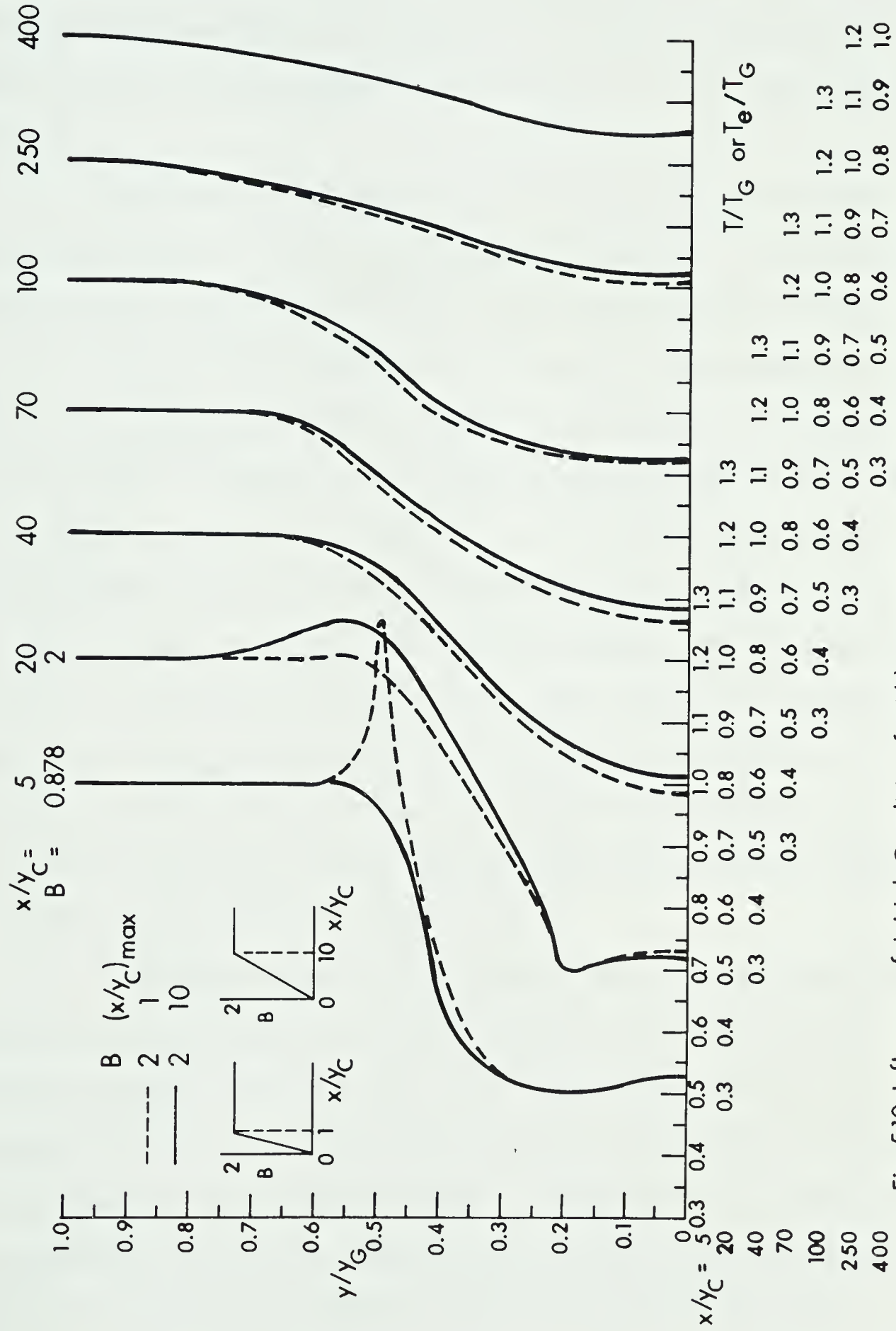


Fig.5.10 Influence of Initial Condition for  $B(x)$  on MHD Film-Cooling Temperature Profiles





$u_{\max}/U_G$  at farther distances downstream. This is a consequence of the increasing mass entrainment into the boundary layer flow, resulting from greater downstream electromagnetic retarding forces on the core flow and the requirement for conservation of mass flow along the channel.

The temperature profiles resulting from the two different functional values for  $B_0(x)$  are plotted on Fig. 5.10. The computational problems are evident from the large temperature overshoot at  $y/y_G \approx .5$  and  $x/y_G = 5$ . The profile at  $x/y_G = 5$  (for the magnetic field equal to its maximum at  $(x/y_G)_{\max} = 1$  (dashed curve)) is seen recovering from the sudden change in magnetic field. The velocity profiles in Fig. 5.9 (for the case of magnetic field which is still developing, having reached approximately 50% of its maximum value at  $x/y_G = 5$ ) are seen to be well behaved. At twenty slot heights, however, the first profile appears to have recovered (solid curve) while the second case profile, that with  $(x/y_G)_{\max} = 10$  is still showing signs of instability. It is noted in Fig. 5.10 that, similar to the downstream convergence of velocity profiles, the temperature profiles become virtually identical at approximately 150 slot heights.

From these results, it was decided that all subsequent computations would be performed with a magnetic field  $B$  reaching its maximum constant value at  $x/y_G = 1$  since, among other reasons, the magnetic field in actual MHD generator ducts would already be fully established at the film-cooling slot. Any instabilities which were encountered in the initial steps of the computational marching procedure were completely damped at twenty slot heights downstream.



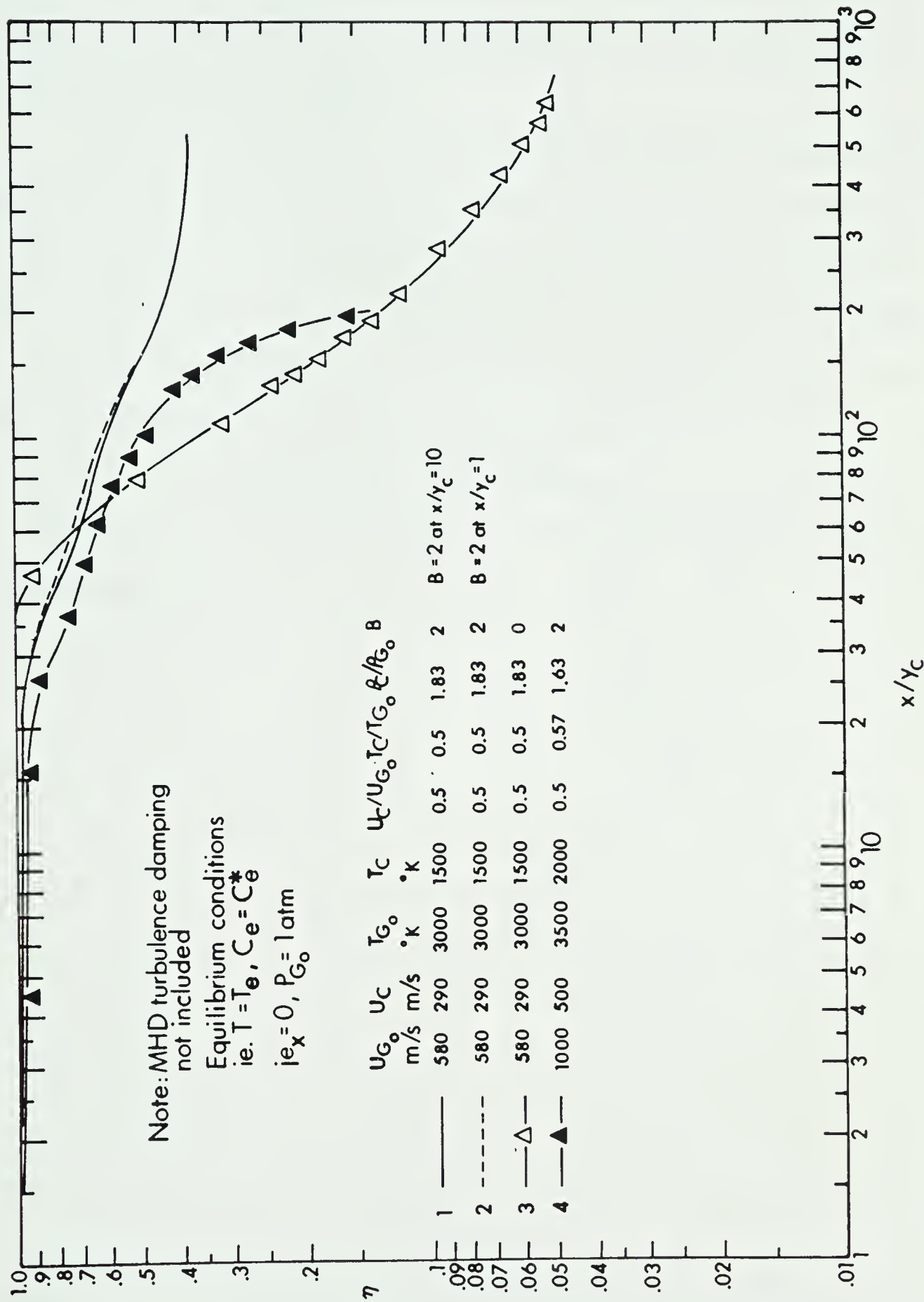


Fig. 5.11 Influence of Initial Condition for  $B(x)$  on MHD Film-Cooling Effectiveness



It should perhaps be noted that damping of any initial instabilities could have been accomplished at even smaller distances by choosing appropriate smaller increments  $\Delta x$  in the forward step of the finite-difference procedure.

Figure 5.12 displays more intermediate developing temperature profiles for the same run conditions shown on Fig. 5.10; solid curves represent  $B_o = B_{\max}$  at  $(x/y_c)_{\max} = 10$ . It can be seen that the profiles converge at the wall for downstream distances up to approximately 30 slot heights, beyond which  $T_{aw}$  increases to its recovery value. The lower boundary of the mixing core emerging from the slot lip is therefore seen to impinge on the film-cooled wall at  $x/y_c \approx 30$  and represents the point at which the film-cooling effectiveness begins to decrease from unity.



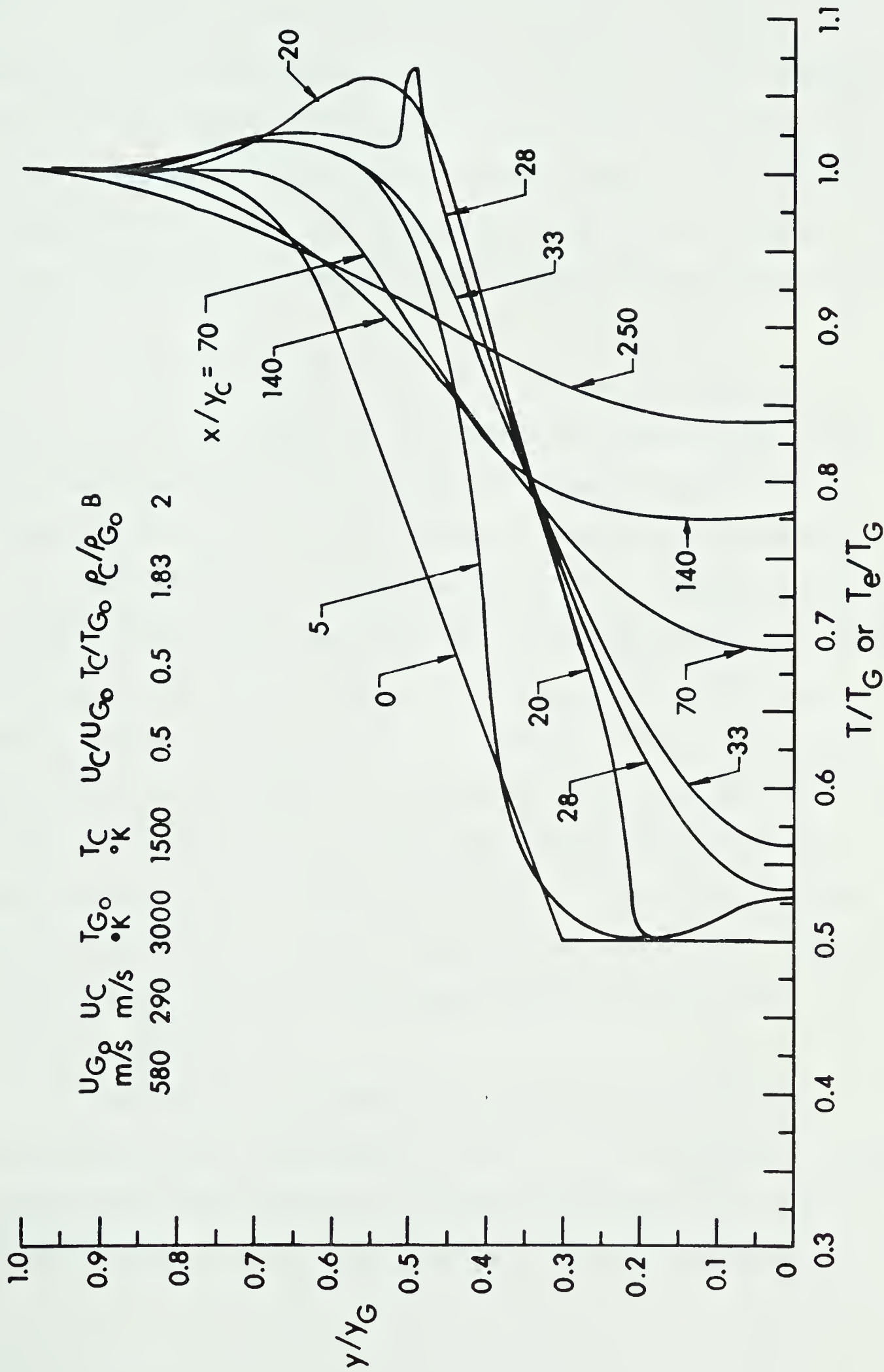


Fig. 5.12 Developing Boundary Layer Temperature Profiles in MHD Film-Cooling for  $B = 2$  at  $x/\gamma_{C,max} = 10$ , Equilibrium Case





#### 5.4 Thermal and Ionizational Non-Equilibrium MHD Film-Cooling

Solutions to Eqs. (2.4) and (2.5), governing electron conservation and temperature, were more difficult to obtain. Because of the strong dependence of the plasma electrical properties on the electron temperature,  $T_e$ , very small forward steps,  $\Delta x \approx 0(10^{-6})$ , and extended precision numerical computations as well as an iteration procedure for the wall electron concentrations and temperatures were required.

The MHD influence on the near-slot velocity profiles are shown in Fig. 5.13, where they are compared with those of similar MHD run conditions but for equilibrium flow. The electromagnetic body forces for non-equilibrium flows are seen to have a similar influence on the velocity profiles as was observed in Fig. 5.2 except that the effect is significantly more pronounced for non-equilibrium conditions. The larger  $\vec{j} \times \vec{B}$  forces resulting from the relative higher current densities (shown plotted in Fig. 5.14) have the effect of destroying the velocity maxima nearer to the film-cooling slot and cause the profiles to become fuller at smaller downstream distances than was the case for equilibrium MHD flows, Fig. 5.13. The velocity profiles farther away from the injection slot are shown in Fig. 5.15. Location of the velocity maxima for the non-equilibrium profiles in this figure is somewhat lower.

The resulting influence on the near-slot boundary-layer temperature profiles can be seen on Fig. 5.16. The temperature in the boundary layer near the wall is increased significantly as a result of the increase in higher temperature core flow becoming entrained



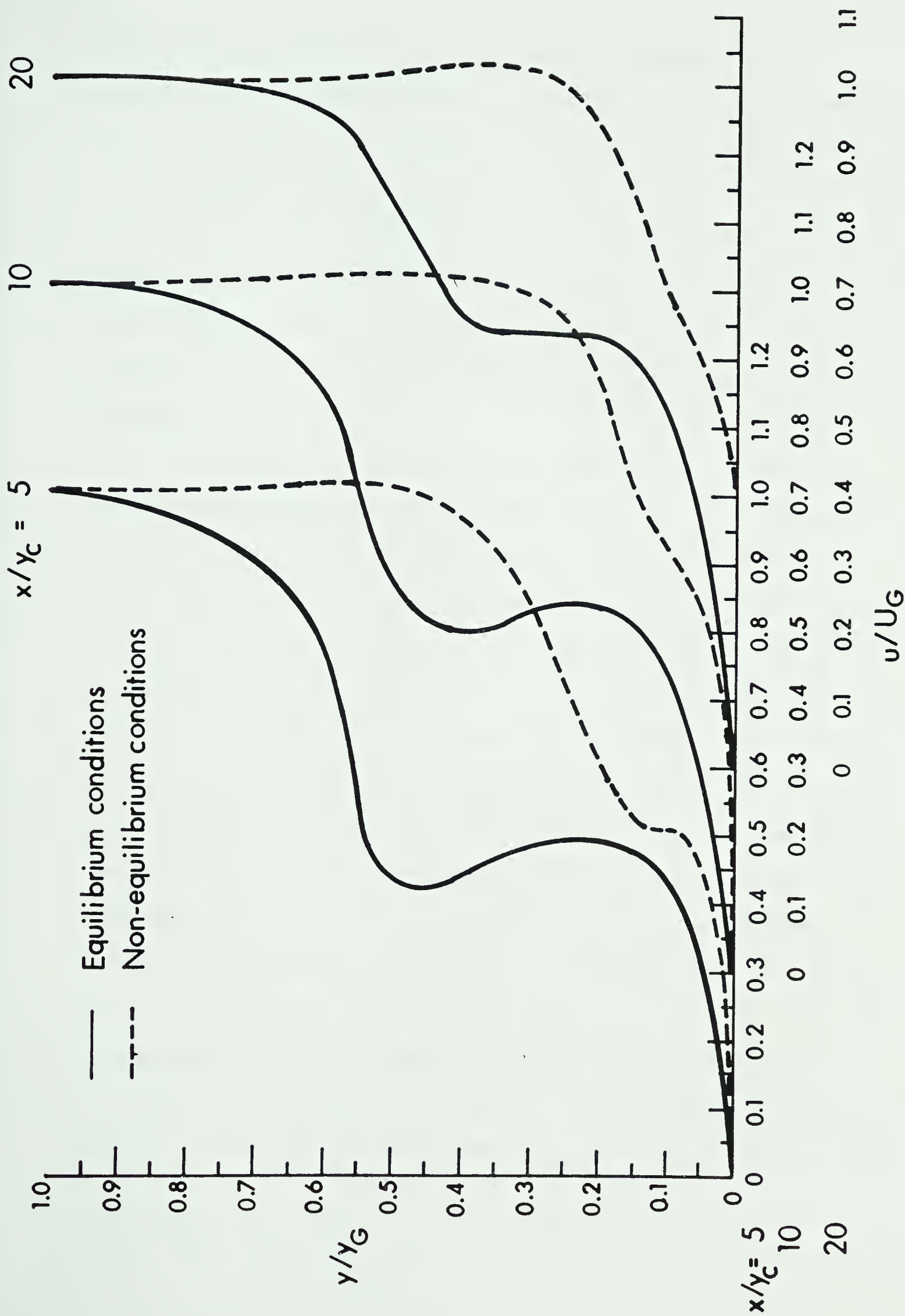


Fig. 5.13 Effect of Non-Equilibrium on MHD Film-Cooling Velocity Profiles



into the mixing region as is evident from the non-equilibrium velocity profiles shown previously in Fig. 5.13. It is noted, however, that the non-equilibrium effect on the adiabatic wall temperature is not as pronounced and  $T_{aw}$  is seen to be increased only slightly above its equilibrium flow counterpart. The electron temperature on the other hand, has its greatest rise above the main gas temperature in the rear wall region although any appreciable increase in heat transfer to the wall due to the higher electron temperature is not evident.

The higher current densities in the near wall region also produce a greater MHD turbulence damping which, in turn, reduce heat transfer from the hotter far-wall boundary layer region towards the colder wall. The tangential injection of the colder secondary fluid is seen to absorb any temperature increases near the wall which would be expected from higher Joule dissipation in the non-equilibrium case. Farther downstream from the film-cooling slot, however, some increase in the near wall boundary layer temperature is evident from Fig. 5.16. This is due to increasing Joule dissipation resulting from the higher non-equilibrium current densities as shown plotted on Fig. 5.14. The magnitude of the maximum current overshoot observed in the present solutions is considerably less than that reported in Ref. [7], where the near wall current densities were as high as eight times their free stream value. It can be expected that the film-cooling fluid acts to reduce the magnitude of the increase in electron temperature above that of the main gas, but when compared to the large current overshoots





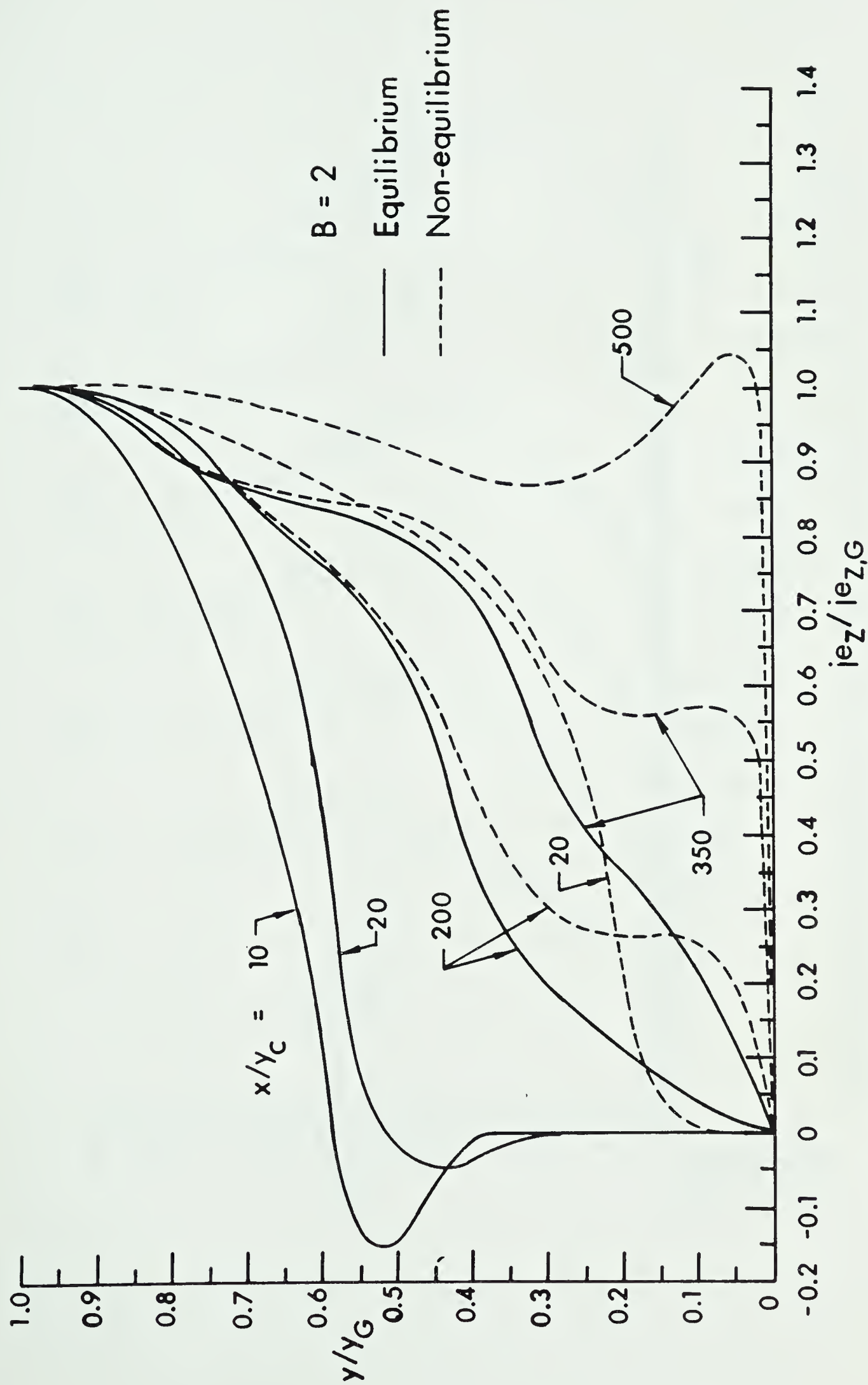


Fig. 5.14 Effect of Non-Equilibrium on Boundary-Layer Current Density Profiles





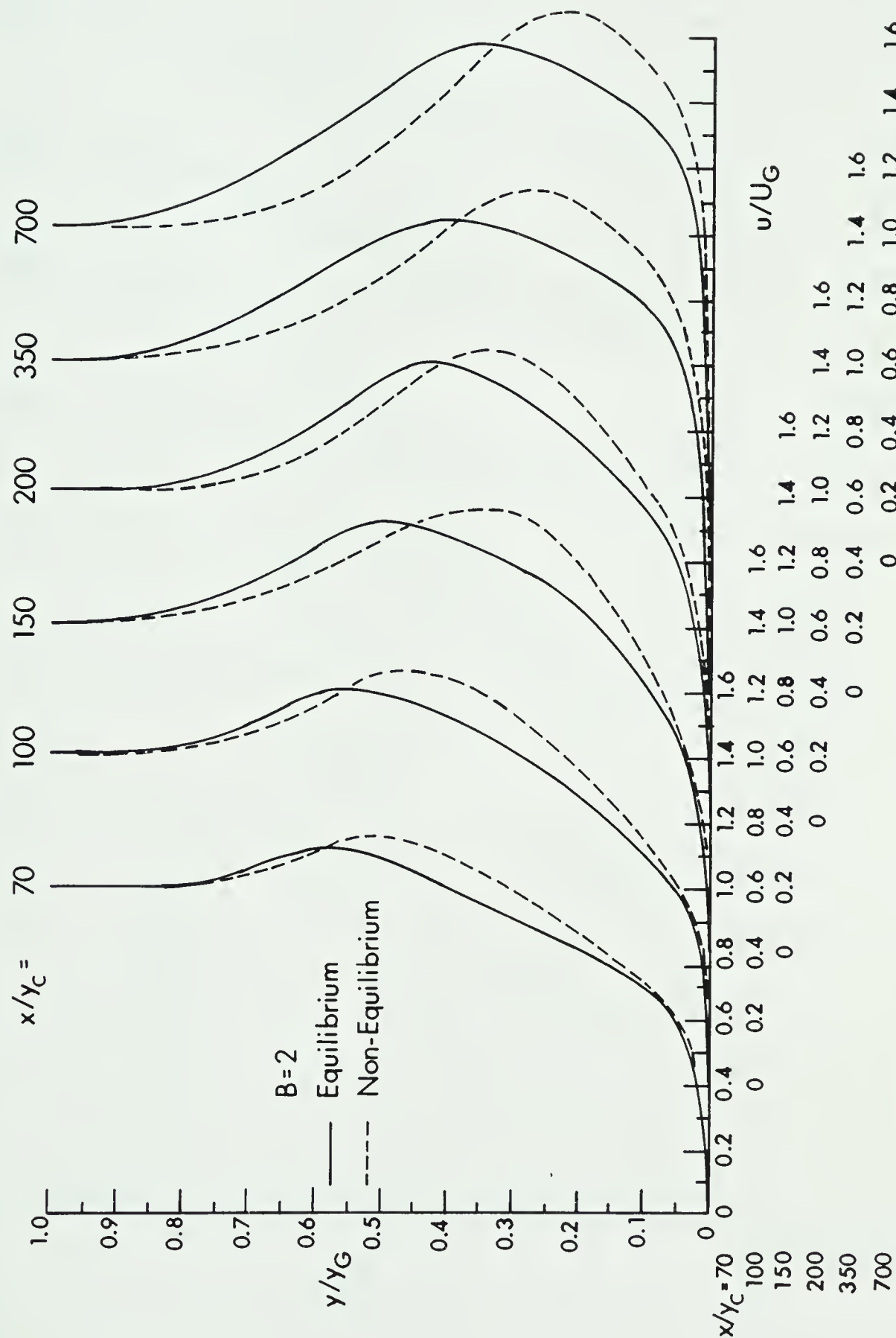


Fig.5.15 Effect of Non-Equilibrium on MHD Film-Cooling Velocity Profiles -Far Slot Region



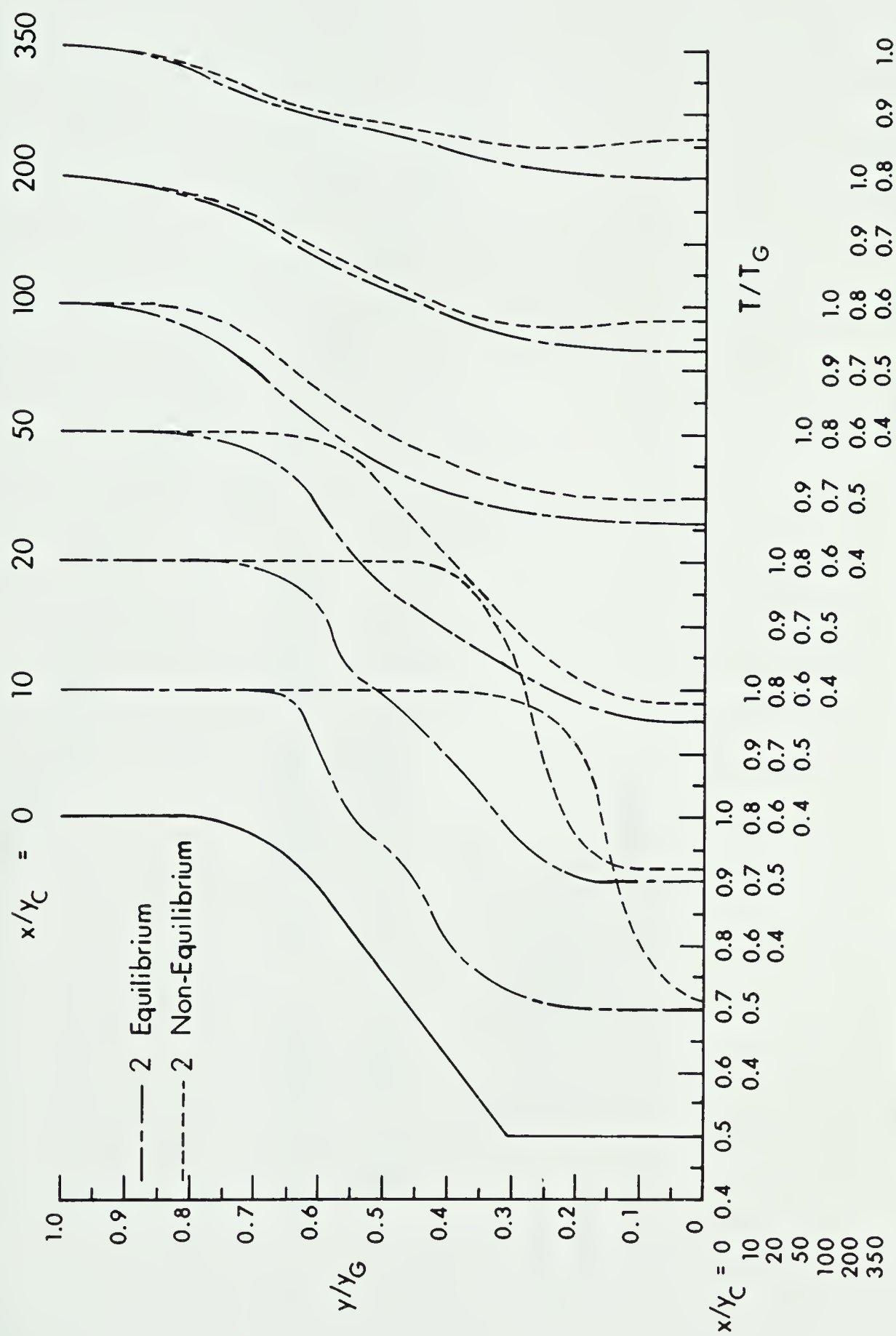


Fig.5.16 Effect of Non-Equilibrium on Boundary Layer Temperature Profiles



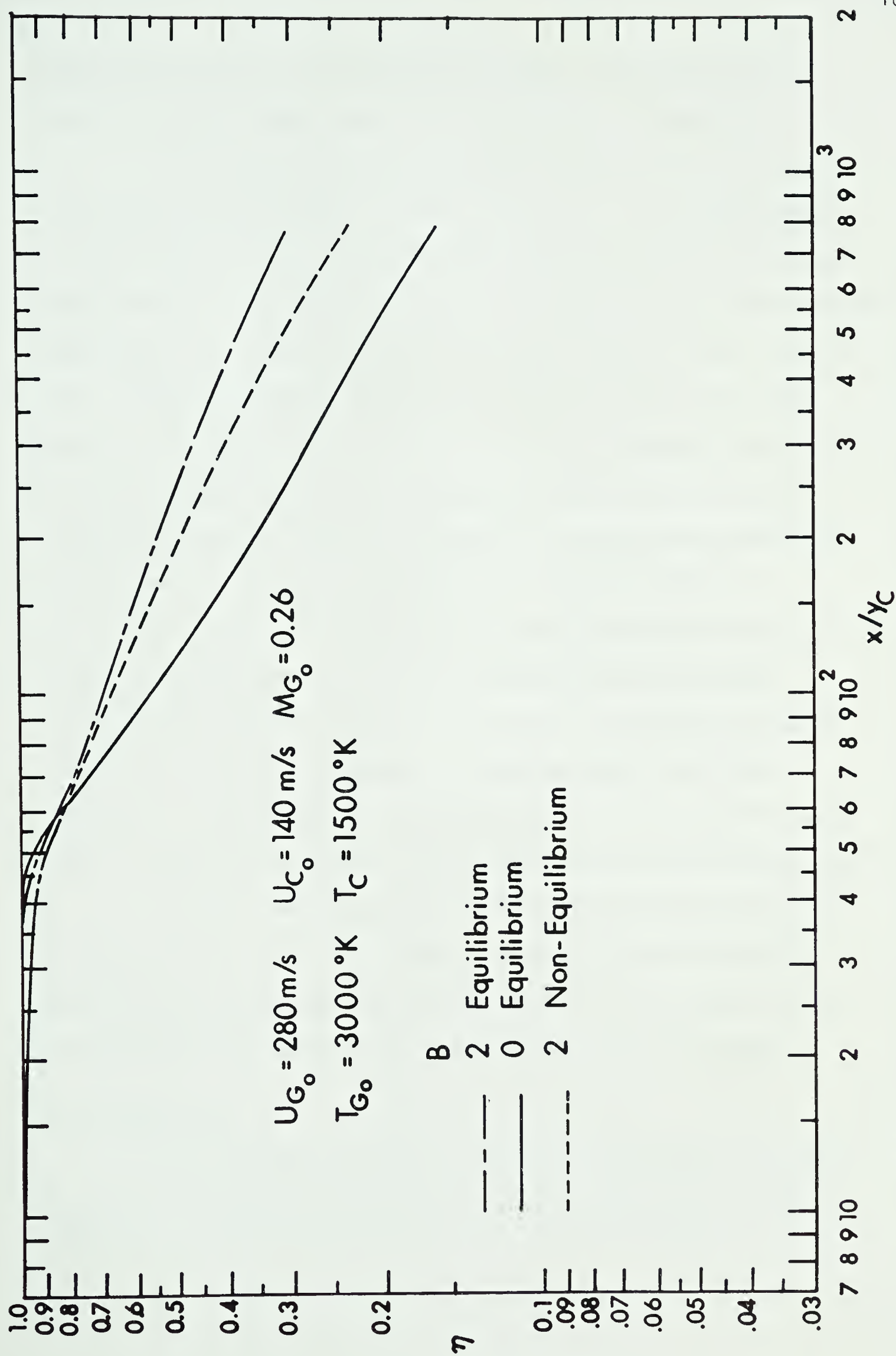


Fig. 5.17 Influence of Non-Equilibrium on MHD Film-Cooling Effectiveness



obtained in Ref. [7], the significantly higher freestream current densities applied there must also be taken into consideration.

The higher adiabatic wall temperatures result in a lower film-cooling effectiveness as shown in Fig. 5.17. The effectiveness is lower than both the equilibrium MHD value and the OHD film-cooling effectiveness in the near-slot region. At approximately 60 slot heights downstream, the non-equilibrium effectiveness becomes greater than its OHD counterpart although it remains less than the equilibrium MHD value at all downstream locations. The difference between equilibrium and non-equilibrium MHD effectiveness also grows larger at greater downstream distances, partly as a result of increased non-equilibrium current densities giving rise to greater Joule dissipation.

The larger  $\vec{j} \times \vec{B}$  forces near the wall can also be seen in Fig. 5.15 to result in a shift of the maximum velocity overshoot closer towards the wall which in turn results in a greater mixing of the hotter free stream fluid with the cooling layer. Both this effect and increasing Joule dissipation near the wall result in lower MHD film-cooling effectiveness when compared with the equilibrium case.

For the cases computed (up to the maximum downstream station indicated by Fig. 5.17), both equilibrium and non-equilibrium film-cooling effectiveness were greater than their OHD counterpart in the far downstream region which is of most interest to the designer.

## 5.5 Conclusions

The fundamental process of tangential-injection film-cooling has been investigated theoretically for cooling the B-walls of both





equilibrium and non-equilibrium MHD generators. The general finite-difference method of Patankar and Spalding for solving heat and mass transfer boundary layer flows has been modified in a universal way to allow MHD heat and mass transfer flow analysis. The free molecular sheath analysis required for non-equilibrium conditions, however, requires individual analysis for the flow conditions under consideration.

The overall influence of electromagnetic body forces on the adiabatic film-cooling effectiveness results in a significant difference over its OHD counterpart. As the magnetic field induction,  $B$ , is increased from zero to moderate values, an increase in  $\eta$  is observed and this increase grows larger with increasing distance downstream from the coolant injection slot. As an example for the flow conditions shown in Fig. 5.3 an increase of 23% is observed at  $x/y_C=100$  and 86% at  $x/y_C=500$  when  $B$  is changed from 0 to 1. As the magnetic field induction is increased further to  $B=2$  the film-cooling effectiveness is not significantly altered farther downstream. Nearer the slot, however,  $\eta$  is decreased and for  $x/y_C \leq 60$  the decrease results in a lower film-cooling effectiveness when compared with the OHD case. As  $B$  is further increased to extremely large values, the film-cooling effectiveness continues to decrease in the near-slot region whereas farther downstream boundary layer separation or choking of the channel flow will occur. Thus, there appears an optimum value of magnetic field intensity which will result in maximum film-cooling effectiveness for any one particular set of flow conditions. For the run conditions of Fig. 5.3, this optimum magnetic field occurs for values of  $B$  between 1 and 2.



Allowance for electromagnetic field damping of turbulent fluctuations has an appreciable influence on the MHD film-cooling effectiveness. With a particular value of  $B=2$ , for example and the flow conditions indicated on Fig. 5.3, MHD damping of turbulent fluctuations results in an average 15% increase in the film-cooling effectiveness. Allowance for MHD turbulence damping should therefore be included in any MHD film-cooling predictions.

The influence of initial flow parameters and injection slot geometry on the film-cooling effectiveness is not the same for MHD flows when compared with OHD flows. Because the velocity profiles are significantly altered in MHD boundary layers, the optimum film-cooling effectiveness is not necessarily obtained with a coolant-to-primary flow velocity ratio of unity as has been shown the case in OHD film-cooling processes. The optimum velocity ratio  $U_C/U_{Go}$  to achieve maximum effectiveness at any given magnetic field intensity has not been investigated in the present work. This could, however, be determined if many more runs were performed with the present numerical method.

The MHD film-cooling effectiveness is influenced to a lesser degree than its OHD counterpart for similar changes in the initial velocity and temperature ratios,  $U_C/U_{Go}$  and  $T_C/T_{Go}$ . The MHD film-cooling effectiveness does, however, depend on the magnitude of these initial profiles. For a constant magnetic field induction, increases in effectiveness are relatively larger at lower values of initial velocities and temperatures. A definite range of magnitudes for initial velocities and temperatures is obtained which result in negligible further changes in effectiveness at any given magnetic field intensity.



These observations were made by keeping the ratios  $U_C/U_{Go}$  and  $T_C/T_{Go}$  constant at 0.5. The influence of variable initial ratios at constant magnetic field has not been investigated here although, again, such sensitivity analysis could be performed with additional runs of the present computational procedure.

The sensitivity of the MHD film-cooling effectiveness to initial flow conditions is no more pronounced than what has been observed in OHD film-cooling studies. The choice of initial condition for the magnetic field induction, however, influences the downstream solution for  $\eta$  in a more significant way. Although the percentage difference in magnitude observed in the effectiveness is relatively small, this difference is sustained for longer distances downstream from the injection slot. It is therefore more important to prescribe initial magnetic field variations as accurately as possible than is necessary for other initial flow conditions in either MHD or OHD film-cooling predictions.

Thermal non-equilibrium and finite-rate ionization have a significant influence on film-cooling effectiveness. The major cause for this is the alterations of the boundary layer velocity profiles resulting from larger  $\vec{j} \times \vec{B}$  forces. These in turn are the result of increased near-wall current densities,  $j_{e_z}$ , due to the strong dependence of plasma electrical properties on electron temperature and number density.

In the near-slot region the coolant fluid precludes any significant thermal non-equilibrium and temperature rise which would be attributed to Joule dissipation. There is a bulk temperature rise





in the mixing region as a result of the flow velocity distribution although the adiabatic wall temperature, and hence the film-cooling effectiveness, is changed only slightly from that in equilibrium MHD flows. Farther downstream, however, an increasing current density over-shoot develops near the wall which influences the film-cooling effectiveness in several ways. First, a larger velocity maxima is produced in the boundary layer and the resulting wall-jet like flow serves to increase the film-cooling effectiveness in a manner similar to the one observed in the equilibrium case. The shifting of this velocity maxima closer to the wall, on the other hand, brings more of the hotter core-flow gases in closer contact with the coolant-gas layer producing a more rapid temperature rise of the coolant gas. Secondly, a larger current density produced greater MHD damping of turbulent fluctuations such that the rate of this temperature rise is tempered to some degree.

Finally, the increasing current densities at larger downstream distances resulting from greater non-equilibrium conditions, produce a slight increase in the near-wall temperature due to Joule dissipation. This increase is noticeable but relatively small for the flow conditions assumed. The net influence of non-equilibrium therefore is to produce a film-cooling effectiveness that is reduced from its equilibrium counterpart, but remains greater than that for an equivalent OHD flow.

For equal wall thermal protection, therefore, more film-cooling slots are required for non-equilibrium MHD generators than for equilibrium, combustion driven generators. As a matter of relative





comparison, if the film-cooling effectiveness for a channel wall were permitted by design to reduce to 50% of its initial value, then for a particular set of flow conditions, the MHD equilibrium channel should have tangential-injection spaced at 250 slot heights, the MHD non-equilibrium channel at 190 slot heights and the OHD channel at 120 slot heights.



## REFERENCES

- [1] Stangeby, P.C., "A Review of the Status of MHD Power Generation Technology Including Suggestions for a Canadian MHD Research Program", UTIAS Review, No. 39, November, 1974.
- [2] Patankar, S.V., Spalding, D.B., "Heat and Mass Transfer in Boundary Layers", International Text Book Company, London, 2nd Edition, 1970, ISBN 0 7002 0154 8.
- [3] Cole, E.H., Spalding, D.B., "The Calculation of Film-Cooling Processes, with Allowance for Non-Uniform Initial-Property Profiles and for the Effects of Free-Stream Turbulence...", Report No. EHT/TN/B/17, Imperial College, London, 1969.
- [4] Cott, Donald Wing, "Ionizational and Electron Thermal Non-Equilibrium Effects in Compressible Magneto Hydrodynamic Boundary Layers", PhD Thesis, University of Tennessee Space Institute, 1969.
- [5] Cott, D.W., "Ionizational and Electron Thermal Non-Equilibrium in MHD Boundary Layers", AIAA Journal, Vol. 9, No. 12, pp 2404 - 2412.
- [6] Patankar, S.V., Spalding, D.B., "A Finite-Difference Procedure for Solving the Equations of the Two-Dimensional Boundary Layer", Int. Journ. Heat and Mass Transfer, Vol. 10, pp 1389 - 1411, Pergamon Press, 1967.



- [7] High, M.D., Felderman, E.J., "Turbulent MHD Boundary Layers with Electron Thermal Non-Equilibrium and Finite Rate Ionization", AIAA, Vol. 10, No. 1, pp 98 - 103, January, 1972.
- [8] Sherman, A., Yeh, H., Reshotko, E., McAssey Jr., E., "MHD Boundary Layers with Non-Equilibrium Ionization and Finite Rates", AIAA paper No. 71 - 139, AIAA 9th Aerospace Sciences Meeting, New York, January, 1971.
- [9] Sherman, A., Yeh, H., McAssey Jr., E., Reshotko, E., "Summary Report MHD Boundary Layers with Non-Equilibrium Ionization and Finite Rates", Computer and Applied Sciences, Inc., Philadelphia, Pennsylvania, 1970.
- [10] Heighway, J.E., Nichols, L.D., "Brayton Cycle Magnetohydrodynamic Power Generation with Non-Equilibrium Conductivity, NASA TN D-2651 Lewis Research Centre, 1965.
- [11] Sherman, A., "Magnetohydrodynamic Channel Flows with Non-Equilibrium Ionization", The Physics of Fluids, Vol. 9, No. 9, September, 1966.
- [12] Ermolaera, G.K., Yuferev, V.S., "Boundary Layer on Nonconducting Wall of MHD Channel", Magnitnaya Gidrodinamika, Vol. 6, No. 2, pp 45 - 50, April - June, 1970.
- [13] Branover, H., Yakhot, Ed. and A., Ed., "MHD-Flows and Turbulence II", Proceedings of the Second Bat-Sheva International Seminar, Israel Universitites Press, ISBN 7065 15919, 1980.
- [14] Scaglione, A., "An Analytical Study of Turbulent Magnetohydrodynamic Channel Flows", PhD Thesis, Michigan State University, 1970.



- [15] Chandrasekhar, S., Proceedings of the Royal Society, London, A233, 330, 1955.
- [16] Napolitano, L.G., "On Turbulent Magneto-Fluid Dynamic Boundary Layers", Reviews of Modern Physics, Vol.32, No. 4, October, 1960.
- [17] Brouillette, E.C., Lykoudis, P.S., "Magneto-Fluid-Mechanic Channel Flow. I. Experiment", Physics of Fluids, Vol. 10, No. 5, pp 995 - 1011, May, 1967.
- [18] Lykoudis, P.S., Brouillette, E.C., "Magneto-Fluid-Mechanic Channel Flow. II. Theory", Physics of Fluids, Vol. 10, No. 5, pp 1002 - 1006, May, 1967.
- [19] Van Driest, E.R., "On Turbulent Flow Near a Wall", J.A.S. Vol. 23, pp 1007 - 1012, November, 1956.
- [20] Klebanoff, P.S., "Characteristics of Turbulence in a Boundary Layer with Zero Pressure Gradient", Tech. Notes, Nat. Adv. Comm. Aero., Washington, No. 3178, 1954.
- [21] Smith, A.M.O., Cebeci, T., "Numerical Solution of the Turbulent Boundary Layer Equations", Douglas Aircraft Division, Report DAC 33735, 1967.
- [22] Cebeci, T., Smith, A.M.O., "A Finite-Difference Solution of the Incompressible Turbulent Boundary Layer Equations by Eddy-Viscosity Concept", Douglas Aircraft Division, Report DAC 67130, October, 1968.





- [23] Levin, V.B., Chinenkov, I.A., "Experimental Investigation of the Effect of a Longitudinal Magnetic Field on the Friction Factor in Turbulent Flow of an Electrically Conducting Liquid in a Pipe", *Magnitnaya Gidrodinamika*, Vol. 6, No. 3, pp 145 - 146, July - September, 1970.
- [24] Levin, V.B., "On the Transition to Turbulence in Magnetohydrodynamic Flows for Finite Disturbances", *Magnitnaya Gidrodinamika*, Vol. 6, No. 3, pp 50 - 56, July - September, 1970.
- [25] Argyropoulos, G.S., Demitriades, S.T., Lackner, K., "Compressible Turbulent Magnetohydrodynamic Boundary Layers", *The Physics of Fluids*, Vol. 11, No. 12, December, 1968.
- [26] Jett, E.S., Denzel, D.L., Wu, Y.C.L., "Eddy Currents in an Infinitely Finely Segmented Hall Generator", *AIAA Journal*, Vol. 8, No. 9, pp 1592 - 1597, February, 1970.
- [27] Moreau, R., "On Magnetohydrodynamic Turbulence", *Magnitnaya Gidrodinamika*, No. 4, pp 31 - 40, October - December, 1970.
- [28] Dzhaugashtin, K.E., "Turbulent Conducting Liquid Jets, I. Problem Formulation", *Magnitnaya Gidrodinamika*, Vol. 6, No. 2, pp 3 - 11, April - June, 1970.
- [29] Dzhaugashtin, K.E., "Turbulent Jet of Conducting Fluid, II Results of Calculation", *Magnitnaya Gidrodinamika*, Vol. 6, No. 3, pp 3 - 15, 1970.
- [30] Bocheninskii, V.P., Tananaev, A.V., "Velocity Profile for Turbulent Flow in the Presence of a Magnetic Field", *Magnitnaya Gidrodinamika*, Vol. 6, No. 2, pp 148 - 152, April - June, 1970.



- [31] Branover, G.G., Gel'fgat, Yu. M., Kit, L.G., Platnicks, I.A.,  
"Effect of a Transverse Magnetic Field on the Intensity  
Profiles of Turbulent Velocity Fluctuations in a Channel of  
Rectangular Cross Section", *Magnitnaya Gidrodinamika*, Vol. 6,  
No. 3, pp 41 - 49, July - September, 1970.
- [32] Branover, G.G., Slyusarev, N.M., Shcherbinin, E.V., "Measurement  
of Velocity Profiles and Fluctuations in a Two-Dimensional  
Channel with the Long Side of the Cross Section Parallel to  
the Transverse Magnetic Field", *Magnitnaya Gidrodinamika*,  
No. 4, pp 54 - 58, October - December, 1970.
- [33] Goldstein, R.J., "Film Cooling", *Advances in Heat Transfer*, Vol. 7,  
pp 321 - 379, 1971.
- [34] Wilson, D.J., "Heat Transfer and Effectiveness in Turbulent Super-  
sonic Film Cooling with Normal Air Injection", MSc Thesis,  
University of Minnesota, August, 1967.
- [35] Goldstein, R.J., Eckert, E.R.G., Wilson, D.J., "Film Cooling with  
Normal Injection into a Supersonic Flow", *Trans. ASME*, pp 584  
- 588, November, 1968.
- [36] Spalding, D.B., "Boundary Layer Theory Applied to Film-Cooling  
Processes", *Progress in Heat and Mass Transfer*, Vol. 4,  
pp 279 - 296, 1971.
- [37] Shiver, W.D., "Development and Evaluation of a Plasma Generator  
with a Film Cooled Anode", MSc Thesis, Georgia Institute of  
Technology, June, 1967.



- [38] Cremers, C.J., Shiver, W.D., Birkebak, R.C., "Film-Cooling of a Plasma Generator Anode", AIAA Journal, Vol. 6, No. 9, pp 1774 - 1776, August, 1967.
- [39] D'Sa, E.R., "Hydromagnetic Wall Jet", AIAA Journal, T.N., Vol. 4, No. 3, pp 537 - 539, 1965.
- [40] Luft, H.B., Rodkiewicz, C.M., "On Flat Plate Boundary Layer Flow Subjected to Suction and Transverse Magnetic Field", Department Mechanical Engineering, University of Alberta, 1973.
- [41] Sych, V.M., "Magnetohydrodynamic Flow in Rectangular Channels with Forced Flow Through Porous Walls", Magnitnaya Gidrodinamika, Vol. 4, No. 1, pp 85 - 92, 1968.
- [42] Jain, R.K., Mehta, K.N., "Laminar Hydromagnetic Flow in an Annulus with Porous Walls", The Physics of Fluids, Vol. 5, No. 10, pp 1207 - 1211, April, 1962.
- [43] Hale, F.J., Kerrebrock, J.L., "Insulator Boundary Layers in Magnetohydrodynamic Channels", AIAA Journal, Vol. 2, No. 3, pp 461 - 469, March, 1964.
- [44] Decher, R., "MHD Generator Characteristics with Insulator Wall Losses", AIAA Journal, Vol. 8, No.1, pp 132 - 137, January, 1970.
- [45] Vasil'ev, V.F., Lavrent'ev, I.V., "Effect of the Conductivity of the Walls and the Velocity Profile on Joule Losses in MHD Channels", Magnitnaya Gidrodinamika, No. 4, pp 125 - 131, October - December, 1970.
- [46] Robben, F., "Nonequilibrium Ionization in a Magnetohydrodynamic Generator", AIAA Journal, Research Notes, pp 1308 - 1309, May, 1962.



- [47] Decher, R., Hoffman, M.A., Kerrebrock, J.L., "Behaviour of a Large Nonequilibrium MHD Generator", AIAA Journal, Vol. 9, No. 3, pp 357 - 364, March, 1971.
- [48] Shohet, J.L., Osterle, J.F., Young, F.J., "Velocity and Temperature Profiles for Laminar Magnetohydrodynamic Flow in the Entrance Region of a Plane Channel", The Physics of Fluids, Vol. 5, No. 5, pp 545-549, May, 1962.
- [49] Shohet, J.L., "Velocity and Temperature Profiles for Laminar Magnetohydrodynamic Flow in the Entrance Region of an Annular Channel", The Physics of Fluids, Vol. 5, No. 8, pp 879 - 884, August, 1962.
- [50] Ching-Lai Hwang, Knieper, P.J., Liang-Tseng Fan, "Heat Transfer to MHD Flow in the Thermal Entrance Region of a Flat Duct", Int. J. Heat Mass Transfer, Vol. 9, pp 773 - 789, Pergamon Press, 1966.
- [51] Chen, T.S., Eaton, T.E., "Magnetohydrodynamic Stability of the Developing Laminar Flow in a Parallel-Plate Channel", The Physics of Fluids, Vol. 15, No. 4, pp 592-596, April, 1972.
- [52] Nihoul, J.C.J., "The Malkus Theory Applied to Magnetohydrodynamic Turbulent Channel Flow", J. Fluid Mech., Vol. 25, Part 1, pp 1 - 16, 1966.
- [53] Moffatt, H.K., "Turbulence in Conducting Fluids", The Mechanics of Turbulence, Gordon and Breach Science Publishers, pp 395 - 405, 1961.





- [54] Kovaszny, S.L.G., "Turbulence in Compressible and Electrically Conductive Media", The Mechanics of Turbulence, Gordon and Breach Science Publishers, pp 356 - 365, 1961.
- [55] Moffatt, H.K., "On the Suppression of Turbulence by a Uniform Magnetic Field", J. Fluid Mech., Vol. 28, Part 3, pp 571 - 592, 1967.
- [56] Seban, R.A., Back, L.H., "Velocity and Temperature Profiles in Turbulent Boundary Layers with Tangential Injection", Journal of Heat Transfer, Trans. ASME, Paper No. 61-SA-24, pp 45 - 54, 1962.
- [57] Pai, B.R., Whitelaw, J.H., "The Influence of Strong Pressure Gradients on Film-Cooling Effectiveness", Imperial College, London, S.W.7, England, Paper No. F C I.11, pp 1 - 10.
- [58] Cary, Jr., A.M., Hefner, J.N., "Film Cooling Effectiveness in Hypersonic Turbulent Flow", AIAA Journal, Vol. 8, No. 11, pp 2090 - 2091, December 1970.
- [59] Demetriades, S.T., Argyropoulos, G.S., "Ohm's Law in Multicomponent Nonisothermal Plasmas with Temperature and Pressure Gradients", Physics Fluids, Vol. 9, No. 11, pp 2136 - 2149, March, 1966.
- [60] Garrison, G.W., "Electrical Conductivity of a Seeded Nitrogen Plasma", AIAA Journal, Vol. 6, No. 7, pp 1264 - 1270, July, 1968.
- [61] Sutton, G.W., Sherman, A., "Engineering Magneto-Hydrodynamics", New York, McGraw Hill Book Co. Inc., 1965.
- [62] Demetriades, S.T., "Determination of Energy-Loss Factors for Slow Electrons in Hot Gases", Physical Review, June 10, 1967.



- [63] Swift-Hook, D.T., Wright, J.K., "The Constant Mach Number MHD Generator", J. Fluid Mech., Vol. 15, pp 97 - 110.
- [64] Burns, W.K., Stollery, J.L., "Film Cooling: The Influence of Foreign-Gas Injection and Slot Geometry on Impervious-Wall Effectiveness", Imperial College, Aero. Dept. Report EHT/TN/12, July, 1968.
- [65] Kacker, S.C., Whitelaw, J.H., "Prediction of Wall-Jet and Wall-Wake Flows", J. Mech. Eng'g Science, Vol. 12, No. 6, pp 404 - 420, 1970.
- [66] Kacker, S.C., Pai, B.R., Whitelaw, J.H., "The Prediction of Wall Jet Flows with Particular Reference to Film-Cooling", Progress in Heat and Mass Transfer, Vol. 2, pp 163 - 186.
- [67] Pai, B.R., Whitelaw, J.H., "The Prediction of Wall Temperature in the Presence of Film-Cooling", Int. J. Heat and Mass Transfer, Vol. 14, pp 409 - 426, Pergamon Press, 1971.
- [68] Bushnell, D.M., "Calculation of Relaxing Turbulent Boundary Layers Downstream of Tangential Slot Injection", J. Spacecraft, Vol. 8, No. 5, pp 550 - 551, 1970.
- [69] Bushnell, D.M., Beckwith, I.E., "Calculation of Non-Equilibrium Hypersonic Turbulent Boundary Layers and Comparisons with Experimental Data", AIAA Journal, Vol. 8, No. 8, pp 1462 - 1469, 1970.
- [70] Maise, G., McDonald, H., "Mixing Length and Kinematic Eddy Viscosity in a Compressible Boundary Layer", AIAA Journal Vol. 6, No. 1, pp 73 - 80, January 1968.



- [71] Kays, W.M., "Heat Transfer to the Transpired Turbulent Boundary Layer", Int. J. Heat and Mass Transfer, Vol. 15, pp 1023 - 1044, 1972.
- [72] Rossow, V.J., "On Flow of Electrically Conducting Fluids Over a Flat Plate in the Presence of Transverse Magnetic Field", NACA TN 3971, May, 1957.
- [73] Lykoudis, P.S., "Transition From Laminar to Turbulent Flow in Magneto-Fluid Mechanic Channels", Rev. Mod. Physics, Vol. 32, No. 4, pp 796 - 798, October, 1960.
- [74] Schlichting, H., "Boundary Layer Theory", McGraw-Hill Book Co. Inc., 6th Edition, pp 369 - 1968.
- [75] Davis, D.S., "Nomography and Empirical Equations", Reinhold Pub. Corp., Chapman and Hall Ltd., London, 1962.
- [76] Levens, A.S., "Graphical Methods in Research", John Wiley & Sons Ltd., 1965.
- [77] Whitelaw, J.H., "The Effect of Slot Height on the Effectiveness of the Uniform Density, Two Dimensional Wall-Jet", Imp. College Report EHT/TN/4, February, 1967.
- [78] Eckert, E.R.G., Birkebak, R.C., "The Effect of Slot Geometry on Film-Cooling", Dean Boelter Anniversary Volume, "Heat Transfer, Thermodynamics and Education", H.A. Johnson ed., McGraw Hill, 1964.
- [79] Seban, R.A., Back, L.H., "Velocity and Temperature Profiles in a Wall Jet", Int. J. Heat Mass Transfer, Vol. 3, pp 255 - 265, Pergamon Press, 1961.



- [80] Seban, R.A., Back, L.H., "Effectiveness and Heat Transfer for a Turbulent Boundary Layer with Tangential Injection and Variable Free-Stream Velocity", Journal of Heat Transfer, pp 235 - 244, Trans. of ASME, August, 1962.
- [81] Kacker, S.C., Whitelaw, J.H., "Dependence of the Impervious Wall Effectiveness of a Two-Dimensional Wall-Jet on the Thickness of the Upper Lip Boundary Layer", Int. J. Heat Mass Transfer, Vol. 10, pp 1623 - 1624, Pergamon Press. 1967.





## APPENDIX A

### On Flat Plate Boundary Layer Flow Subjected to Suction and Transverse Magnetic Field

Bernard H. Luft and Czeslaw M. Rodkiewicz  
Department of Mechanical Engineering  
University of Alberta, Edmonton, Canada

#### Abstract

The Karman-Pohlhausen technique is applied to obtain a solution of MHD boundary layer flow over an insulated semi-infinite flat plate in the presence of a uniform transverse magnetic field and uniform suction applied at the plate surface. The fluid assumed to be incompressible and have a constant coefficient of electrical conductivity. The usual MHD assumptions are adopted among which the magnetic Reynolds number is considered to be small enough such that induced current effects become negligible. Two cases are considered: the first is usually referred to as magnetic field fixed relative to the fluid far from the plate and the second designated as magnetid field fixed relative to the plate. For the first case an asymptotic - MHD suction profile is obtained and the advent of the fully developed boundary layer is illustrated for combined Hartmann numbers and suction coefficients. Developing velocity profiles and average skin friction coefficients are also derived. For the second case, boundary layer separation is predicted for an impermeable wall at a Stuart number of unity in spite of a nonexistent pressure gradient. Unfortunately, the



integral method with a fourth order polynomial velocity profile was not able to predict the points of separation for suction and magnetic field applied simultaneously.



## Nomenclature

$\bar{B}$	= magnetic field
$c_f'$	= local skin friction coefficient $(=\tau_w/\frac{1}{2} \rho U_\infty^2)$
$C_F$	= average skin friction coefficient
$C_Q$	= suction coefficient $(= v_w /U_\infty)$
$L$	= reference plate length
$M$	= Hartmann number $(= BL\sqrt{\sigma/\mu_f})$
$N$	= interaction parameter $(= \sigma B^2 L/\rho U_\infty)$
$N_x$	= Stuart number or local interaction parameter $(=\sigma B^2 x/\rho U_\infty)$
$Re_L$	= Reynolds number $(=U_\infty L/\nu)$
$Re_x$	= local Reynolds number $(=U_\infty x/\nu)$
$U_e$	= free stream velocity
$U_\infty$	= uniform upstream velocity
$u$	= x-component of velocity
$v_w$	= uniform suction velocity
$x, y$	= coordinates parallel and normal to plate, respectively
$\delta$	= boundary layer thickness
$\delta_1$	= displacement thickness
$\delta_2$	= momentum thickness
$\mu_f$	= fluid dynamic viscosity
$\nu$	= fluid kinematic viscosity
$\rho$	= fluid mass density
$\sigma$	= fluid electrically conductivity
$\tau_w$	= wall shear stress



## Subscripts

B	= magnetic field
e	= free-stream conditions
r	= reference based on plate length L
s	= separation
w	= evaluated at the wall
0	= zero suction
$\infty$	= uniform upstream conditions





## Introduction

Magnetohydrodynamic (MHD) flows over a porous surface are encountered in studying vortex type MHD generators<sup>1</sup> or when considering the possibility of applying transpiration cooling to the channel walls of an MHD converter. In such cases it becomes necessary to solve the flow equations in the presence of permeable wall boundary conditions. Hydromagnetic flows with porous walls have interested previous authors among which are E.R. D'Sa<sup>2</sup> who obtained a series solution for the hydromagnetic wall jet including the effects of suction and blowing at the wall and R.K. Jain and K.N. Mehta<sup>3</sup> considered the problem of laminar hydromagnetic flow in an annulus with porous walls. In general the problem is complicated but simplifying assumptions are possible that permit solutions from which first order effects can be inferred.

The Kármán-Pohlhausen method has already been found useful in solving the MHD boundary layer equations in the absence of suction or blowing. Maciulaitis and Loeffler<sup>4</sup> used a parabolic velocity profile in their investigation of MHD channel entrance flows, W.C. Moffatt<sup>5</sup> chose a profile that was a function of the Hartmann number in his study of hydromagnetic channel entrance flows. Heiser and Bornhorst<sup>6</sup> proposed a modified fourth degree polynomial velocity profile to include adverse free-stream pressure gradients for flows of incompressible, conducting fluids over semi-infinite boundaries. The modification relinquishes the usual ordinary hydrodynamic (OHD) condition that  $\partial^2 u / \partial y^2$  vanish in the free stream and replaces this by a condition on the third derivative at the wall. Later, Ramamoorthy<sup>7</sup> resolves the problems treated by Rossow<sup>8</sup> and others using the Karman-Pohlhausen



method with the modified velocity profile and obtains excellent agreement as well as improvements over the solutions obtained earlier. In the present investigation the modified fourth degree polynomial profile is not necessitated since an adverse pressure gradient is not considered. For the case referred to by Rossow as "magnetic field fixed relative to the fluid", an exponential profile similar to that prescribed by H.G. Lew<sup>9</sup> for OHD flat plate flow with uniform suction will be employed. For the second case referred to as "magnetic field fixed relative to the plate", the usual fourth degree polynomial profile is adopted since in general this yields slightly better results than the exponential assumption.

#### Governing Equations and Solutions

Our mathematical model consists of a boundary layer flow over an electrically insulated flat plate in the presence of a constant transverse magnetic field  $\bar{B}$  which may be stationary or moving with constant velocity  $U_B$  relative to the plate. The fluid is assumed to be incompressible with constant electrical conductivity  $\sigma$ , density  $\rho$  and viscosity  $\nu$ . We further assume that no electric field is applied and that the uniform upstream velocity  $U_\infty$  is undisturbed; that is, the magnetic field is assumed to vanish abruptly upstream from the leading edge of the plate.

Application of the integral method results in the following general differential equation which is comparable to that given in References 4, 5 and 6 in the absence of wall suction:

$$U_e^2 \frac{d\delta_2}{dx} + (2\delta_2 + \delta_1) U_e \frac{dU_e}{dx} + \frac{\sigma B^2}{\rho} U_e \delta_1 - U_e v_w = \frac{\tau_w}{\rho} \quad (1)$$



The first case of interest arises when  $U_B = U_e = U_\infty$  are constant.

Following Lew<sup>9</sup> we introduce new variables  $\lambda$  and  $\xi$  defined by

$\lambda(\xi) = -\text{Re}_L C_Q \delta_r(\xi)/2$  and  $\xi = \text{Re}_L^2 C_Q^2 \bar{x} = C_Q^2 \text{Re}_x$  with  $\delta_r = \delta/L$ ,  $\bar{x} = x/L\text{Re}_L$ ,  $\bar{y} = y/\delta$  and  $\bar{u} = u/U_\infty$  we obtain the following dimensionless equation:

$$2 \frac{d}{d\xi} \left[ \lambda \int_0^\infty \bar{u}(1-\bar{u}) d\bar{y} \right] + 2I\lambda \int_0^\infty (1-\bar{u}) d\bar{y} = 1 + \left( \frac{\partial \bar{u}}{\partial \bar{y}} \right)_w / 2\lambda \quad (2)$$

where the combined magnetic and suction effects are related by a single parameter  $I$  defined by  $I = N/\text{Re}_L C_Q^2 = (M/\text{Re}_L C_Q)^2$ . Even for an impermeable wall the boundary layer behaves asymptotically as  $x \rightarrow \infty$ . This asymptotic solution, as given by Gurevich et al<sup>10</sup>, is

$$\bar{u} = 1 - e^{-My_r} \quad (3)$$

where  $y_r = \delta_r \bar{y} = y/L$ . To solve equation (2) we will want to choose an exponential profile of a particular form and to illustrate the justification for this choice we first resolve the momentum equation for zero suction and compare the results with several existing solutions. The non-dimensional equation to be solved is now

$$\frac{d}{d\xi_0} \left[ \lambda_0 \int_0^\infty \bar{u}(1-\bar{u}) d\bar{y} \right] + \left( \frac{M}{\text{Re}_L} \right)^2 \lambda_0 \int_0^\infty (1-\bar{u}) d\bar{y} = \frac{1}{4\lambda_0} \left( \frac{\partial \bar{u}}{\partial \bar{y}} \right)_w \quad (4)$$

with  $\lambda_0 = \text{Re}_L \delta_r/2$  and  $\xi_0 = \text{Re}_L^2 \bar{x}$ . Considering the asymptotic solution (3) we are led to assume a velocity distribution of the form



$$\bar{u} = 1 - e^{-M\bar{y}} (1 - M\bar{y}K(\bar{x})) \quad (5)$$

where  $K(\bar{x}) = \frac{1}{2} (\delta_r^2(\bar{x}) - 1)$  as determined from the boundary condition  $(\partial^2 \bar{u} / \partial \bar{y}^2)_w = -M^2 \delta_r$ . Expression (5) satisfies the remaining boundary conditions  $\bar{u}(0) = \bar{u}'(\infty) = \bar{u}''(\infty) = \bar{u}(\infty) - 1 = 0$  and we note that when  $\delta_r = 1$ ,  $K = 0$ ,  $\bar{y} = y_r$  and hence the required asymptotic solution (3) is recovered. Substitution of (5) into equation (4) and defining  $\phi_0 = \lambda_0 / \text{Re}_L$  results in the differential equation

$$\frac{d\phi_0}{d\xi_0} = 2\left(\frac{M}{\text{Re}_L}\right)^2 \left\{ \frac{8\phi_0^4 - 10\phi_0^2 + 1}{\phi_0(-4\phi_0^4 - 16\phi_0^3 - 12\phi_0^2 + 11)} \right\} \quad (6)$$

The solution of (6) subject to  $\phi_0 = 0$  at  $\xi_0 = 0$  is easily found to be

$$\begin{aligned} \left(\frac{M}{\text{Re}_L}\right)^2 \xi_0 = N_x = & -\frac{1}{8} \phi_0^2 - \phi_0 \\ & - \frac{1}{16} \ln \left\{ \frac{(\phi_0 + a_1)^{C_1} (a_1 - \phi_0)^{C_2} (\phi_0 + a_2)^{C_3} (a_2 - \phi_0)^{C_4}}{a_1^{C_5} a_2^{C_6}} \right\} \end{aligned} \quad (7)$$

with the constants given by

$$\begin{aligned} C_1 &= \frac{17a_1^3 - 20a_1^2 - 11\frac{1}{2}a_1 + 2}{2a_1(a_1^2 - a_2^2)}, & C_2 &= \frac{17a_1^3 + 20a_1^2 - 11\frac{1}{2}a_1 - 2}{2a_1(a_1^2 - a_2^2)} \\ C_3 &= \frac{-17a_2^3 + 20a_2^2 + 11\frac{1}{2}a_2 - 2}{2a_2(a_1^2 - a_2^2)}, & C_4 &= \frac{-17a_2^3 - 20a_2^2 + 11\frac{1}{2}a_2 + 2}{2a_2(a_1^2 - a_2^2)} \end{aligned}$$





$$c_5 = \frac{34a_1^2 - 23}{2(a_1^2 - a_2^2)}, \quad c_6 = \frac{-34a_2^2 + 23}{2(a_1^2 - a_2^2)}$$

$$a_1 = \left(\frac{5+\sqrt{17}}{8}\right)^{1/2}, \quad a_2 = \left(\frac{5-\sqrt{17}}{8}\right)^{1/2}$$

Using solution (7) the local skin friction coefficient and displacement thickness can now be plotted as a function of Stuart number  $N_x$  given that

$$c_f' \frac{Re_L}{M} = \frac{1}{\phi_0} (2\phi_0^2 + \frac{1}{2}) \quad (8)$$

and

$$\frac{\delta_1 M}{L} = 2\phi_0 \left(\frac{3}{2} - 2\phi_0^2\right) \quad (9)$$

Figure 1 shows fairly good agreement with the other results shown although a somewhat higher skin friction coefficient is obtained.\*

Returning now to the solution of equation (2) with suction present, an asymptotic - MHD suction profile is easily shown to be

$$u = 1 - e^{-A\eta} \quad (10)$$

where  $A = \frac{1}{2} + \sqrt{\frac{1}{4} + I}$  and  $\eta = y|v_w|/\nu$ . An obvious choice for  $\bar{u}$  now is expression (5) with A simply replacing the Hartmann number M. Hence we assume

---

\* It appears that Ramamoorthy<sup>7</sup> incorrectly plotted  $c_f' M$  instead of  $c_f' Re_L / M$ . Expressions used to plot Rossow's results<sup>8</sup> for  $N_x \leq .2$  are  $c_f' Re_L / M = (.664 + 2.29N_x - 2.768N_x^2)/\sqrt{N_x}$  and  $\delta_1 M / L = (1.73 - 2.21N_x)\sqrt{N_x}$



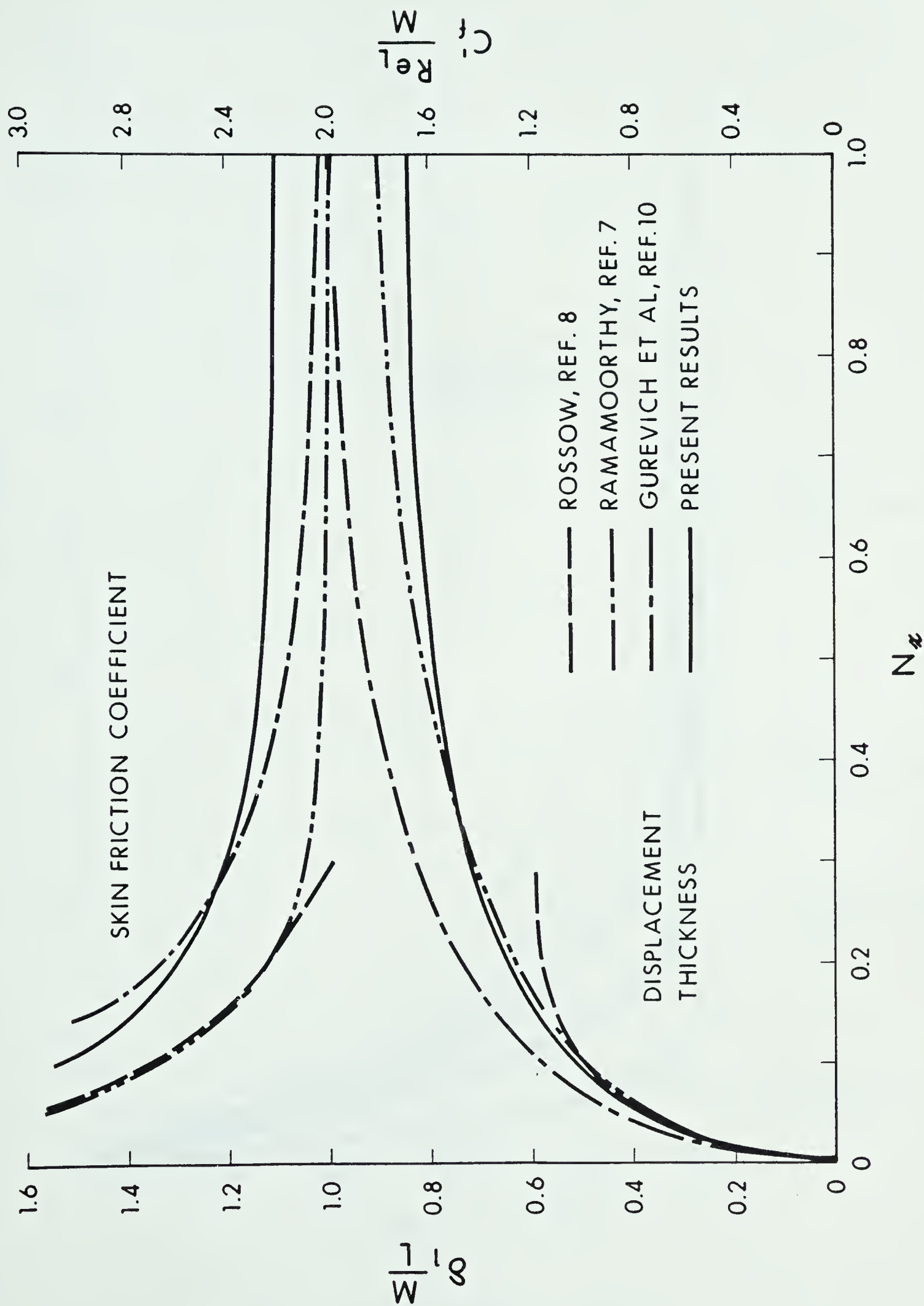


Fig.1 Displacement Thickness and Skin-Friction Coefficient



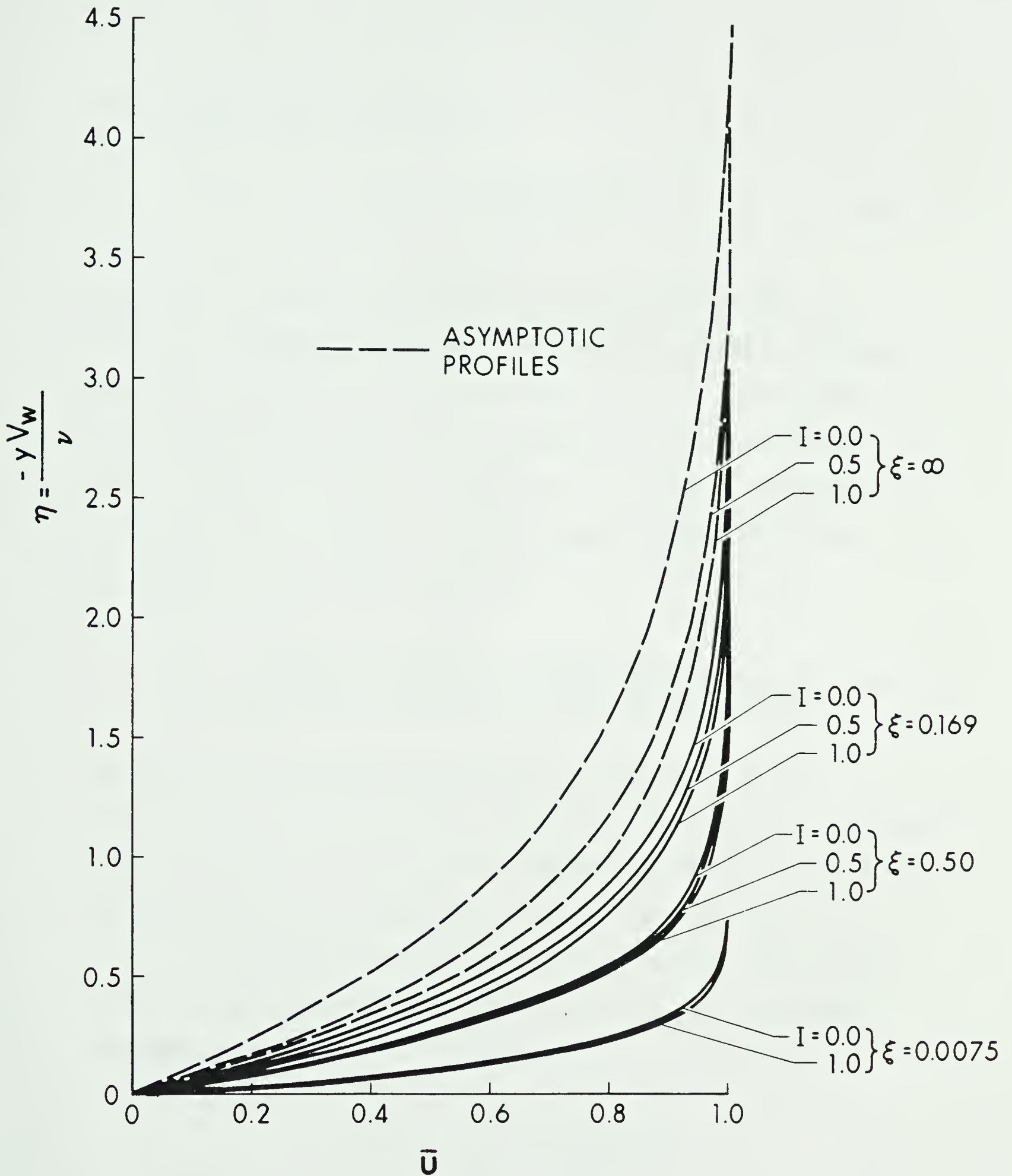


Fig. 2 Velocity Profiles at Various Locations and Along Plate Length



$$\bar{u} = 1 - e^{-A\bar{y}} (1 - A\bar{y}K(\bar{x})) \quad (11)$$

The parameter  $K(\bar{x})$  is then given by

$$K(\bar{x}) = - \frac{[A(A+2\lambda) - 4I\lambda^2]}{2A(\lambda+A)} \quad (12)$$

obtained from the condition that at the plate surface -  $Re_L C_Q \delta_r$   
 $(\partial\bar{u}/\partial\bar{y})_w = (\partial^2\bar{u}/\partial\bar{y}^2)_w + N Re_L \delta_r^2$ . The remaining boundary conditions are again automatically satisfied by expression (11). Furthermore, the asymptotic solution is also recovered with  $K = 0$ , which occurs when  $\lambda = (A - A\sqrt{1+4I})/4I = -\frac{1}{2}$ , since with  $|\lambda| = \frac{1}{2}$ ,  $\bar{y} = \eta$  in view of  $\eta = 2|\lambda|\bar{y}$ . Insertion of (11) into the Kármán equation (2) results in the ordinary differential equation

$$\frac{d\lambda}{d\xi} = \frac{2A(\lambda+A)^2[(2A\lambda+A^2)^2 + 8I\lambda^2(2I\lambda^2 - 2A\lambda - A^2)]}{12A^2\lambda^4 + 36A^3\lambda^3 + 37A^4\lambda^2 + 11A^5\lambda - 8I\lambda^3(6I\lambda^3 + 10AI\lambda^2 + A^2\lambda + 3A^3)} \quad (13)$$

which agrees with the non-magnetic case of Lew<sup>9</sup> for  $I = 0$  ( $A=1$ ) specialized for zero Mach number and with the coefficient of  $\lambda^2$  corrected to 37. Equation (13) is not easily integrated in closed form for  $I \neq 0$  and a numerical solution was obtained subject to  $\lambda = 0$  when  $\xi = 0$ .

The developing velocity profiles for several values of the magnetic suction parameter  $I$  are shown in Fig. 2. The displacement thickness, defined by

$$\frac{\delta_1 |v_w|}{\nu} = - \frac{\lambda}{A^2} \left\{ \frac{4A\lambda + 3A^2 - 4I\lambda^2}{\lambda + A} \right\} \quad (14)$$





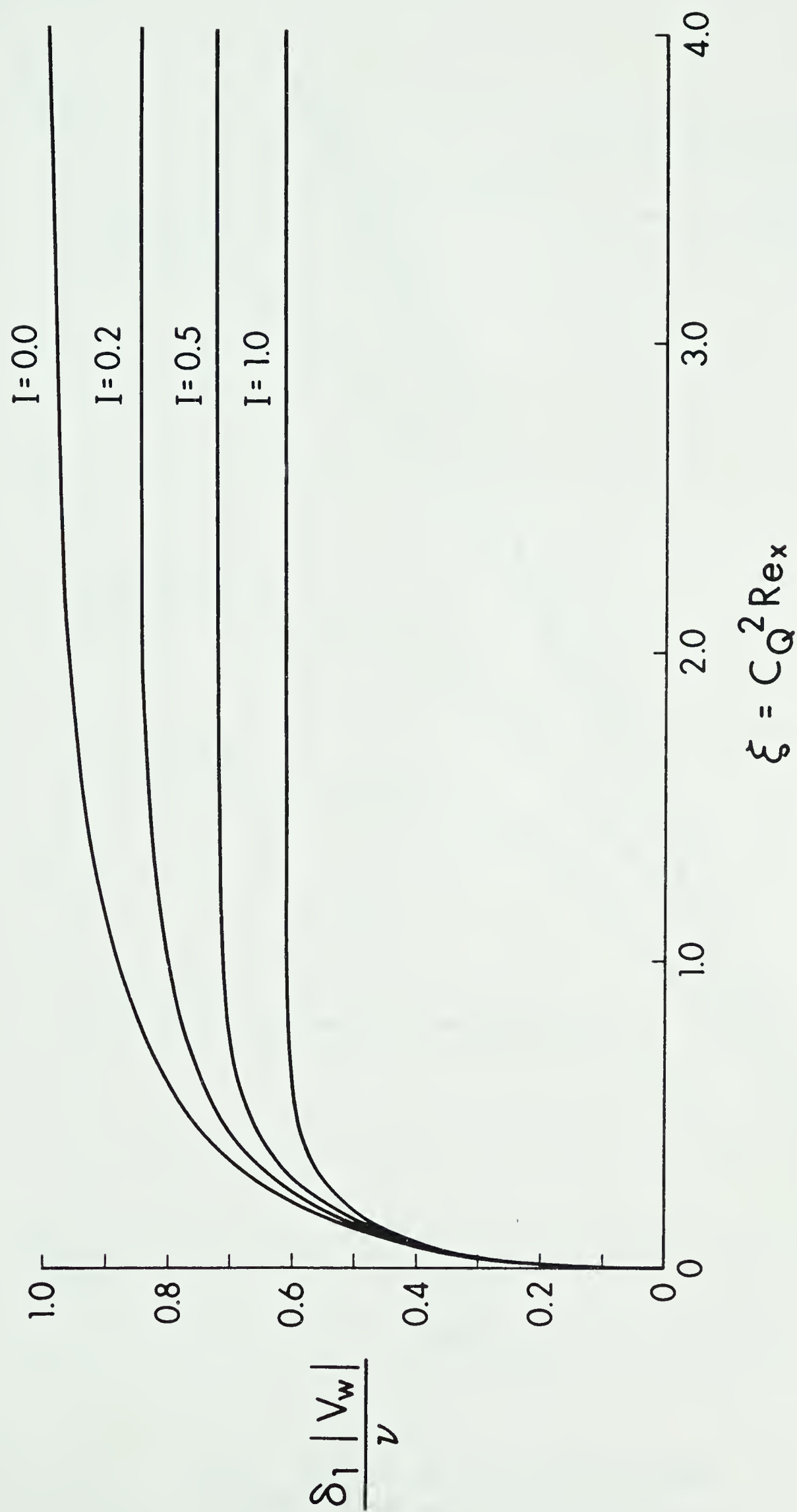


Fig. 3 Displacement thickness along  
plate length,  $\bar{B}$  fixed to fluid



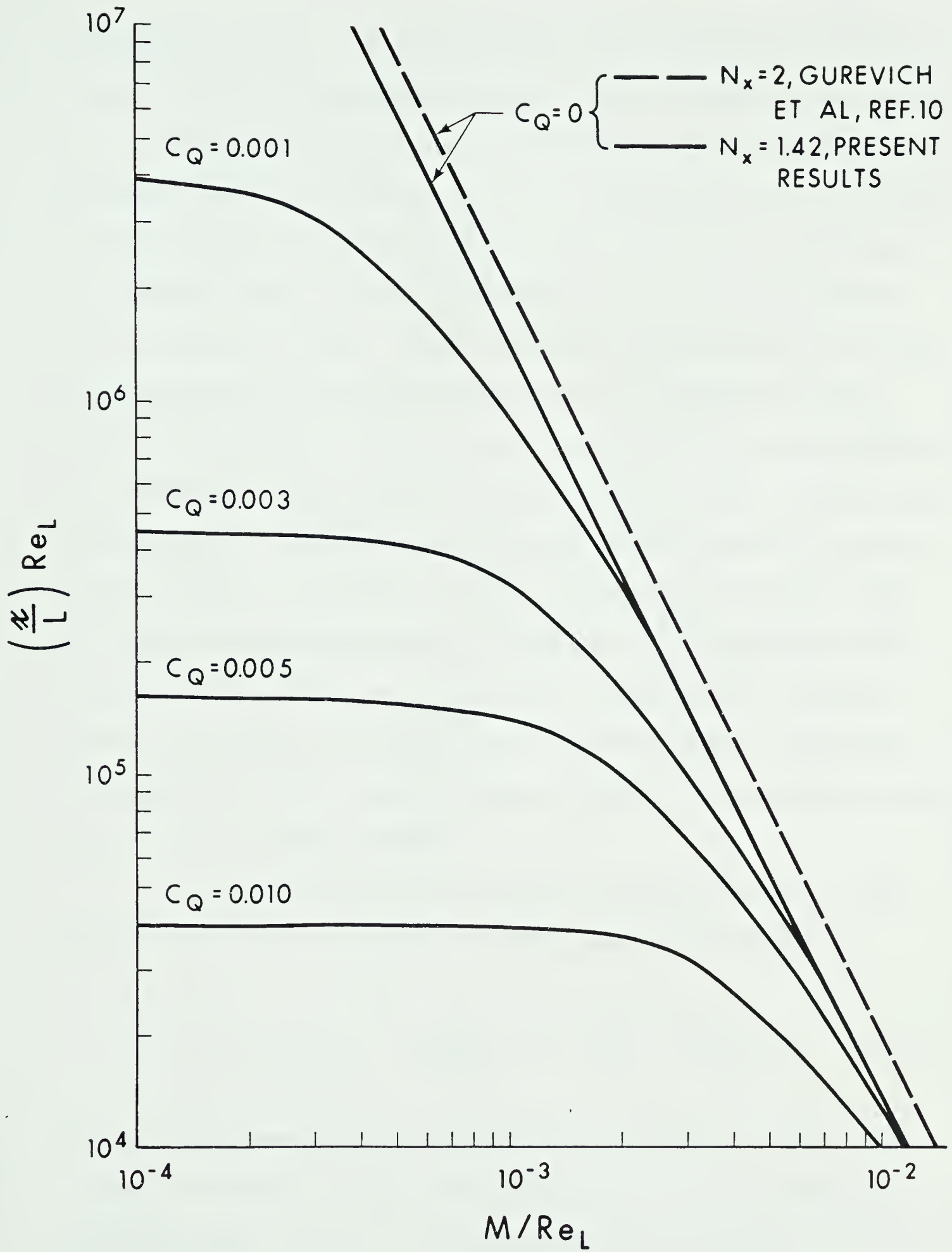


Fig. 4 Position of fully developed MHD boundary layer with uniform suction,  $B$  fixed to fluid



is plotted in Fig. 3. It is evident that the displacement thickness is reduced and the fully developed boundary layer is approached at smaller  $\xi$  as  $I$  increases. Expression (14) is easily verified to approach its asymptotic value of  $1/A$  when  $\lambda = -1/2$ . Defining the fully developed condition to occur at 99% of this value it is possible to illustrate the combined effect of suction and magnetic field on the attainment of the asymptotic state. Figure 4 indicates the position on the plate corresponding to fully developed conditions as a function of  $M/Re_L$  (ratio of ponderomotive force to inertia force) with  $C_0$  as a parameter. For sufficiently weak magnetic fields (or low electrical conductivity) the magnitude of suction primarily determines the asymptotic position. Conversely, for large values of  $M/Re_L$  the behaviour corresponds more as if the plate were impermeable. Gurevich et al<sup>10</sup> determine from a series solution without suction that at a Stuart number of approximately 2 or larger, the boundary layer behaviour differs little from its asymptotic state. From the present analysis a corresponding value of  $N_x = 1.42$  has been obtained.

It is also desired to know the influence of magnetic field and suction on the average skin friction coefficient defined as

$$C_F = \frac{1}{\frac{1}{2} \rho U_\infty^2 x} \int_0^x \mu_f \left( \frac{\partial u}{\partial y} \right)_w dx = - \frac{C_0}{\xi} \int_0^\xi \frac{1}{\lambda} \left( \frac{\partial \bar{u}}{\partial y} \right)_w d\xi \quad (15)$$

Figure 5 shows the behaviour of  $C_F$  with local Reynolds number. The asymptotic solution of  $2AC_0$  is indicated as well and the approximate Reynolds number at which it is approached can be determined from Fig. 4.



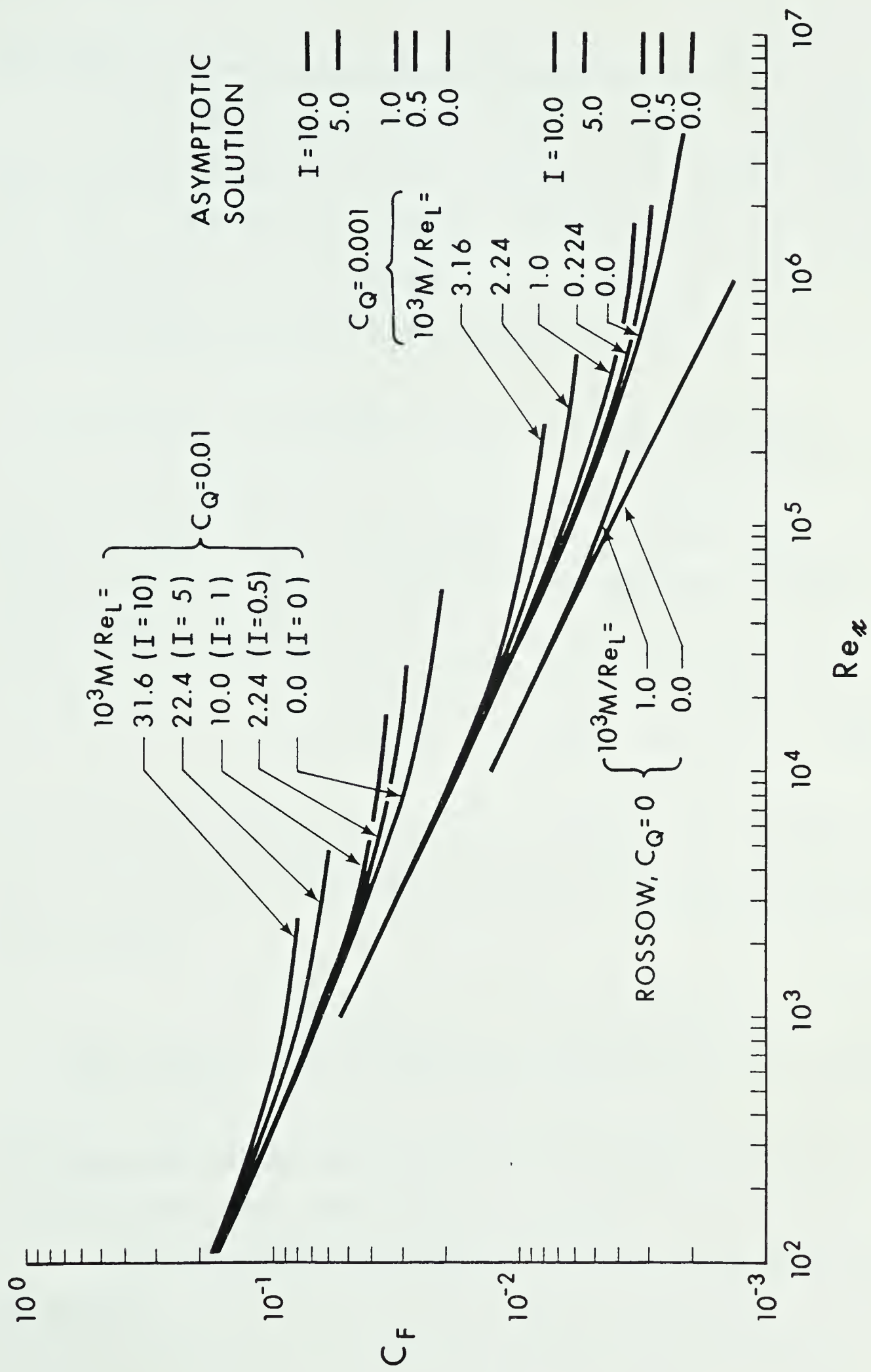


Fig. 5 Average Skin-Friction Coefficient, B fixed to fluid





Also shown are some zero suction results obtained by Rossow<sup>8</sup>.

The second case of interest occurs when  $U_B = 0$ . The resulting differential equation is that considered by V.J. Rossow<sup>8,11</sup> and E.R. D'Sa<sup>2</sup>. Assuming that no magnetic interaction occurs with  $U_\infty$ , the free stream velocity is now given by  $U_e = U_\infty - \sigma B^2 x / \rho$  or  $U_e / U_\infty = 1 - I\xi$ . The dimensionless momentum integral equation is now

$$2(1-I\xi) \frac{d}{d\xi} \left[ \lambda \int_0^1 u^*(1-u^*) d\bar{y} \right] - 4I\lambda \int_0^1 u^*(1-u^*) d\bar{y} = 1 + \left( \frac{\partial u^*}{\partial \bar{y}} \right)_w / 2\lambda \quad (16)$$

where  $u^* = u/U_e$ . Since in this case there is no a priori reason to assume a velocity profile of a particular form, the usual polynomial distribution is adopted—viz.,

$$u^* = a\bar{y} + b\bar{y}^2 + c\bar{y}^3 + d\bar{y}^4 \quad (17)$$

with coefficients given by  $a = 6/(\lambda+3)$ ,  $b = 6\lambda/(\lambda+3)$ ,  $c = -2(4\lambda+3)/(\lambda+3)$  and  $d = 3(\lambda+1)/(\lambda+3)$ . Substitution of (17) into equation (16) results in the equation

$$\frac{d\lambda}{d\xi} = \frac{1}{2(1-I\xi)} \left\{ \frac{35(\lambda+3)^2(\lambda^2+3\lambda+3) + 4I\lambda^2(\lambda+3)(4\lambda^2+26\lambda+37)}{4\lambda^4 + 36\lambda^3 + 119\lambda^2 + 111\lambda} \right\} \quad (18)$$

which once again can be made to agree with the incompressible version of Lew's<sup>9</sup> equation (19) when  $I = 0$ .

The displacement thickness and local shear stress coefficient are given by



$$\delta_1 \frac{|v_w|}{v} = - \frac{\lambda(4\lambda+9)}{5(\lambda+3)} \quad (19)$$

and

$$c'_f = - \frac{6C_0(1-I\xi)}{\lambda(\lambda+3)} \quad (20)$$

An unfortunate shortcoming of assumption (17) is that the asymptotic state for the non-magnetic case cannot be attained. As  $x \rightarrow \infty$ ,  $\delta_1 |v_w|/v \rightarrow 1$  and equation (19) shows that  $\lambda$  for this value is imaginary. Lew has shown that the useful range of values for  $\lambda$  is only  $0 \geq \lambda > -1\frac{1}{2}$  which also turns out to be the case for  $I \neq 0$ .

Again we resolve the purely magnetic case using (17) without the modification proposed in Ref. 6, and compare the results with an existing solution. The non-dimensional equation to be solved for this case is

$$\begin{aligned} & \left[ 1 - \left( \frac{M}{Re_L} \right)_{\xi_0}^2 \frac{d}{d\xi_0} \left[ \lambda_0 \int_0^1 u^*(1-u^*) d\bar{y} \right] \right. \\ & \left. - 2 \left( \frac{M}{Re_L} \right)^2 \lambda_0 \int_0^1 u^*(1-u^*) d\bar{y} \right] = \frac{1}{4\lambda_0} \left( \frac{\partial u^*}{\partial \bar{y}} \right)_w \end{aligned} \quad (21)$$

and the coefficients in (17) take the values of  $a = 2$ ,  $b = 0$ ,  $c = -2$  and  $d = 1$ . The solution for the Stuart number\* is now

$$N_x = 1 - \frac{1}{\left[ 1 + \frac{148}{315} (M\phi_0)^2 \right]^{1/4}} \quad (22)$$

---

\*The Stuart number  $N_x$  is identical with the parameter  $mx$  defined by Rossow<sup>8,11</sup>.



and the expression for the average skin friction becomes

$$C_F = \frac{M}{Re_L} \frac{148}{315} \left\{ \frac{M\phi_0}{\sqrt{(1 + \frac{148}{315} (M\phi_0)^2)}} \right\} \frac{1}{N_x} \quad (23)$$

A comparison of  $C_F$  obtained from the polynomial distribution with that obtained by Rossow<sup>8</sup> with  $M/Re_L = 10^{-3}$  is shown in Table 1.\*

$N_x$	Rossow**	Eqn. (23)
0.01	0.0132	0.0133
0.10	0.0038	0.0040
0.15	0.0029	0.0032
0.20	0.0024	0.0026

Table 1 Comparison of Average Skin Friction  
Coefficient  $C_F$ ,  $M/Re_L = 10^{-3}$

Equation (18) was again integrated numerically satisfying the condition  $\lambda = 0$  at  $\xi = 0$ . The local skin friction from equation (20) is plotted in Fig. 6 at a particular location on the plate given by  $Re_x = 10^4$ . The restricted range of  $\lambda$  is seen to be a limitation on the magnetic parameter  $M/Re_L$  for which a solution is obtained when suction is present and a continuation up to the point of separation ( $c_f' = 0$ ) was, therefore, not possible. Nevertheless, the combined

---

\* Rossow's result is  $C_F = \frac{1.328 - 1.19N_x}{\sqrt{Re_x}} = \frac{M}{Re_L} \left\{ \frac{1.328 - 1.19N_x}{\sqrt{N_x}} \right\}$ ,  $N_x \leq .2$



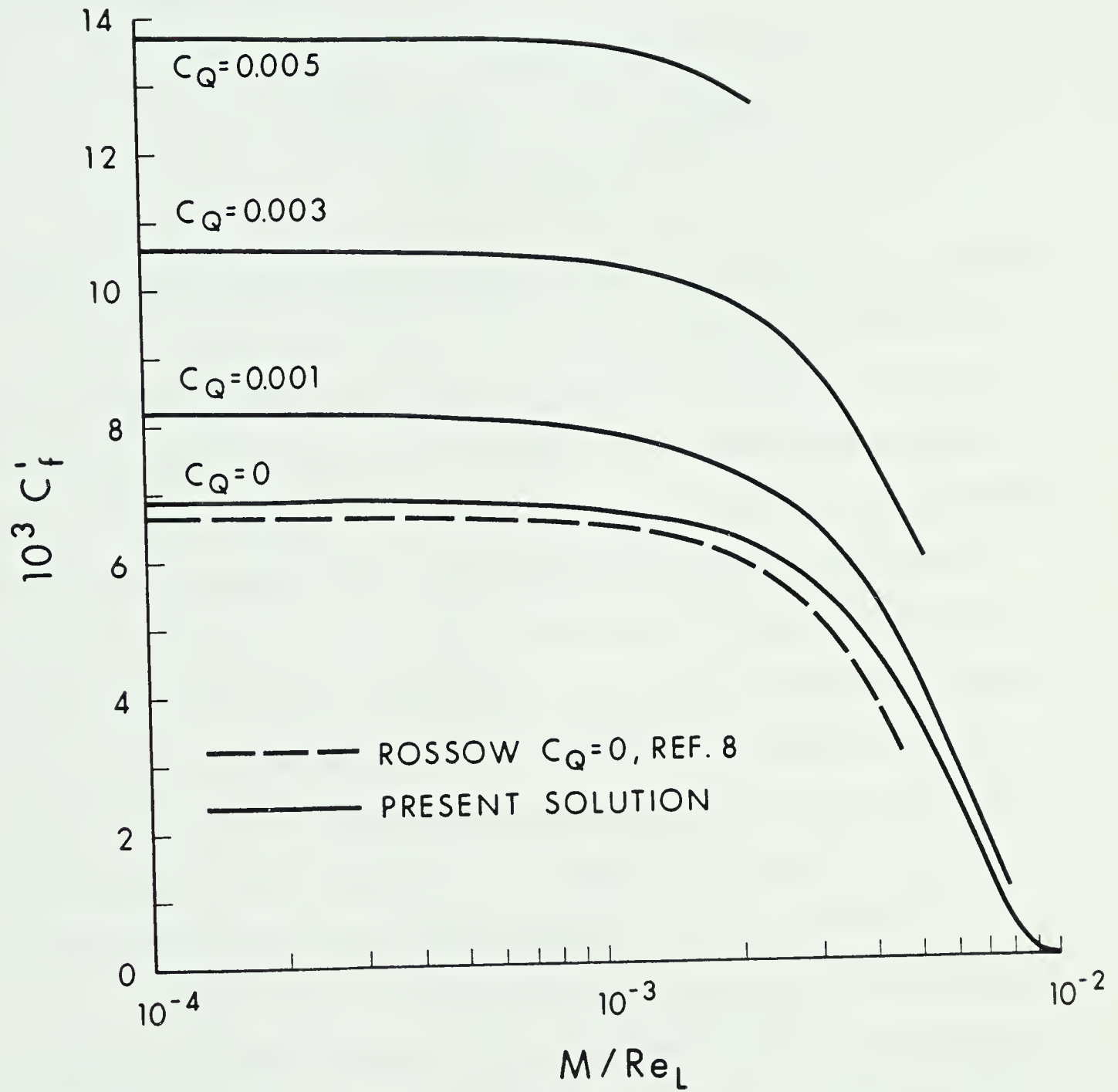


Fig. 6 Local skin-friction variation at a particular location given by  $Re_x = 10^4$ ,  $\bar{B}$  fixed to plate





effect of suction and magnetic field on the local shear stress before separation, is indicated. When  $C_Q = 0$ , however, the expression for the local shear stress

$$c_f' \frac{Re_L}{M} = \frac{2(1-N_x)}{\left\{ \frac{315}{148} \left[ \frac{1}{(1-N_x)^4} - 1 \right] \right\}^{1/2}} \quad (24)$$

indicates that separation occurs when the Stuart number  $N_x = 1$ , which in Fig. 6\* occurs when  $M/Re_L = 10^{-2}$ . If a dimensionless point of separating is defined by  $\hat{x}_s = (U_\infty/\nu)x_s$  we can plot the relationship between  $k$  and  $\hat{x}_s$  where  $k$  is a constant in the free-stream potential flow of the form  $U_e/U_\infty = 1 - (kU_\infty/\nu)x$ . Figure 7 shows  $\hat{x}_s$  as a function of  $k$  and is compared with  $\hat{x}_s$  when separation is due to an adverse pressure gradient. In the latter case the well known relationship in Reference 12 is  $\hat{x}_s = 0.125/k$  whereas from the present analysis we obtain  $\hat{x}_s = 1/k$ . The reason for the downstream displacement of the separation point for the magnetic case is a result of the fact that a hydrodynamic pressure gradient is transmitted to the plate surface whereas the magnetic body force vanishes there for this case.

It would be of interest to include suction or blowing in the analysis of channel entrance region problems considered in References 4 and 5. If a polynomial profile were assumed the modification proposed by Heiser and Bornhorst would require  $(\partial^3 u^*/\partial \bar{y}^3)_w = NRe_L \delta_r^2 (\partial u^*/\partial \bar{y})_w - C_Q Re_L \delta_r (\partial^2 u^*/\partial \bar{y}^2)_w$ .

---

\* Rossow's result shown for comparison, was terminated at  $M/Re_L \approx 4.5 \times 10^{-3}$  since it ceases to be valid beyond  $N_x = 0.2$ .



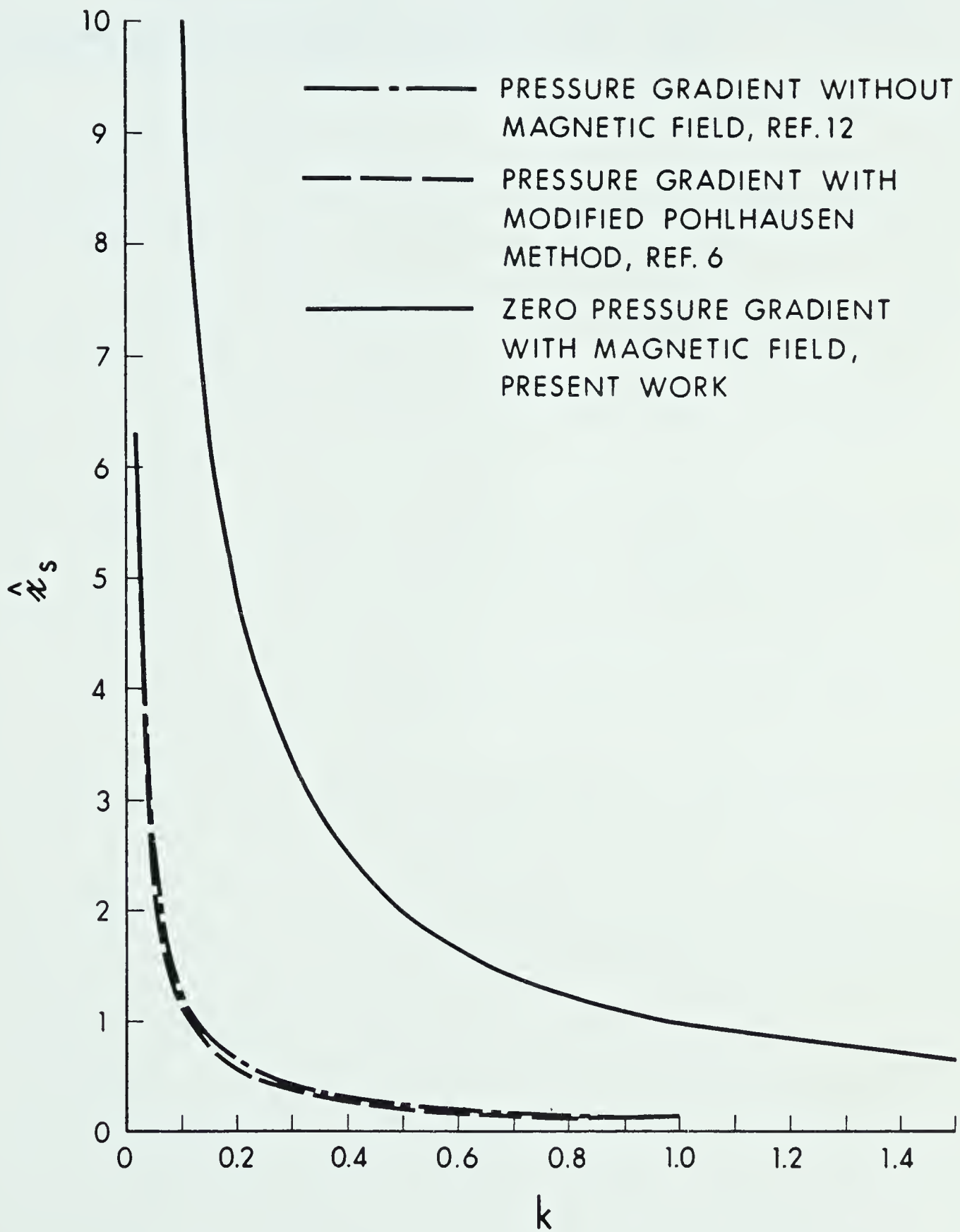


Fig. 7 Dimensionless point of separation for uniformly decelerated flows of the form  $U_e/U_\infty = 1 - k\hat{x}$



## Acknowledgement

This research was financially supported by the National Research Council of Canada through Grant NRC C-0083.



## References

1. Sych, V.M., "Magnetohydrodynamic flow in rectangular channels with forced flow through porous walls", *Magnitnaya Gidrodinamika* 4, 85-92 (1968). Translation in "Magnetohydrodynamics", Faraday Press, Inc.
2. D'Sa, E.R., "Hydromagnetic wall jet", *AIAA J.* 4, 537-539 (1966).
3. Jain, R.K. and Mehta, K.N., "Laminar hydromagnetic flow in an annulus with porous walls", *Phys. Fluids* 5, 1207-1211 (1962).
4. Maciulaitis, A. and Hoeffler, Jr. A.L., "A theoretical investigation of MHD channel entrance flows", *AIAA J.* 2, 2100-2103 (1964).
5. Moffatt, W.C., "Analysis of MHD channel entrance flows using the momentum integral method", *AIAA J.* 2, 1495-1497 (1964).
6. Heiser, W.H. and Bornhorst, W.J., "A modified Pohlhausen velocity profile for MHD boundary layer problems", *AIAA J.* 4, 1139-1141 (1966).
7. Ramamoorthy, P., "Kármán-Pohlhausen method for MHD boundary layers", *AIAA J.* 6, 1407-1409 (1968).
8. Rossow, V.J., "On flow of electrically conducting fluids over a flat plate in the presence of a transverse magnetic field", *NACA TN* 3971 (1957).
9. Lew, H.G., "On the compressible boundary layer over a flat plate with uniform suction", *Reissner Annivers. Vol. Contr. Appl. Mech.*, Ann Arbor Mich., 43-60 (1949).





10. Gurevich, B. Ya., Miller, R.L., Tsinober, A.B. and Shtern, A.G.,  
"Flow of an electrically conducting fluid over a flat plate  
in a perpendicular magnetic field", *Magnitnaya Gidrodinamika*  
2, 69-77 (1966). Translation in "Magnetohydrodynamics",  
Faraday Press, Inc.
11. Rossow, V.J., "On magneto-aerodynamic boundary layers", *ZAMP*  
IXb, 519-527 (1958).
12. Schlichting, H., "Boundary Layer Theory" (McGraw-Hill Book Co.  
Inc., 1968).











**B30373**